ISSN 1949-8470 (online)

World Journal of *Radiology*

World J Radiol 2012 July 28; 4(7): 291-344

Baishideng Publishing Group
www.wjgnet.com

WJR World Journal of Radiology

A peer-reviewed, online, open-access journal of Radiology

Editorial Board

2009-2013

The *World Journal of Radiology* Editorial Board consists of 319 members, representing a team of worldwide experts in radiology. They are from 40 countries, including Australia (3), Austria (4), Belgium (5), Brazil (3), Canada (9), Chile (1), China (25), Czech (1), Denmark (1), Egypt (4), Estonia (1), Finland (1), France (6), Germany (17), Greece (8), Hungary (1), India (9), Iran (5), Ireland (1), Israel (4), Italy (28), Japan (14), Lebanon (1), Libya (1), Malaysia (2), Mexico (1), Netherlands (4), New Zealand (1), Norway (1), Saudi Arabia (3), Serbia (1), Singapore (2), Slovakia (1), South Korea (16), Spain (8), Switzerland (5), Thailand (1), Turkey (20), United Kingdom (16), and United States (82).

France

Alain Chapel, *Fontenay-Aux-Roses*
Nathalie Lassau, *Villejuif*
Youlia M Kirova, *Paris*
Géraldine Le Duc, *Grenoble Cedex*
Laurent Pierot, *Reims*
Frank Pilleul, *Lyon*
Pascal Pommier, *Lyon*

Germany

Ambros J Beer, *München*
Thomas Deserno, *Aachen*
Frederik L Giesel, *Heidelberg*
Ulf Jensen, *Kiel*
Markus Sebastian Juchems, *Ulm*
Kai U Juergens, *Bremen*
Melanie Kettering, *Jena*
Jennifer Linn, *Munich*
Christian Lohrmann, *Freiburg*
David Maintz, *Münster*
Henrik J Michaely, *Mannheim*
Oliver Micke, *Bielefeld*
Thoralf Niendorf, *Berlin-Buch*
Silvia Obenauer, *Duesseldorf*
Steffen Rickes, *Halberstadt*
Lars V Baron von Engelhardt, *Bochum*
Goetz H Welsch, *Erlangen*

Greece

Panagiotis Antoniou, *Alexandroupolis*
George C Kagadis, *Rion*
Dimitris Karacostas, *Thessaloniki*
George Panayiotakis, *Patras*
Alexander D Rapidis, *Athens*
C Triantopoulou, *Athens*
Ioannis Tsalafoutas, *Athens*
Virginia Tsapaki, *Anixi*
Ioannis Valais, *Athens*

Hungary

Peter Laszlo Lakatos, *Budapest*

India

Anil Kumar Anand, *New Delhi*
Surendra Babu, *Tamilnadu*
Sandip Basu, *Bombay*
Kundan Singh Chufal, *New Delhi*
Shivanand Gamanagatti, *New Delhi*
Vimoj J Nair, *Haryana*
R Prabhakar, *New Delhi*
Sanjeeb Kumar Sahoo, *Orissa*

Iran

Vahid Reza Dabbagh Kakhki, *Mashhad*
Mehran Karimi, *Shiraz*
Farideh Nejat, *Tehran*
Alireza Shirazi, *Tehran*
Hadi Rokni Yazdi, *Tehran*

Ireland

Joseph Simon Butler, *Dublin*

Israel

Amit Gefen, *Tel Aviv*
Eyal Sheiner, *Be'er-Sheva*
Jacob Sosna, *Jerusalem*
Simcha Yagel, *Jerusalem*

Italy

Mohssen Ansarin, *Milan*
Stefano Arcangeli, *Rome*
Tommaso Bartalena, *Imola*
Sergio Casciaro, *Lecce*
Laura Crocetti, *Pisa*
Alberto Cuocolo, *Napoli*
Mirko D'Onofrio, *Verona*
Massimo Filippi, *Milan*
Claudio Fiorino, *Milano*
Alessandro Franchello, *Turin*
Roberto Grassi, *Naples*
Stefano Guerriero, *Cagliari*
Francesco Lassandro, *Napoli*
Nicola Limbucci, *L'Aquila*
Raffaele Lodi, *Bologna*
Francesca Maccioni, *Rome*
Laura Martincich, *Candiolo*
Mario Mascalchi, *Florence*
Roberto Miraglia, *Palermo*
Eugenio Picano, *Pisa*
Antonio Pinto, *Naples*
Stefania Romano, *Naples*
Luca Saba, *Cagliari*
Sergio Sartori, *Ferrara*
Mariano Scaglione, *Castel Volturno*
Lidia Strigari, *Rome*
Vincenzo Valentini, *Rome*

Japan

Shigeru Ehara, *Morioka*
Nobuyuki Hamada, *Chiba*
Takao Hiraki, *Okayama*
Akio Hiwatashi, *Fukuoka*
Masahiro Jinzaki, *Tokyo*
Hiroshi Matsuda, *Saitama*
Yasunori Minami, *Osaka*
Jun-Ichi Nishizawa, *Tokyo*
Tetsu Niwa, *Yokohama*
Kazushi Numata, *Kanagawa*
Kazuhiko Ogawa, *Okinawa*
Hitoshi Shibuya, *Tokyo*
Akira Uchino, *Saitama*
Haiquan Yang, *Kanagawa*

Lebanon

Aghiad Al-Kutoubi, *Beirut*

Libya

Anuj Mishra, *Tripoli*

Malaysia

R Logeswaran, *Cyberjaya*
Kwan-Hoong Ng, *Kuala Lumpur*

Mexico

Heriberto Medina-Franco, *Mexico City*

Netherlands

Jurgen J Fütterer, *Nijmegen*
Raffaella Rossin, *Eindhoven*
Paul E Sijens, *Groningen*

New Zealand

W Howell Round, *Hamilton*

Norway

Arne Sigmund Borthne, *Lørenskog*

Saudi Arabia

Mohammed Al-Omran, *Riyadh*
Ragab Hani Donkol, *Abha*
Volker Rudat, *Al Khobar*

Serbia

Djordjije Saranovic, *Belgrade*

Singapore

Uei Pua, *Singapore*
Lim CC Tchoyoson, *Singapore*

Slovakia

František Dubecký, *Bratislava*

South Korea

Bo-Young Choe, *Seoul*
Joon Koo Han, *Seoul*
Seung Jae Huh, *Seoul*
Chan Kyo Kim, *Seoul*
Myeong-Jin Kim, *Seoul*
Seung Hyup Kim, *Seoul*
Kyoung Ho Lee, *Gyeonggi-do*
Won-Jin Moon, *Seoul*
Wazir Muhammad, *Daegu*
Jai Soung Park, *Bucheon*
Noh Hyuck Park, *Kyunggi*
Sang-Hyun Park, *Daejeon*
Joon Beom Seo, *Seoul*
Ji-Hoon Shin, *Seoul*
Jin-Suck Suh, *Seoul*
Hong-Gyun Wu, *Seoul*

WJR World Journal of Radiology

Contents

Monthly Volume 4 Number 7 July 28, 2012

World Journal of Radiology
Volume 4 Number 7 July 28, 2012

Contents

NAME OF JOURNAL
World Journal of Radiology

ISSN
ISSN 1949-8470 (online)

LAUNCH DATE
December 31, 2009

FREQUENCY
Monthly

EDITING
Editorial Board of *World Journal of Radiology,*
Room 903, Building D, Ocean International Center,
No. 62 Dongsihuan Zhonglu, Chaoyang District,
Beijing 100025, China
Telephone: +86-10-59080039
Fax: +86-10-85381893
E-mail: wjr@wjgnet.com
http://www.wjgnet.com

EDITOR-IN-CHIEF
Filippo Cademartiri, MD, PhD, FESC, FSCCT, Professor, Cardio-Vascular Imaging Unit-Giovanni XXIII Hospital, Via Giovanni XXIII, 7-31050-Monastier di Treviso (TV), Italy

EDITORIAL OFFICE
Jian-Xia Cheng, Director
World Journal of Radiology
Room 903, Building D, Ocean International Center,
No. 62 Dongsihuan Zhonglu, Chaoyang District,
Beijing 100025, China
Telephone: +86-10-59080039
Fax: +86-10-85381893
E-mail: wjr@wjgnet.com
http://www.wjgnet.com

PUBLISHING
Baishideng Publishing Group Co., Limited
Room 1701, 17/F, Henan Building,
No.90 Jaffe Road, Wanchai, Hong Kong, China
Fax: +852-31158812
Telephone: +852-58042046

PUBLICATION DATE
July 28, 2012

INSTRUCTIONS TO AUTHORS
Full instructions are available online at http://www.wjgnet.com/1949-8470/g_info_20100316162358.htm.

ONLINE SUBMISSION
http://www.wjgnet.com/esps/

World Journal of Radiology

Online Submissions: http://www.wjgnet.com/esps/
wjr@wjgnet.com
doi:10.4329/wjr.v4.i7.291

World J Radiol 2012 July 28; 4(7): 291-301
ISSN 1949-8470 (online)

ORIGINAL ARTICLE

Impact of the arterial input function on microvascularization parameter measurements using dynamic contrast-enhanced ultrasonography

Marianne Gauthier, Stéphanie Pitre-Champagnat, Farid Tabarout, Ingrid Leguerney, Mélanie Polrot, Nathalie Lassau

Marianne Gauthier, Stéphanie Pitre-Champagnat, Farid Tabarout, Ingrid Leguerney, Nathalie Lassau, IR4M-UMR 8081, Institut Gustave Roussy, 94805 Villejuif cedex, France
Mélanie Polrot, Service Commun d'Expérimentation Animale, Institut Gustave Roussy, 94805 Villejuif cedex, France
Nathalie Lassau, Institut de recherche en cancérologie à Villejuif, Institut Gustave Roussy, 94805 Villejuif cedex, France
Author contributions: Gauthier M performed the majority of experiments, designed the study and wrote the manuscript; Pitre-Champagnat S and Polrot M provided substantial contributions to conception, design, acquisition, analysis and interpretation of the data; Tabarout F provided substantial contributions to conception and design; Leguerney I was involved in analyzing results and editing the manuscript; and Lassau N managed each step of the study, provided contribution to data analyses and was involved in editing the manuscript.
Correspondence to: Marianne Gauthier, PhD, IR4M-UMR 8081, Institut Gustave Roussy, Pavillon de recherche I, 39 rue Camille Desmoulins, 94805 Villejuif cedex, France. gauthier.marianne@gmail.com
Telephone: +33-1-42116215 Fax: +33-1-42115495
Received: April 22, 2012 Revised: June 5, 2012
Accepted: June 12, 2012
Published online: July 28, 2012

Abstract

AIM: To evaluate the sources of variation influencing the microvascularization parameters measured by dynamic contrast-enhanced ultrasonography (DCE-US).

METHODS: Firstly, we evaluated, *in vitro*, the impact of the manual repositioning of the ultrasound probe and the variations in flow rates. Experiments were conducted using a custom-made phantom setup simulating a tumor and its associated arterial input. Secondly, we evaluated, *in vivo*, the impact of multiple contrast agent injections and of examination day, as well as the influence of the size of region of interest (ROI) associated with the arterial input function (AIF). Experiments were conducted on xenografted B16F10 female nude mice. For all of the experiments, an ultrasound scanner along with a linear transducer was used to perform pulse inversion imaging based on linear raw data throughout the experiments. Semi-quantitative and quantitative analyses were performed using two signal-processing methods.

RESULTS: *In vitro*, no microvascularization parameters, whether semi-quantitative or quantitative, were significantly correlated (*P* values from 0.059 to 0.860) with the repositioning of the probe. In addition, all semi-quantitative microvascularization parameters were correlated with the flow variation while only one quantitative parameter, the tumor blood flow, exhibited *P* value lower than 0.05 (*P* = 0.004). *In vivo*, multiple contrast agent injections had no significant impact (*P* values from 0.060 to 0.885) on microvascularization parameters. In addition, it was demonstrated that semi-quantitative microvascularization parameters were correlated with the tumor growth while among the quantitative parameters, only the tissue blood flow exhibited *P* value lower than 0.05 (*P* = 0.015). Based on these results, it was demonstrated that the ROI size of the AIF had significant influence on microvascularization parameters: in the context of larger arterial ROI (from 1.17 ± 0.6 mm^3 to 3.65 ± 0.3 mm^3), tumor blood flow and tumor blood volume were correlated with the tumor growth, exhibiting *P* values lower than 0.001.

CONCLUSION: AIF selection is an essential aspect of the deconvolution process to validate the quantitative DCE-US method.

Key words: Dynamic contrast-enhanced ultrasonography; Angiogenesis; Linear raw data; Arterial input function; Functional imaging

Peer reviewers: Zhonghua Sun, MD, PhD, Associate Professor, Discipline of Medical Imaging, Department of Imaging and Applied Physics, Curtin University of Technology, GPO Box U 1987, Perth, Western Australia 6845, Australia; Dr. Kazushi Kishi, Department of Radiology, Wakayama Medical University, Kimiidera 811-1, Wakayama City 641-8510, Japan

Gauthier M, Pitre-Champagnat S, Tabarout F, Leguerney I, Polrot M, Lassau N. Impact of the arterial input function on microvascularization parameter measurements using dynamic contrast-enhanced ultrasonography. *World J Radiol* 2012; 4(7): 291-301 Available from: URL: http://www.wjgnet.com/1949-8470/full/v4/i7/291.htm DOI: http://dx.doi.org/10.4329/wjr.v4.i7.291

INTRODUCTION

Tumor angiogenesis is a process characterized by the development of new blood vessels supplying tumors with nutrients and oxygen[1,2]. This process is an essential step for tumor growth as well as the initiation of metastasis. In this context, research is currently focused on developing anti-angiogenic treatments resulting in the destruction of neoblood vessels, which often occurs initially without any morphological changes[3-5].

Since February 2000, Response Evaluation Criteria in Solid Tumors has been used by the entire cancer clinical research community as an essential tool in evaluating responses to anti-tumor treatments[6]. As this involves analyzing morphological information[7], it is commonly recognized that these criteria are no longer optimal in the early assessment of anti-angiogenic therapies, which primarily target microvasculature. Consequently, functional imaging is recognized as the best modality for evaluating such treatments.

However, the current microvascularization parameters on which therapy evaluations are based do not properly correlate with the vascular physiology, which might interfere with the final interpretation. Such parameters are defined as semi-quantitative since they only provide a relative access to the physiological parameters through the current ultrasound imaging mode. These limits may be overcome by working with the arterial input function (AIF), which takes into account physiological variations such as the cardiac flow rate, the arterial blood pressure, the vascular structure, and the way the contrast agent is injected[8]. This is done through a deconvolution process which allows access to quantitatively-defined microvascularization parameters, since it provides absolute evaluation of microvasculature parameters. Deconvolution has been already performed using other imaging modalities[9-11]. Previous studies have been performed to develop a deconvolution technique based on Tikhonov regularization[12,13]: preliminary results demonstrated a diminution in microvascularization parameter coefficients of variation from 30% to 13%, respectively measured without and with the deconvolution process.

Considering these results, the aim of this study was to determine and analyze sources of variation that impact microvascularization parameters measured using dynamic contrast-enhanced ultrasonography (DCE-US) combined with a deconvolution process, both *in vitro* and *in vivo*, following bolus injections of SonoVue® (Bracco, Milan, Italy).

MATERIALS AND METHODS

Contrast agent

DCE-US data were acquired following bolus injections of SonoVue®, a second generation echo contrast agent made of microbubbles filled with sulphur hexafluoride (SF_6) and stabilized by a shell of amphiphilic phospholipids[14,15]. The diameter of the microbubbles, ranging from 1 to 10 μm[15], allowed a purely intravascular circulation through the whole blood volume, which made it ideal for the evaluation of microvascularization[15]. SF_6 is an innocuous, stable and inert gas that does not interact with any other molecules found in the body. In addition, SonoVue® is highly resistant to pressure changes and exhibits a non-linear response of the microbubbles when insonated at low acoustic power, thus provides continuous real-time ultrasonographic (US) imaging without any bubble destruction[14,16,17]. SonoVue® is available as a kit which includes one vial of SF_6, a powder combining phospholipids and pharmaceutical grade polyethyleneglycol, and one syringe pre-filled with 5 mL of 0.9% sodium chloride. Before any US exam, reconstruction of the contrast agent was performed by introducing the content of the syringe into the vial followed by manual shaking for at least 20 s. After a few minutes of no use, the microbubbles tend to accumulate at the upper surface because of buoyancy. Thus, to inject a homogeneous bolus of contrast agent, the vial was manually checked before each injection. SonoVue® is stable for 6 h, and all experiments were conducted within this limit[14].

Time intensity method

The time-intensity method is based on the dye-dilution theory, which provides a mathematical method for estimating microvascularization parameters based on monitoring the tracer concentration as a function of time generating a time intensity curve (TIC). Microvascularization parameters to be analyzed are extracted from the TIC[18,19]. To be valid, a series of assumptions must be verified[20]: (1) flow must be constant to ensure the amount of microbubbles injected has no effect on the flux; (2) blood and contrast agent must be mixed homogeneously; (3) recirculation should not interfere with the first pass; and (4) the mixing of the contrast agent must exhibit linearity and stability[21]. In this context, linearity refers to the linear relationship between the injected concentration of contrast agents and the measured US signal. This was confirmed for low doses[15] and in the context of bolus injections of contrast agent[22].

In this study, these conditions were assumed to be satisfied, allowing the direct extraction of the microvascularization parameters from the TIC.

Ultrasound imaging mode

Images were acquired using a Toshiba Aplio® XG ultrasound scanner (Toshiba, Japan) connected to a 7-14 MHz linear transducer (PLT 1202S probe). (1) B-mode and Doppler imaging were performed at 14 MHz; and (2) Harmonic imaging was performed at 10 MHz using the pulse inversion mode in which two pulses were sent into the tissue, the second pulse being an inverted copy of the first one. Thus, the associated echoes were detected and summed[23]. Linear scattering from the two pulses produced echoes that were inverted copies of each other, resulting in a null signal. Linear scattering dominates in tissue. Conversely, non-linear scattering of the two pulses, which dominates in microbubbles, produced echoes that were no longer inverted, resulting in a non-null signal[24].

Data analysis

Semi-quantitative microvascularization parameters (the current method): Acquisitions and analyses were based on linear raw data (uncompressed data before standard video visualization). Such data exhibit the advantage of a linear dynamic range, which is the essential aspect of TIC analysis[25,26]. Following bolus injections of SonoVue®, several harmonic images were acquired. Image analysis followed a protocol described in previous studies[27,28] using dedicated software called CHIQ® (Toshiba). Thus, the current method allowed one to graphically extract semi-quantitative microvascularization parameters following the fitting of the tumor TIC based on minimizing the differences between the parameters of the raw curve and the coefficients of the IGR equation (Patent: WO/2008/053268 entitled "Method and system for quantification of tumoral vascularization"):

$$I(t) = a_0 + (a_1 - a_0) * \left(\frac{A + \left(\frac{t}{a_2} \right)^p}{B + \left(\frac{t}{a_2} \right)^q} \right)$$

I(t) describes the variation in the intensity of contrast uptake as a function of time. a_0 is the intensity before the arrival of the contrast agent. a_1 is linked to the maximum value of contrast uptake. a_2 is linked to the rise time to the peak intensity (PI). p is a coefficient related to the increase in intensity. q is a coefficient related to the decrease in intensity. A and B are arbitrary parameters.

Semi-quantitative microvascularization parameters have already been described in previous studies[27,28]. These are PI, the time to peak intensity (T_{PI}), the area under the curve (AUC), the wash-in (AUWI), the wash-out (AUWO) and the full width at half maximum (FWHM) (Figure 1[12]).

Quantitative microvascularization parameters (the deconvolution process): Based on the dye-dilution theory, the influence of the arterial input manifests itself through the following fundamental convolution equation:

$$C_t(t) = \frac{\rho}{k_H} \cdot (BF) \cdot [C_a(t) \otimes R(t)]$$

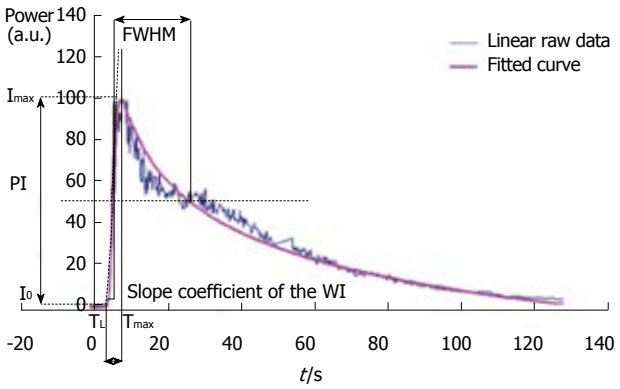

Figure 1 Graph displaying an example of a time intensity curve with four of its seven associated microvascularization parameters: the peak intensity, the time to peak intensity, the slope coefficient of the wash-in and the full width at half maximum. The three other microvascularization parameters extracted from the time intensity curve are the area under the curve, the area under the wash-in and the area under the wash-out. WI: Wash-in; FWHM: The full width at half maximum; PI: The peak intensity; I_{max}: Maximal intensity value; I_0: Initial intensity value; T_L is the latency time and is defined as the time at the intersection between y = I_0 and the tangent at $T_{max}/2$ where T_{max} is the time associated with I_{max}.

where $C_t(t)$ is the concentration of the contrast agent measured in the tumor as a function of time, $C_a(t)$ is the AIF, BF is the tissue blood flow (unit: mL/min per 100 g of tissue), ρ is the tissue density (unit: g/mL) and k_H represents the difference in hematocrit between capillaries and arteries: ρ and k_H are commonly approximated by 1[29,30]. *R(t)* is the residue function and is defined as the relative amount of tracer in the region of interest (ROI) under the hypothesis of an instantaneous unit bolus injection [R(0) = 1 ; R(∞) = 0]. The shape of the *R(t)* function reflects the properties of both the vasculature and the tissue[31].

In order to derive quantitative parameters from this equation, the residue function *R(t)* can be determined using a process called deconvolution. The deconvolution method developed in our lab and dedicated to the DCE-US imaging is based on the Tikhonov regularization and was previously described by Gauthier *et al*[12].

Three quantitative microvascularization parameters are thus graphically extracted from the residue function: the BF, the tissue blood volume (BV) and the mean transit time (MTT) (Figure 2[27]).

In vitro analysis

Three-intertwined pipe phantom: The phantom used in the *in vitro* experiments consisted of three-intertwined silicone pipes simulating a heterogeneous structure akin to that of vessels in tumor and feeding pipes which simulated the arterial input (Figure 3).

The phantom was immersed in a custom-made water tank connected to a peristaltic pump (SP vario/ PD 5101, Heidolph®, Germany) which provided a water flow rate set as required for the experiments. The three silicone pipes had an internal diameter of 2 mm with a 1 mm thick wall. Both the input and the output of the phantom were composed of three-way taps (Discofix®, B. Braun, Melsungen, Germany) allowing linkage between the three

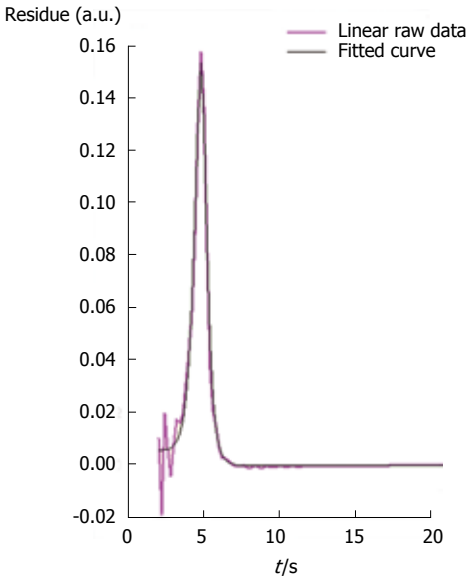

Figure 2 Graph displaying an example of a residue function. From this curve, three quantitative microvascularization parameters are graphically extracted: Blood flow corresponds to the maximum value reached by the residue function, blood volume is defined as the area under the curve and the mean transit time is defined as the ratio between blood volume and blood flow.

pipes. A new ROI, containing both pipes, feeding pipe and water spaces, was drawn for each injection and the associated TIC was obtained.

The total amount of water in the circuit was set at 60 mL. The amount of injected contrast agent was 0.06 mL. This volume corresponded to the ratio granted by French marketing approval ("Autorisation de Mise sur le Marché": AMM) (2.4 mL of SonoVue® for 5 L of blood): this was defined as the AMM ratio. The second volume was associated with the ratio routinely used for clinical exams (4.8 mL of SonoVue® for 5 L of blood). In particular, this ratio was used in four studies led by the IGR involving 117 patients and 800 DCE-US exams[32,33] as well as in a French national project supported by the "Institut National du Cancer" (French National Cancer Institute)[34]. This ratio was defined as the internal growth rate ratio.

US protocol

Bolus injections of SonoVue® were performed using a 1 mL syringe (Terumo®, Belgium). To minimize potential errors due to SonoVue® residues, all of the injection materials were changed before each injection: the circuit was entirely emptied, rinsed and reset with water. Thus no contrast agent residues were present in the circuit, allowing the initial conditions to be exactly the same throughout all of the experiments[27].

Before the series of acquisitions, a Doppler image was acquired to help the operator image the same setup through all the experiments.

Acquisitions were performed at a low mechanical index (MI = 0.21) and at a rate of 5 frames per second (fps). Two ROIs were selected to be analyzed (Figure 4[12]): the first one was associated with the three-intertwined pipe phantom while the second was associated with its feeding pipe. Deconvolution was performed between the two TICs extracted from these ROIs through the CHIQ® software.

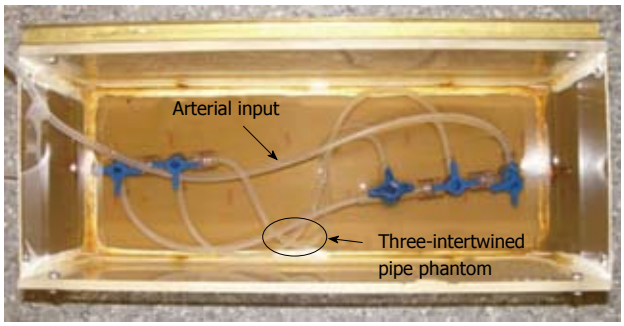

Figure 3 Three-intertwined silicone pipe phantom and its feeding pipe simulating the heterogeneous structure of a tumor and one of its arterial inputs.

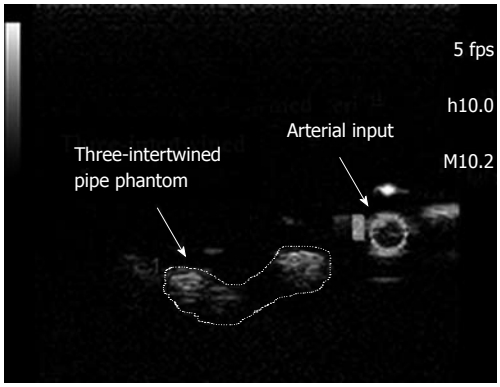

Figure 4 Pulse inversion image of the three-intertwined pipe phantom. The figure displays the selection of the region of interests associated with the phantom and its feeding pipe. fps: Frames per second.

Repositioning of the US probe

Experimental protocol: Sources of DCE-US variability include the repositioning of the US probe before each examination: this has to be the same for each acquisition of the therapeutic evaluation process which can last several months or years. Indeed, evaluation of therapy is based on analyzing evolution of microvascularization parameters linked to a specific target along the whole duration of the treatment. In this context, the aim of this study was to evaluate the impact of the repositioning of the US probe on microvascularization parameters. The experiments consisted of: (1) 10 consecutive contrast agent injections with the US probe unchanged; and (2) 10 consecutive contrast agent injections with the US probe manually replaced before each exam.

Variation in flow

Experimental protocol: The absolute evaluation of the microvascularization parameters is not possible through the methodology which does not take into account the arterial input[8]. Until now, different studies have investigated and used the link between the microvascularization

Figure 5 ***In vivo*** **experiments were conducted on xenografted B16F10 female nude mice.**

parameters directly extracted from the tumor TIC and the physiological parameters of interest[35-38].

Thus, the BF is linked to the slope of the WI and the TPI, which are currently the two parameters mentioned in the literature. None of the semi-quantitative microvascularization parameters are specific to the BF. On the contrary, as expected by definition, only one quantitative microvascularization parameter should be specific to the blood flow: it is BF.

To perform the study, 4 injections per flow rate were performed and 3 flow rates were tested: 21.2 mL/min, 42.4 mL/min and 63.6 mL/min. Variations in flow rates were controlled using the peristaltic pump.

In vivo analysis

Animals and tumor model: Animal experiments were conducted with five nude female mice aged from six to eight weeks with the approval of the European Convention for the Protection of Vertebrate Animals used for experimental and other scientific purposes (Strasbourg, 18.Ⅲ.1986; text amended according to the provisions of protocol ETS No. 170 as of its entry into force on 2nd December 2005). The tumor model B16F10 (CRL-6475, ATCC, American Type Culture Collection) melanoma cell line, a murine skin cancer, was selected to perform the *in vivo* experiments. Tumor cells were prepared and cultured in Dulbeco Minimum Essential Medium (Gibco Life Technologies, France) combined with 10% fetal bovine serum, 1% penicillin/streptomycin and glutamate (Invitrogen Life Technologies, Inc., France) to avoid bacterial contamination of the solution. While growing, cells were maintained in an incubator at 37 ℃. Tumors were xenografted onto the right flank (Figure 5[12,27]) of five mice through a subcutaneous injection of 2×10^6 melanoma cells in 0.2 mL of phosphate buffered saline. DCE-US exams were performed following three 0.1 mL injections of SonoVue® according to the methodology used in our lab.

Anesthesia

Mice received chemical anesthesia based upon their weight. Product was injected intraperitoneally using the 1 mL syringe. The solution consisted of ketamine (10 mg/mL, Ketalar®, Parapharm, France) and xylazine (2%, Rompum®, Bayer, France). To ensure the mice remained asleep throughout the experiment, 150 μL/g per mouse was systematically injected.

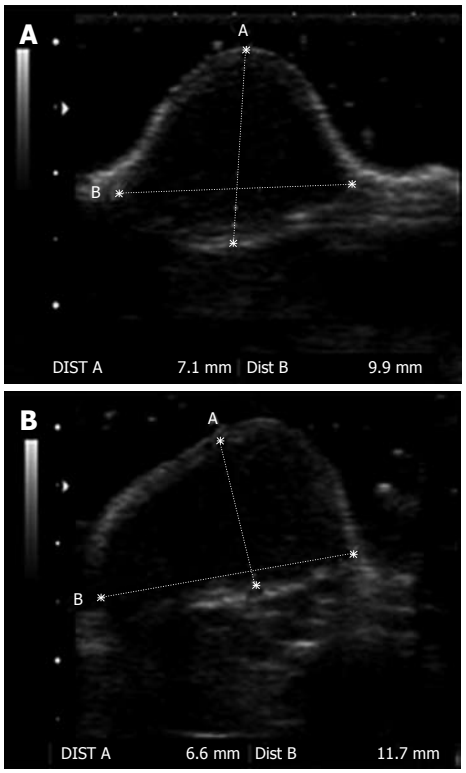

Figure 6 Volume evaluation was performed for each mouse using transversal (A) and longitudinal (B) B-mode images of the tumor.

Acquisition protocol

In vivo images were acquired using the same ultrasound machine and probe as the *in vitro* experiments. Images were acquired using a mechanical index set at 0.21 and a rate of 5 fps. In addition, preliminary fundamental B-mode images were acquired to evaluate the tumor volume prior to the SonoVue® injection (Figure 6[12]). The three perpendicular tumor diameters were determined and the tumor volume was derived according to the following formula:

$$V = \frac{1}{2} \times (depth \times width \times length)$$

In the following study, two new ROIs were selected for each acquisition. The first ROI included only the tumor while the second ROI was associated with an arterial input. We gave preference to the location of the arterial ROI instead of its size to avoid any delay or dispersion effects that can impact the quantitative microvascularization parameters[30]. Two TICs were extracted from these ROIs. To ensure the complete elimination of the contrast agent between each acquisition, a break of 15 min and 3 min of insonation at high MI (MI = 1.04) were observed. Mice were kept asleep no more than 2 h[39]. This duration included the time required for the mice to obtain a stable

Table 1 Characteristics of the *in vivo* experiments

Mouse number	Number of days	Number of injections
Multiple injections and day of examination		
1	4	3
		4
		3
		4
2	2	3
		2
3	2	2
		4
Influence of the size of the arterial region of interest		
1	3	3
		3
		2
2	3	2
		3
		3
3	2	4
		3
4	2	4
		3

heart rate after the administration of anesthesia, acquisition time and the time of the break between each injection.

Evaluated sources of variation

Multiple injections/day of examination: The first evaluated factor was the order of injection. This is a parameter of interest especially in the context of DCE-US exams that sometimes require the re-injection of the contrast agent. This study aimed to confirm that multiple injections had no significant impact on semi-quantitative and quantitative microvascularization parameters.

The second factor included different parameters. It was defined as the examination day to ensure no restriction of its meaning. Because melanoma cell lines exhibit a high doubling time of about 20 h[40-42], the examination day may be a source of variation. Thus, to analyze this second factor amounts to evaluating whether any morphological or functional modification of the tumor significantly interferes with the microvascularization parameters.

For logistic reasons, a total of 3 mice were evaluated over 4 d following a maximum of 4 contrast agent injections performed during the study (Table 1).

Size of the arterial ROI

Until now, no consensus has existed concerning the ideal location to select the AIF. In the literature, the need to find a compromise between the size of the arterial input and its location with regards to the tumor is often highlighted. Indeed, to avoid any partial volume effects which affect the ROI, the AIF must be extracted from an artery exhibiting a diameter larger than the intrinsic resolution of the functional imaging technique used[43,44]. On the other hand, an AIF measured too far from the tissue of interest causes additional delay and dispersion involving wrong estimation of quantitative parameters, in particular, an underestimation of the BF and an overestimation of MTT[8,44,45].

In the previous *in vivo* study, the arterial ROI was selected as close to the tumor as possible, whatever its size. In the second *in vivo* study (Table 1), the impact of the examination day on microvascularization parameters, giving preference in the selection of the arterial input to its size rather than its location, was evaluated.

Statistical analysis in vitro and in vivo

The aim of the first *in vitro* study was to determine whether there is an impact on the microvascularization parameters while repositioning the US probe during experiments. Statistical analysis was based on comparing the variances of both the series of 10 acquisitions with the US probe unchanged and replaced. To do so, a bilateral Fisher test was performed. It consisted of calculating:

$$F = \frac{s_1}{s_2}$$

where s_1 and s_2 are the variances of each of the series. The determined value of F was compared to the F-value with $(n_1 - 1)(n_2 - 1)$ degrees of freedom where n_1 and n_2 are the number of experiments performed in the two series of acquisitions ($n_1 = n_2 = 10$).

Results were significant for a P-value lower than 0.05.

The aim of the second *in vitro* study was to determine whether there was significant modification of the microvascularization parameters while the flow rate was modified. Thus, statistical analysis was based on comparing the means of microvascularization parameters for the three series of acquisitions. To do so, an analysis of variance (ANOVA) was performed between the 3 series of experimentations. Results were significant for a P-value lower than 0.05.

In vivo, statistical analyses were performed using the same multivariate ANOVA as the second *in vitro* study: the two parameters included in the process were the order of injection and the day of examination. Results were significant for P-value lower than 0.05.

RESULTS

In vitro

Repositioning of the US probe: *In vitro*, no microvascularization parameters, whether semi-quantitative or quantitative, were significantly correlated with the repositioning of the probe. Table 2 provides P-values associated with each of the microvascularization parameters.

Variation of the flow rate: No semi-quantitative microvascularization parameter was specific to the flow rate: none of the semi-quantitative parameters were correlated with the factor of interest. In addition, among the quantitative microvascularization parameter, only BF varied significantly with the flow rate: BF exhibited a P-value of 0.004. All the P-values are summarized in Table 2.

Table 2 *In vitro* and *in vivo* experiments: Statistical analyses

	In vitro results		*In vivo* results	
	Repositioning of the probe: Fisher's test *P* values	Variation of the flow rate: ANOVA *P* values	Multiple injections: ANOVA *P* values	Day of examination: ANOVA *P* values
Semi-quantitative microvascularization parameters				
PI	0.077	< 0.001	0.080	< 0.001
T_{PI}	0.302	0.004	0.595	0.641
Slope of the WI	0.059	0.006	0.141	< 0.001
MTT	0.562	< 0.001	0.885	0.016
AUC	0.731	< 0.001	0.073	0.01
AUWI	0.276	0.024	0.060	0.001
AUWO	0.860	0.006	0.078	0.016
Quantitative microvascularization parameters				
BF	0.055	0.004	0.071	0.116
BV	0.063	0.053	0.429	0.015
MTT	0.131	0.649	0.126	0.645

ANOVA: Analysis of variance; PI: Peak intensity; T_{PI}: Time to peak intensity; WI: The wash-in; MTT: The mean transit time; AUC: The area under the curve; AUWI: The area under the wash-in; AUWO: The area under the wash-out; BF: The tissue blood flow; BV: The tissue blood volume.

Table 3 Areas of the arterial region of interests associated with the two *in vivo* studies described in the article

	Mean (mm^2)	SD	Min	Max
First *in vivo* study	1.17	0.6	0.4	2.3
Second *in vivo* study	3.65	0.3	3.5	4.1

SD: Standard deviation.

Table 4 Influence of the size of the arterial region of interest (*in vivo* experiments: Statistical analyses)

	Day of examination : *P*-ANOVA values
Semi-quantitative microvascularization parameters	
PI	0.027
T_{PI}	0.010
Slope of the WI	0.070
MTT	< 0.001
AUC	0.808
AUWI	0.562
AUWO	0.832
Quantitative microvascularization parameters	
BF	< 0.001
BV	< 0.001
MTT	0.033

ANOVA: Analysis of variance; PI: Peak intensity; T_{PI}: Time to peak intensity; MTT: The mean transit time; AUC: The area under the curve; AUWI: The area under the wash-in; AUWO: The area under the wash-out; BF: The tissue blood flow; BV: The tissue blood volume.

In vivo

Multiple injections/day of examination: Multiple injections had no significant impact on the microvascularization parameters. Indeed, no parameter exhibited *P*-value lower than 0.05. All the *P*-values are summarized in Table 2.

On the other hand, to perform therapy evaluation, it is expected to obtain microvascularization parameters varying significantly with the tumor growth: any modification in microvascularization would be detected through the analysis of the microvascularization parameters. In the study, it was demonstrated that semi-quantitative microvascularization parameters were correlated with the tumor growth while among the quantitative microvascularization parameter, only the BV was.

Size of the arterial ROI

The impact of the size of the arterial ROI on microvascularization parameters was evaluated according to the same protocol used in the previous *in vivo* study.

It was demonstrated that for larger arterial ROIs (from 1.17 ± 0.6 mm^3 to 3.65 ± 0.3 mm^3) (Table 3), all quantitative microvascularization parameters were correlated with the tumor growth. Table 4 summarizes all of the *P*-values associated with this study.

DISCUSSION

In vitro, it was demonstrated that semi-quantitative and quantitative microvascularization parameters were not significantly correlated with the repositioning of the US probe before each acquisition. This is a promising result as in the context of therapy evaluation, the same target must be imaged during the entire treatment as evaluation is based on analyzing the microvascularization parameter evolution of a specific target through these exams. Results associated with the variation of the flow rates study were in agreement with the remarks mentioned before the experiments: all of the semi-quantitative microvascularization parameters were correlated with the flow rate while among the quantitative microvascularization parameters, only *BF* was specific to the flow rate.

In vivo, the importance of the size of the arterial ROI was shown through the first study: the arterial ROI must be large enough to allow the deconvolution process to be relevant in the context of therapy evaluation. This result is consistent with previous studies evaluating the importance of the arterial ROI selection[9]. In particular, the partial volume effect on the AIF and its consequences on analyses have been reported in the literature[46]. Here, the first results demonstrated significant correlation between

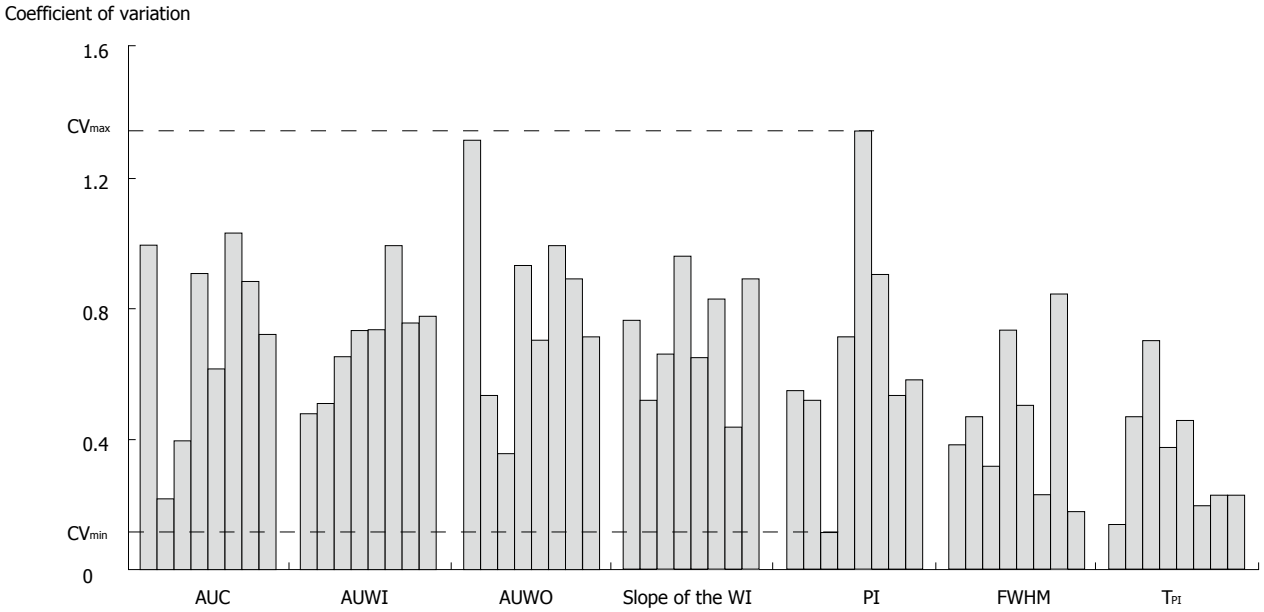

Figure 7 Display of the coefficients of variation, expressed as %, associated with the semi-quantitative microvascularization parameters extracted from the arterial region of interest. CV: Coefficient of variation; AUC: The area under the curve; WI: The wash-in; AUWI: The area under the wash-in; AUWO: The area under the wash-out; PI: Peak intensity; T_{PI}: Time to peak intensity; FWHM: The full width at half maximum.

semi-quantitative and quantitative microvascularization parameters except for T_{PI}, BF and MTT. In the context of experiments performed on mice, the T_{PI} and MTT were extremely short (in the order of a few seconds). Consequently, such low values make it difficult to distinguish modification in times linked to modification in microvascularization because of high statistical fluctuations. Previous studies showed the existing link between semi-quantitative microvascularization parameters and microvascularization quantitative ones. In particular, Lassen *et al*[47] pointed out that the BF was related to the time to peak parameter. Thus, the same explanation may justify the absence of significance concerning this parameter. Further investigations have been performed to better interpret these first results. Coefficients of variation associated with the semi-quantitative microvascularization parameters extracted from the arterial ROI were evaluated (Figure 7). This evaluation provided a mean CV value of 0.63% ± 0.28% which is high compared to previous intra-operator findings (< 30%)[27,48-53]. Such a result may be due to the very small arterial ROI prone to partial volume effects which induce noise in the deconvolution process, leading to the loss of correlation between quantitative microvascularization parameters and the tumor growth. Finally, the last experiments performed *in vivo* demonstrated significant correlation between quantitative microvascularization parameters and tumor growth for larger arterial ROIs. Identical results were obtained in the case of the semi-quantitative microvascularization parameters except for the areas where $P > 0.05$. One explanation may involve the high inter-subject variability noticed in the study. Thus, this high variability implies fluctuations in semi-quantitative microvascularization mean values that hide modifications in BV. On the other hand, as deconvolution allows freeing oneself from inter-subject variability, results associated with the quantitative microvascularization parameters were significant.

Study limitations

In vitro, both the fluid and the pipes used did not exhibit the same ultrasound properties as blood and vessels, respectively[54-56]. *In vivo,* quantification may have been difficult to perform because of the mouse's respiratory and cardiac movements which lead to instability in ROI locations. Another limitation involved the stability of the ultrasound contrast agent. Indeed, even if each experiment duration was less than 2 h on account of the stability of SonoVue® (6 h after its reconstitution as described by Schneider[14]), recent studies have reported a significant incidence of spontaneous gas diffusion phenomena on temporal evolution of contrast microbubble size[57-59]. This study did not take into account gas diffusion phenomena occurring for 2 h from initial formation of contrast agent. This assumption might have impacted the final results.

Further studies

The last *in vivo* study presented in the article was a preliminary study investigating the best selection of the arterial input. Further analysis must be performed to improve such a difficult selection. Indeed, Calamante *et al*[60] have demonstrated that an arterial ROI not selected directly at the entrance of the tumor may lead to an underestimation of the BF and an overestimation of the MTT. Such wrong estimations were due to the delay and dispersion occurring between the site of injection and the arterial ROI. On the other hand, it may sometimes be difficult to access an arterial ROI large enough and in the close vicinity of the tumor leading to partial volume effect influencing the results[16]. Thus, a trade-off between size and location of the arterial ROI must be determined.

Additional corrections to the deconvolution process may be required, as mentioned by van Osch *et al*[61], to ensure microvascularization parameters are accurately evaluated. Modeling of the AIF might also be necessary for the deconvolution process to be applicable in all cases [62]. Finally, a proof of concept may be interesting in evaluating the robustness of the deconvolution method in a clinical context: additional studies may be performed to definitely validate the deconvolution process.

Advantage of the quantitative evaluation

As already mentioned, the current DCE-US method does not take into account the arterial input, which greatly depends on patient physiological conditions as well as on which contrast agent is injected. Parameters determined according to the method are graphically extracted from the tumor TIC and if studies demonstrated correlation between some of them and the physiological parameters, absolute quantification is not possible through that method. On the other hand, the deconvolution process allows absolute quantification providing clinically meaningful microvascularization parameters.

In addition, results presented in the article support the possible use of the deconvolution method in a similar context to the current DCE-US, as the last *in vivo* study exhibited identical results whatever the quantification process applied.

In the study, sources of variation that impact the microvascularization parameters measured using DCE-US were evaluated, both taking and not taking into account the arterial input.

Throughout all of the experiments, two main conclusions can be drawn. First of all, it is necessary to pay attention to the selection of the arterial ROI as a small ROI may be at the origin of noise in the deconvolution method leading to its impossible use as a quantification tool. Finally, when the arterial ROI is large enough, deconvolution exhibits similar results as the current DCE-US. Such results suggest that the deconvolution method may be useful in a similar context with the advantage of providing absolute quantification of the microvascularization.

COMMENTS

Background

The early and functional evaluation of new treatments in oncology, such as anti-angiogenic therapies, is a main goal. Today, dynamic contrast-enhanced ultrasonography (DCE-US) is commonly recognized as a functional imaging technique. It is a highly available and sensitive modality which allows early predicting of the tumor response to treatments involving changes in microvascularity before any morphological ones occur.

Research frontiers

Microbubble contrast agents for DCE-US have developed over the past 10 years and are currently approved in Europe, Asia and Canada. As it provides real time imaging, is widely available, non-ionizing, and low cost, ultrasound imaging is recognized as an ideal modality for angiogenesis. Recently, a deconvolution method dedicated to DCE-US imaging was developed to take into account the arterial input function which provides an absolute evaluation of microvasculature parameters. In this study, the authors aim to evaluate the sources of variation influencing the microvascularization parameters measured using the routinely used DCE-US imaging method and the deconvolution method.

Innovations and breakthroughs

DCE-US is supported by the French National Cancer Institute which is currently studying the technique in several pathologies to establish the optimal microvascularization parameters and timing for quantitative anticancer efficacy assessments. This study firstly suggests the selection of the arterial region of interest (ROI) is important when using the deconvolution process, and secondly, when using the appropriate arterial ROI, analyses using deconvolution DCE-US and routine DCE-US exhibit similar results.

Applications

By comparing the deconvolution DCE-US and the routine DCE-US methods, this study may confirm the use of the deconvolution method in a similar context to the current routinely used DCE-US method. The deconvolution method exhibits the additional advantage of allowing absolute microvascularization quantification.

Terminology

DCE-US imaging involves the use of microbubble contrast agents and specialized imaging techniques to evaluate semi-quantitative microvascularization parameters. The deconvolution method is based on the Tikhonov regularization and aims to perform an absolute quantification of the microvascularization.

Peer review

This is part of an enthusiastic series of works, and is well organized. Other articles of the same authors are open. The end point of this study is clear: To evaluate the sources of variation influencing the microvascularization parameters measured by DCE-US. They performed an intensive experimental study using an *in vitro* and an *in vivo* model, and the results were clearly described. Even though a clinical situation may be further complicated, their study showed that their semi-quantitative microvascularization parameters might reflect reliable information of the nature of each parameter.

REFERENCES

1 **Lanza GM**, Caruthers SD, Winter PM, Hughes MS, Schmieder AH, Hu G, Wickline SA. Angiogenesis imaging with vascular-constrained particles: the why and how. *Eur J Nucl Med Mol Imaging* 2010; **37** Suppl 1: S114-S126

2 **Eisenbrey JR**, Forsberg F. Contrast-enhanced ultrasound for molecular imaging of angiogenesis. *Eur J Nucl Med Mol Imaging* 2010; **37** Suppl 1: S138-S146

3 **Kalva SP,** Namasivayam S, Vasuedo Sahani D. Imaging Angiogenesis. In: Teicher BA, Ellis LM, editors. Cancer Drug Discovery and Development: Antiangiogenic Agents in Cancer Therapy. Totowa, NJ: Humana Press, 2008: 189-203

4 **Lassau N,** Chami L, Pronneau P. Imagerie de contraste ultrasonore pour l'valuation prcoce des thrapeutiques cibles. In: Tranquart F, Correas JM, Bouakaz A, editors. Echographie de contraste. Paris: Springer, 2007: 81-86

5 **Miller JC**, Pien HH, Sahani D, Sorensen AG, Thrall JH. Imaging angiogenesis: applications and potential for drug development. *J Natl Cancer Inst* 2005; **97**: 172-187

6 **Therasse P**, Arbuck SG, Eisenhauer EA, Wanders J, Kaplan RS, Rubinstein L, Verweij J, Van Glabbeke M, van Oosterom AT, Christian MC, Gwyther SG. New guidelines to evaluate the response to treatment in solid tumors. European Organization for Research and Treatment of Cancer, National Cancer Institute of the United States, National Cancer Institute of Canada. *J Natl Cancer Inst* 2000; **92**: 205-216

7 **Eisenhauer EA**, Therasse P, Bogaerts J, Schwartz LH, Sargent D, Ford R, Dancey J, Arbuck S, Gwyther S, Mooney M, Rubinstein L, Shankar L, Dodd L, Kaplan R, Lacombe D, Verweij J. New response evaluation criteria in solid tumours: revised RECIST guideline (version 1.1). *Eur J Cancer* 2009; **45**: 228-247

8 **de Marco G,** Dassonvalle P, Henry-Feugeas MC, Onen F, Idy-Peretti I. Cerebral perfusion: dynamic suceptibility contrast MR imaging. Part 2: vascular models and data extraction. *Mdecine nuclaire* 2004; **28:** 35-48

9 **Lythgoe DJ**, Ostergaard L, William SC, Cluckie A, Buxton-Thomas M, Simmons A, Markus HS. Quantitative perfusion

imaging in carotid artery stenosis using dynamic susceptibility contrast-enhanced magnetic resonance imaging. *Magn Reson Imaging* 2000; **18**: 1-11
10 **Rumboldt Z**, Al-Okaili R, Deveikis JP. Perfusion CT for head and neck tumors: pilot study. *AJNR Am J Neuroradiol* 2005; **26**: 1178-1185
11 **Li PC**, Yeh CK, Wang SW. Time-intensity-based volumetric flow measurements: an in vitro study. *Ultrasound Med Biol* 2002; **28**: 349-358
12 **Gauthier M**, Tabarout F, Leguerney I, Polrot M, Pitre S, Peronneau P, Lassau N. Assessment of quantitative perfusion parameters by dynamic contrast-enhanced sonography using a deconvolution method: an in vitro and in vivo study. *J Ultrasound Med* 2012; **31**: 595-608
13 **Gauthier M,** Tabarout F, Leguerney I, Thalmensi J, Roche A, Lassau N. Assessment of quantitative tumor perfusion parameters by dynamic contrast-enhanced ultrasonography using a deconvolution method: an in vitro and in vivo study. *J Ultrasound Med* 2012; **31:** 595-608
14 **Schneider M**. Characteristics of SonoVuetrade mark. *Echocardiography* 1999; **16**: 743-746
15 **Greis C**. Technology overview: SonoVue (Bracco, Milan). *Eur Radiol* 2004; **14** Suppl 8: P11-P15
16 **Quaia E**, Calliada F, Bertolotto M, Rossi S, Garioni L, Rosa L, Pozzi-Mucelli R. Characterization of focal liver lesions with contrast-specific US modes and a sulfur hexafluoride-filled microbubble contrast agent: diagnostic performance and confidence. *Radiology* 2004; **232**: 420-430
17 **von Herbay A**, Vogt C, Willers R, Häussinger D. Real-time imaging with the sonographic contrast agent SonoVue: differentiation between benign and malignant hepatic lesions. *J Ultrasound Med* 2004; **23**: 1557-1568
18 **Hamilton WF,** Moore JW Kinsman MJ. Studies on the circulation: IV. Further analysis of the injection method, and of changes in hemodynamics under physiological and pathological conditions. *Am J Physiol* 1929; **99:** 534-551
19 **Kinsman MJ,** Moore JW Hamilton WF. Studies on the circulation: I. Injection methods: physical and mathematical considerations. *Am J Physiol* 1929; **89:** 322-330
20 **Mischi M,** Del Prete Z, Korsten HHM. Indicator dilution techniques in cardiovascular quantification. In: Leondes CT, editor. Biomechanical Systems Technology: Cardiovascular Systems. Singapore: World Scientific Publishing Company, 2007: 89-156
21 **Li PC**, Yang MJ. Transfer function analysis of ultrasonic time-intensity measurements. *Ultrasound Med Biol* 2003; **29**: 1493-1500
22 **Lampaskis M**, Averkiou M. Investigation of the relationship of nonlinear backscattered ultrasound intensity with microbubble concentration at low MI. *Ultrasound Med Biol* 2010; **36**: 306-312
23 **Burns PN**, Wilson SR, Simpson DH. Pulse inversion imaging of liver blood flow: improved method for characterizing focal masses with microbubble contrast. *Invest Radiol* 2000; **35**: 58-71
24 **Whittingham TA.** Contrast-specific imaging techniques: technical perspective. In: Quaia E, editor. Contrast media in ultrasonography: basic principles and clinical applications. Berlin, Heidelberg, New York: Springer, 2005: 43-70
25 **Verbeek XA**, Willigers JM, Prinzen FW, Peschar M, Ledoux LA, Hoeks AP. High-resolution functional imaging with ultrasound contrast agents based on RF processing in an in vivo kidney experiment. *Ultrasound Med Biol* 2001; **27**: 223-233
26 **Peronneau P**, Lassau N, Leguerney I, Roche A, Cosgrove D. Contrast ultrasonography: necessity of linear data processing for the quantification of tumor vascularization. *Ultraschall Med* 2010; **31**: 370-378
27 **Gauthier M**, Leguerney I, Thalmensi J, Chebil M, Parisot S, Peronneau P, Roche A, Lassau N. Estimation of intra-operator variability in perfusion parameter measurements using DCE-US. *World J Radiol* 2011; **3**: 70-81
28 **Lavisse S**, Lejeune P, Rouffiac V, Elie N, Bribes E, Demers B, Vrignaud P, Bissery MC, Brulé A, Koscielny S, Péronneau P, Lassau N. Early quantitative evaluation of a tumor vasculature disruptive agent AVE8062 using dynamic contrast-enhanced ultrasonography. *Invest Radiol* 2008; **43**: 100-111
29 **Xiong Z**, Cheng Z, Zhang X, Patel M, Wu JC, Gambhir SS, Chen X. Imaging chemically modified adenovirus for targeting tumors expressing integrin alphavbeta3 in living mice with mutant herpes simplex virus type 1 thymidine kinase PET reporter gene. *J Nucl Med* 2006; **47**: 130-139
30 **Calamante F**, Gadian DG, Connelly A. Delay and dispersion effects in dynamic susceptibility contrast MRI: simulations using singular value decomposition. *Magn Reson Med* 2000; **44**: 466-473
31 **Willats L**, Connelly A, Calamante F. Improved deconvolution of perfusion MRI data in the presence of bolus delay and dispersion. *Magn Reson Med* 2006; **56**: 146-156
32 **Lassau N**, Koscielny S, Albiges L, Chami L, Benatsou B, Chebil M, Roche A, Escudier BJ. Metastatic renal cell carcinoma treated with sunitinib: early evaluation of treatment response using dynamic contrast-enhanced ultrasonography. *Clin Cancer Res* 2010; **16**: 1216-1225
33 **Lassau N,** Koscielny S, Chebil M, Chami L, Bendjilali R, Roche A, Escudier B, Le Cesne A Soria J. Functional imaging using DCE-US: Which parameter for the early evaluation of antiangiogenic therapies [abstract]? *J Clin Oncol* 2009; **27 (**15 Suppl): 3524
34 **Lassau N,** Lacroix J, Aziza R, Vilgrain V, Taeb S Koscielny S. French Multicentric Prospective Evaluation of Dynamic Contrast-enhanced Ultrasound (DCE-US) for the Evaluation of Antiangiogenic Treatments. 95th Scientific Assembly and Annual Meeting; 2009 Nov29 - Dec 4, Mc Cormick Place, Chicago: Radiological Society of North America, 2009
35 **Ugolini P**, Delouche A, Herment A, Diebold B. In vitro flow quantification with contrast power Doppler imaging. *Ultrasound Med Biol* 2000; **26**: 113-120
36 **Thijssen JM**, de Korte CL. Modeling ultrasound contrast measurement of blood flow and perfusion in biological tissue. *Ultrasound Med Biol* 2005; **31**: 279-285
37 **Krix M**, Kiessling F, Farhan N, Schmidt K, Hoffend J, Delorme S. A multivessel model describing replenishment kinetics of ultrasound contrast agent for quantification of tissue perfusion. *Ultrasound Med Biol* 2003; **29**: 1421-1430
38 **Vicenzini E**, Delfini R, Magri F, Puccinelli F, Altieri M, Santoro A, Giannoni MF, Bozzao L, Di Piero V, Lenzi GL. Semiquantitative human cerebral perfusion assessment with ultrasound in brain space-occupying lesions: preliminary data. *J Ultrasound Med* 2008; **27**: 685-692
39 **Workman P**, Aboagye EO, Balkwill F, Balmain A, Bruder G, Chaplin DJ, Double JA, Everitt J, Farningham DA, Glennie MJ, Kelland LR, Robinson V, Stratford IJ, Tozer GM, Watson S, Wedge SR, Eccles SA. Guidelines for the welfare and use of animals in cancer research. *Br J Cancer* 2010; **102**: 1555-1577
40 **Kwee JK**, Mitidieri E, Affonso OR. Lowered superoxide dismutase in highly metastatic B16 melanoma cells. *Cancer Lett* 1991; **57**: 199-202
41 **Ohira T**, Ohe Y, Heike Y, Podack ER, Olsen KJ, Nishio K, Nishio M, Miyahara Y, Funayama Y, Ogasawara H. In vitro and in vivo growth of B16F10 melanoma cells transfected with interleukin-4 cDNA and gene therapy with the transfectant. *J Cancer Res Clin Oncol* 1994; **120**: 631-635
42 **Yerlikaya A**, Erin N. Differential sensitivity of breast cancer and melanoma cells to proteasome inhibitor Velcade. *Int J Mol Med* 2008; **22**: 817-823
43 **Lüdemann L**, Wust P, Gellermann J. Perfusion measurement using DCE-MRI: implications for hyperthermia. *Int J Hyperthermia* 2008; **24**: 91-96
44 **Calamante F**, Gadian DG, Connelly A. Quantification of perfusion using bolus tracking magnetic resonance imaging in

stroke: assumptions, limitations, and potential implications for clinical use. *Stroke* 2002; **33**: 1146-1151
45 **Duhamel G**, Schlaug G, Alsop DC. Measurement of arterial input functions for dynamic susceptibility contrast magnetic resonance imaging using echoplanar images: comparison of physical simulations with in vivo results. *Magn Reson Med* 2006; **55**: 514-523
46 **Hansen AE**, Pedersen H, Rostrup E, Larsson HB. Partial volume effect (PVE) on the arterial input function (AIF) in T1-weighted perfusion imaging and limitations of the multiplicative rescaling approach. *Magn Reson Med* 2009; **62**: 1055-1059
47 **Lassen N,** Perl W. Tracer Kinetic Methods in Medical Physiology. New York: Raven, 1979
48 **Cenic A**, Nabavi DG, Craen RA, Gelb AW, Lee TY. Dynamic CT measurement of cerebral blood flow: a validation study. *AJNR Am J Neuroradiol* 1999; **20**: 63-73
49 **Evelhoch JL**, LoRusso PM, He Z, DelProposto Z, Polin L, Corbett TH, Langmuir P, Wheeler C, Stone A, Leadbetter J, Ryan AJ, Blakey DC, Waterton JC. Magnetic resonance imaging measurements of the response of murine and human tumors to the vascular-targeting agent ZD6126. *Clin Cancer Res* 2004; **10**: 3650-3657
50 **Groves AM**, Goh V, Rajasekharan S, Kayani I, Endozo R, Dickson JC, Menezes LJ, Shastry M, Habib SB, Ell PJ, Hutton BF. CT coronary angiography: quantitative assessment of myocardial perfusion using test bolus data-initial experience. *Eur Radiol* 2008; **18**: 2155-2163
51 **Marcus CD**, Ladam-Marcus V, Cucu C, Bouché O, Lucas L, Hoeffel C. Imaging techniques to evaluate the response to treatment in oncology: current standards and perspectives. *Crit Rev Oncol Hematol* 2009; **72**: 217-238
52 **Morgan B**, Utting JF, Higginson A, Thomas AL, Steward WP, Horsfield MA. A simple, reproducible method for monitoring the treatment of tumours using dynamic contrast-enhanced MR imaging. *Br J Cancer* 2006; **94**: 1420-1427
53 **Ng CS**, Raunig DL, Jackson EF, Ashton EA, Kelcz F, Kim KB, Kurzrock R, McShane TM. Reproducibility of perfusion parameters in dynamic contrast-enhanced MRI of lung and liver tumors: effect on estimates of patient sample size in clinical trials and on individual patient responses. *AJR Am J Roentgenol* 2010; **194**: W134-W140
54 **Gupta LC,** Sahu UC. Diagnostic Ultrasound. New Delhi: Jaypee Brothers Publishers, 2007
55 **Hedrick W,** Hykes D Starchman D. Ultrasound physics and instrumentation. Saint-Louis, MO: Mosby, 1995
56 **Goldstein A,** Powis RL. Medical Ultrasonic Diagnostics. In: Papadakis P, editor. Ultrasonic Instruments and Devices: Reference for Modern Instrumentation, Techniques, and Technology. San Diego, CA: Academic Press, 1999: 46-193
57 **Sarkar K**, Katiyar A, Jain P. Growth and dissolution of an encapsulated contrast microbubble: effects of encapsulation permeability. *Ultrasound Med Biol* 2009; **35**: 1385-1396
58 **Kwan JJ**, Borden MA. Microbubble dissolution in a multigas environment. *Langmuir* 2010; **26**: 6542-6548
59 **Casciaro S**, Palmizio Errico R, Conversano F, Demitri C, Distante A. Experimental investigations of nonlinearities and destruction mechanisms of an experimental phospholipid-based ultrasound contrast agent. *Invest Radiol* 2007; **42**: 95-104
60 **Calamante F**. Bolus dispersion issues related to the quantification of perfusion MRI data. *J Magn Reson Imaging* 2005; **22**: 718-722
61 **van Osch MJ**, Vonken EJ, Bakker CJ, Viergever MA. Correcting partial volume artifacts of the arterial input function in quantitative cerebral perfusion MRI. *Magn Reson Med* 2001; **45**: 477-485
62 **Maxwell RJ**, Wilson J, Prise VE, Vojnovic B, Rustin GJ, Lodge MA, Tozer GM. Evaluation of the anti-vascular effects of combretastatin in rodent tumours by dynamic contrast enhanced MRI. *NMR Biomed* 2002; **15**: 89-98

S- Editor Cheng JX **L- Editor** Logan S **E- Editor** Xiong L

World Journal of Radiology

Online Submissions: http://www.wjgnet.com/esps/
wjr@wjgnet.com
doi:10.4329/wjr.v4.i7.302

World J Radiol 2012 July 28; 4(7): 302-310
ISSN 1949-8470 (online)

ORIGINAL ARTICLE

Diffusion-weighted MRI in a liver protocol: Its role in focal lesion detection

Stefano Palmucci, Letizia Antonella Mauro, Martina Messina, Brunella Russo, Giovanni Failla, Pietro Milone, Massimiliano Berretta, Giovanni Carlo Ettorre

Stefano Palmucci, Letizia Antonella Mauro, Martina Messina, Brunella Russo, Giovanni Failla, Pietro Milone, Giovanni Carlo Ettorre, Radiodiagnostic and Oncological Radiotherapy Unit, University Hospital "Policlinico-Vittorio Emanuele", 95123 Catania, Italy

Massimiliano Berretta, Department of Medical Oncology, National Cancer Institute, 33081 Aviano (PN), Italy

Author contributions: Palmucci S, Messina M and Russo B planned the research, performed the study and analyzed the data; Ettorre GC approved the research; Milone P provided some magnetic resonance imaging studies; Palmucci S and Berretta M were involved in the collection of clinical data; Palmucci S and Failla G critically revised the data; Palmucci S wrote the paper, assisted by Russo B and Messina M; and Mauro LA corrected the manuscript.

Correspondence to: Stefano Palmucci, MD, Radiodiagnostic and Oncological Radiotherapy Unit, University Hospital "Policlinico-Vittorio Emanuele", 95123 Catania, Italy. spalmucci@sirm.org
Telephone: +39-95-3782360 Fax: +39-95-3782360

Received: September 8, 2011 Revised: February 21, 2012
Accepted: March 1, 2012
Published online: July 28, 2012

Abstract

AIM: To evaluate the role of diffusion-weighted imaging (DWI) in the detection of focal liver lesions (FLLs), using a conventional magnetic resonance imaging (MRI) protocol.

METHODS: Fifty-two patients (22 males, average age 55.6 years, range: 25-82 years), studied using a 1.5 Tesla magnetic resonance scanner, were retrospectively analyzed; detection of FLLs was evaluated by considering the number of lesions observed with the following sequences: (1) respiratory-triggered diffusion-weighted single-shot echo-planar (DW SS-EP) sequences; (2) fat-suppressed fast spin-echo (fs-FSE) T2 weighted sequences; (3) steady-state free precession (SSFP) images; and (4) dynamic triphasic gadolinium-enhanced images, acquired with three-dimensional fast spoiled gradient-echo (3D FSPGR). Two radiologists independently reviewed the images: they were blinded to their respective reports. DW SS-EP sequences were compared to fs-FSE, SSFP and dynamic gadolinium-enhanced acquisitions using a *t*-test. Pairs were compared for the detection of: (1) all FLLs; (2) benign FLLs; (3) malignant FLLs; (4) metastases; and (5) hepatocellular carcinoma (HCC).

RESULTS: Interobserver agreement was very good (weighted κ = 0.926, CI = 0.880-0.971); on the consensus reading, 277 FLLs were detected. In the comparison with fs-FSE, DW SS-EP sequences had a significantly higher score in the detection of all FLLs, benign FLLs, malignant FLLs and metastases; no statistical difference was observed in the detection of hepatocellular carcinoma (HCCs). In the comparison with SSFP sequences, DW SS-EP had significantly higher scores ($P < 0.05$) in the detection of all lesions, benign lesions, malignant lesions, metastases and HCC. All FLLs were better detected by dynamic 3D FSGR enhanced acquisition, with $P = 0.0023$ for reader 1 and $P = 0.0086$ for reader 2 in the comparison with DW SS-EP sequences; with reference to benign FLLs, DW SS-EP showed lower values than 3D FSPGR enhanced acquisition ($P < 0.05$). No statistical differences were observed in the detection of malignant lesions and metastases; considering HCCs, a very slight difference was reported by reader 1 ($P = 0.049$), whereas no difference was found by reader 2 ($P = 0.06$).

CONCLUSION: In lesion detection, DWI had higher scores than T2 sequences; considering malignant FLLs, no statistical difference was observed between DWI and dynamic gadolinium images.

Key words: Diffusion weighted magnetic resonance imaging; Liver; Liver disease; Magnetic resonance imaging

Peer reviewers: Roberto Miraglia, MD, Department of Diagnostic and Interventional Radiology, Mediterranean Institute for Transplantation and Advanced Specialized Therapies (IsMeTT), Via Tricomi 1, 90100 Palermo, Italy; Yasunori Minami, MD, PhD, Division of Gastroenterology and Hepatology, Department of Internal Medicine, 377-2 Ohno-higashi, Osaka-sayama, Osaka 589-8511, Japan; Yicheng Ni, MD, PhD, Professor, Biomedical Imaging, Interventional Therapy and Contrast Media Research, Department of Radiology, University Hospitals, KU Leuven, Herestraat 49, B-3000 Leuven, Belgium

Palmucci S, Mauro LA, Messina M, Russo B, Failla G, Milone P, Berretta M, Ettorre GC. Diffusion-weighted MRI in a liver protocol: Its role in focal lesion detection. *World J Radiol* 2012; 4(7): 302-310 Available from: URL: http://www.wjgnet.com/1949-8470/full/v4/i7/302.htm DOI: http://dx.doi.org/10.4329/wjr.v4.i7.302

INTRODUCTION

In the past twenty years, several magnetic resonance imaging (MRI) diagnostic techniques have gradually been introduced in the study of focal liver lesions (FLLs), increasing to the greatest possible extent the high contrast resolution inherent in the method. For instance, long echo-time T2 weighted sequences are widely used to characterize fluid-filled cystic lesions or hemangiomas; fat-containing lesions (adenomas, atypical focal nodular hyperplasia) can be diagnosed in cases of signal decay in out-of-phase T1-weighted spoiled gradient echo sequences[1]. More recently a gradual introduction of new hepato-specific agents - gadolinium-ethoxybenzyl-diethylenetriamine pentaacetic acid (Gd-EOB-DTPA, Primovist, Bayer Schering) and gadopentate dimeglumine (Gd-BOPTA, Multihance, Bracco Imaging) has significantly increased the diagnostic potential of MRI, especially in the preoperative management of patients with liver metastases[2,3]. In addition, three-dimensional gradient echo imaging allows a dynamic study of the liver, evaluating the behavior of FLLs in the arterial and portal phase after contrast administration[4]. In view of these considerations, non-invasive characterization of FLLs is a current diagnostic challenge.

The introduction of diffusion weighted imaging (DWI) in liver MRI fuelled high expectations with several encouraging studies[5-7]. High values of *b* - required for characterization - cannot be used to identify FLLs. It has been shown that the use of diffusion weighted single-shot echo-planar (DW SS-EP) sequences with a low *b*-value is important for the detection of hepatic lesions, especially for small-sized lesions. The acquisition of "black blood" images with DW SS-EP sequences makes it possible to easily differentiate vessels from focal small-sized lesions in the liver[8,9]. Parallel techniques reduce artifacts, such as "blurring" or magnetic susceptibility artifacts, increasing the signal-to-noise ratio (SNR)[10,11]; moreover, respiratory-triggered sequences offer a better possibility of SNR compared to breath-hold techniques[12]. Many studies have recently started to compare DWI to T1-weighted acquisition in the detection and characterization of liver lesions[13-15].

In diffusion imaging of the liver, the first difficulty concerns the choice of the appropriate *b*-value, which means the degree of weighting in diffusion. High b-values cannot be used because of the low SNR they determine: for these reasons, in this study we retrospectively evaluated the ability to detect lesions using relatively low *b*-value DWI (*b*-values extended from $b = 0\text{-}10$ to $b = 0\text{-}500$) in a routine liver MRI protocol. The characterization of FLLs was not considered in our work, because the role of DWI in this regard has already been widely debated in previous studies[5,15], and seems to be limited by overlapping[16].

In the detection of FLLs, diffusion weighted sequences were compared to fat suppressed fast spin-echo (fs-FSE) T2-weighted sequences, steady state free-precession (SSFP) sequences and dynamic triphasic gadolinium-enhanced acquisition, acquired with 3D fast spoiled gradient echo (FSPGR), emphasizing their advantages and limits.

MATERIALS AND METHODS

Patients and lesions

The study included 70 patients with a liver MRI study, performed on the basis of a clinical suspicion of FLL and/or for a morphological suspicion of FLL derived from a previous diagnostic exam (computed tomography or ultrasonography). In the revision analysis, the following exclusion criteria were adopted: (1) diffuse or "miliary" involvement of liver parenchyma (2 patients); (2) sequences with image quality damaged by artifacts, not included in the analysis (5 patients); and (3) incomplete liver MRI study (11 patients).

We retrospectively evaluated a total of 52 patients (22 males, 30 females, average age 55.6 years, range: 25-82 years), studied from November 2009 to February 2011. For detection and characterization of FLLs, the standard of reference in our study was based on: (1) the presence of previous diagnostic examinations and/or the follow-up; (2) the presence of the typical radiological pattern; and (3) the histopathology. On the consensus reading, 277 FLLs were detected: 135 of them were benign lesions, whereas 142 were malignant; the number of metastases and hepatocellular carcinomas (HCCs) observed were 114 and 28, respectively. Metastases were reported in 12 patients, whereas HCCs were found in 8 patients (Table 1).

The benign lesions detected were as follows: 44 hemangiomas were found in 14 patients, 77 cysts in 17 patients and 14 focal nodular hyperplasias (FNHs) in 9 patients (Table 1).

The diagnosis of cysts was made for hyperintense lesions in T2-weighted images, even with long echo-time, without any enhancement during contrast administration. The diagnosis of hemangioma was established as follows: (1) typical MRI findings of cavernous hemangiomas, represented by signal hyperintensity in T2-weighted images - even with long echo-time - and globular centripetal

Table 1 Patients and lesions

Total number of patients	52
Age (yr)	55.6
Gender	30 females, 22 males
FLLs distribution	
Patients with benign FLLs	35
Patients with hemangiomas	14
Patients with cysts	17
Patients with FNHs	9
Patients with malignant FLLs	20
Patients with metastases	12
Patients affected by breast cancer	1
Patients affected by colo-rectal cancer	9
Patients affected by melanoma	1
Patients affected by pancreatic cancrer	1
Patients with HCCs	8

Characteristics of the patients included in our study. The distribution of benign and malignant focal liver lesions (FLLs) among the patients is also reported, according to the different categories of lesions observed. HCC: Hepatocellular carcinoma.

enhancement during contrast administration[17,18]; and (2) typical behavior of capillary hemangiomas or high-flow related hemangiomas, with a hypervascular pattern on arterial phase and slight signal hyperintensity or isointensity in the delayed equilibrium phase[17,18]. In addition, the stability of lesion size was detected on serial cross-sectional imaging studies obtained from our archive or acquired with a mean follow-up of 8 mo.

The diagnosis of FNH was determined by histopathology in only one patient; the remaining FNHs were defined considering the following features: (1) a hypervascular aspect in MRI images during the arterial phase after contrast administration; (2) retention of hepato-specific contrast on delayed images (20 min after Gd-EOB-DTPA and 120 min after Gd-BOPTA); and (3) presence of a central scar, observed in cases of typical FNH. The uptake of hepato-specific contrast in the hepatobiliary phase and the absence of estrogen exposure were adopted as criteria to differentiate FNHs from adenomas. The diagnosis was also validated by the size stability of the lesions on serial cross-sectional imaging studies during follow-up (mean time of 9 mo and 24 d).

The diagnosis of HCC was determined by histopathology in 6 patients; in the remaining cases the presence of HCC was established on the basis of the typical imaging features (enhancement on the arterial phase, rapid wash-out and pseudocapsule on the delayed phase), according to clinical tests and a biomarker (increased serum levels of alpha-fetoprotein).

Metastatic malignant lesions were confirmed by biopsy in 6 patients; the remaining metastases were confirmed by diagnostic imaging features (target appearance for colic metastases) and by their enlarged size, which was evident after a mean follow-up time of 123.4 d (90 d was the shortest follow-up, 174 was the longest). The primary sites of metastases included breast carcinoma (n = 1), colorectal carcinoma (n = 9), melanoma (n = 1) and pancreatic carcinoma (n = 1).

Imaging protocol

The exams were performed using a 1.5 Tesla Magnetic Resonance (General Electric, Signa HDxt); an eight-channel phased-array coil was used for acquisition of liver images. Synchronization with patients' breath was achieved by placing a "respiratory" belt around their abdomen.

The study protocol included: (1) axial breath-hold FSPGR T1-weighted, with the following parameters: TR = 180 ms, TE = 2.2-4.4 ms (in and out of phase); flip angle 80; thickness = 6 mm; spacing = 1 mm; acquisition matrix = 256 × 224; number of averages = 1; acquisition type = 2D; (2) axial breath-hold SSFP - Fiesta - TR = 4.0 ms; TE = 1.7 ms; thickness = 6 mm; spacing = 1 mm; flip angle = 75; acquisition matrix = 256 × 224; number of averages = 1; acquisition type = 2D; and (3) axial breath-hold fs-FSE T2-weighted - spatial fat saturation; TR = 2100 ms; TE > 100 ms; thickness = 6 mm; spacing = 1 mm, flip angle = 90; acquisition matrix = 256 × 224; number of averages = 1; acquisition type = 2D.

DWI was acquired using a respiratory-triggered SS-EP technique with several b values (0-10/0-40/0-150/0-300/0-500); images obtained with b = 10 and b = 40 were also included in the evaluation and in the comparison with the other sequences.

Diffusion sequences were performed with the following parameters: TR = 1R-R, TE = 40 ms, EPI factor = 80, slice thickness = 6 mm, gap = 1 mm, flip angle = 90, acceleration factor = 2, FOV 32-44 cm, NSA = 2, acquisition time 39 s, half scan-factor = 2, band-width = 250 KHz, scan percentage = 100%, acquisition voxel = N/A, reconstruction voxel = N/A, acquisition matrix 192 × 160, reconstruction matrix = 256 × 256, spatial fat saturation = Yes - Water Excitation, isotropic motion gradient = SI, RL and AP with the Stejskal-Tanner Diffusion scheme.

All examinations included a dynamic multiphase 3D FSPGR T1-weighted sequence, acquired before and after a hepato-specific-gadolinium contrast agent (Gd-BOPTA 0.1 mmol/kg, Multihance 0.5 mol, Bracco Imaging, Italy or Gd-EOB-DTPA 25 μmol/kg - 0.1 mL/kg - Bayer Schering, Germany). Three-dimensional FSPGR sequences were acquired with the following parameters: TR = 4.2 ms; TE = 2.0 ms; thickness = 3 mm; flip angle = 12; acquisition matrix = 320 × 192; acquisition type = 3D. A dynamic multiphase hepatic acquisition (arterial, portal and delayed phases) was carried out using the smart prep system; when necessary, some studies were also completed with a delayed hepato-specific phase, acquired 20 min after Gd-EOB-DTPA, and 120 min after Gd-BOPTA administration. The contrast medium was administered by a MedRad double testis injector with a contrast injection rate of 2 mL/s for Gd-BOPTA and 1 mL/s for Gd-EOB-DTPA. In all patients an immediate bolus of physiological saline was injected after the contrast agent.

Detection of FLLs

Detection of FLLs was evaluated considering the number of liver lesions observed with different sequences: (1)

Table 2 Detection rate

	Tri-Gd T1	SSFP	fs-FSE	DWI	Consensus
All FLLs					277
Reader 1	266 (96)	161 (58)	187 (68)	234 (84)	
Reader 2	256 (92)	185 (67)	185 (67)	222 (80)	
Mean	261 (84)	186 (67)	186 (67)	228 (82)	
Benignant					135
Reader 1	134 (99)	89 (66)	89 (66)	116 (86)	
Reader 2	127 (94)	88 (65)	88 (65)	105 (78)	
Mean	130.5 (97)	88.5 (66)	88.5 (66)	110.5 (82)	
Malignant					142
Reader 1	132 (93)	99 (70)	99 (70)	118 (83)	
Reader 2	129 (91)	97 (68)	97 (68)	114 (80)	
Mean	130.5 (92)	98 (69)	98 (69)	116 (82)	
Metastases					114
Reader 1	104 (91)	82 (72)	82 (72)	100 (88)	
Reader 2	101 (89)	79 (69)	79 (69)	97 (85)	
Mean	102.5 (90)	80.5 (71)	80.5 (71)	98.5 (86)	
HCC					28
Reader 1	28 (100)	17 (60)	17 (60)	18 (64)	
Reader 2	28 (100)	18 (64)	18 (64)	17 (60)	
Mean	28 (100)	17.5 (62)	17.5 (62)	17.5 (62)	

Detection rate observed by triphasic gadolinium-enhanced T1 sequences (Tri-Gd T1), steady-state free precession (SSFP), fat-suppressed fast spin-echo (fs-FSE) and diffusion-weighted imaging (DWI) sequences. The values are divided according to the different categories of lesions analyzed in the study. HCC: Hepatocellular carcinoma; FLLs: Focal liver lesions.

respiratory-triggered DW SS-EP; (2) fs-FSE T2 weighted sequences with long TE (> 100 ms); (3) SSFP images; and (4) dynamic triphasic gadolinium-enhanced acquisition, acquired with multiphase 3D FSPGR T1-weighted sequences.

Location and size (maximum axial diameter) were reported for each lesion.

The measurements were carried out by two radiologists with more than two years of experience in body MRI. Radiologists reviewed images independently; sequences were randomized. The following pairs were compared in the number of FLLs detected: (1) DW SS-EP sequences *vs* fs-FSE; (2) DW SS-EP sequences *vs* SSFP; and (3) DW SS-EP sequences *vs* dynamic gadolinium-enhanced acquisition.

In the detection of lesions, these compared pairs were studied for: (1) all FLLs; (2) benign FLLs; (3) malignant FLLs; (4) metastases; and (5) HCC.

The number of FLLs was finally confirmed by viewing: (1) all sequences performed in the MR examination, including unenhanced T1 sequences, conventional T2 sequences, DWI sequences and enhanced 3D FSPGR acquisitions; when available, the hepato-specific phase was also considered to validate the number of lesions; and (2) previous or subsequent MR examinations; patient history was also considered to assess the number of lesions, in patients who underwent surgical intervention or biopsy.

Statistical analysis

A statistical analysis was performed using Win-Stat Software and a MedCalc program (MedCalc® version 11.4.4.0., MedCalc Software bvba). Interobserver agreement was evaluated for both radiologists involved in the detection analysis, by calculating the simple κ coefficient. The k-value was interpreted according to the following classification: < 0.20 poor; 0.20-0-40 fair; 0.41-0.60 moderate; 0.61-0.80 good; 0.81-1.00 very good. For the different classes of FLLs (all lesions, benign lesions, malignant lesions, metastases, HCCs) the detection rate was calculated as: the number of lesions observed/total number provided by consensus reading for each category. The number of lesions observed with conventional T2 sequences (fs-FSE), SSFP sequences, respiratory-triggered DW SS-EP sequences (acquired from b = 0-10 to b = 0-500 values) and 3D FSPGR post-gadolinium acquisitions were compared using a paired samples t-test.

RESULTS

Interobserver agreement was very good (weighted κ = 0.923, CI = 0.873-0.972). Detection rates for all FLLs, benign lesions, malignant lesions, metastases and HCC are shown in Table 2.

DW SS-EP sequences vs fs-FSE

DW SS-EP sequences showed a higher score when compared with conventional breath-hold T2-weighted sequence fs-FSE, with P = 0.001 for reader 1 and P = 0.0019 for reader 2 (Figure 1A). Considering benign FLLs (Figure 1B), DW SS-EP sequences showed higher values than fs-FSE sequences (P = 0.00 017 for reader 1 and P = 0.01 for reader 2) and SSFP sequences (P = 0.00 013 for reader 1 and P = 0.02 for reader 2); in the evaluation of malignant lesions (Figure 1C), DW SS-EP showed higher scores than fs-FSE only for reader 1 (P = 0.023), whereas no statistical difference was observed by reader 2 (P = 0.053). In the detection of metastases (Figure 1D), a significant statistical difference was observed for both readers, with P = 0.026 for both readers; no statistical difference was found in the detection of HCC (Figure 1E).

DW SS-EP sequences vs SSFP

With reference to all FLLs (Figure 1A), DW SS-EP sequences showed the highest score compared with SSFP sequences, with P = 0.001 for reader 1 and P = 0.00 035 for reader 2. The number of benign FLLs (Figure 1B) detected by DW SS-EP sequences was significantly higher, with P = 0.00 013 and P = 0.02 for reader 1 and reader 2, respectively.

DW SS-EP sequences also had higher scores in evaluating malignant lesions, metastases and HCC (Figure 1C-E), with significant P values (P < 0.05); in fact, the mean percentage of metastases detected by DW SS-EP was 86.4%, whereas the value observed using fs-FSE was 70%; also in the detection of HCCs, diffusion sequences were slightly superior to fs-FSE images.

DW SS-EP sequences vs dynamic 3D FSPGR gadolinium-enhanced acquisition

All FLLs were better detected by dynamic 3D FSPGR enhanced acquisition, with P = 0.0023 for reader 1 and P

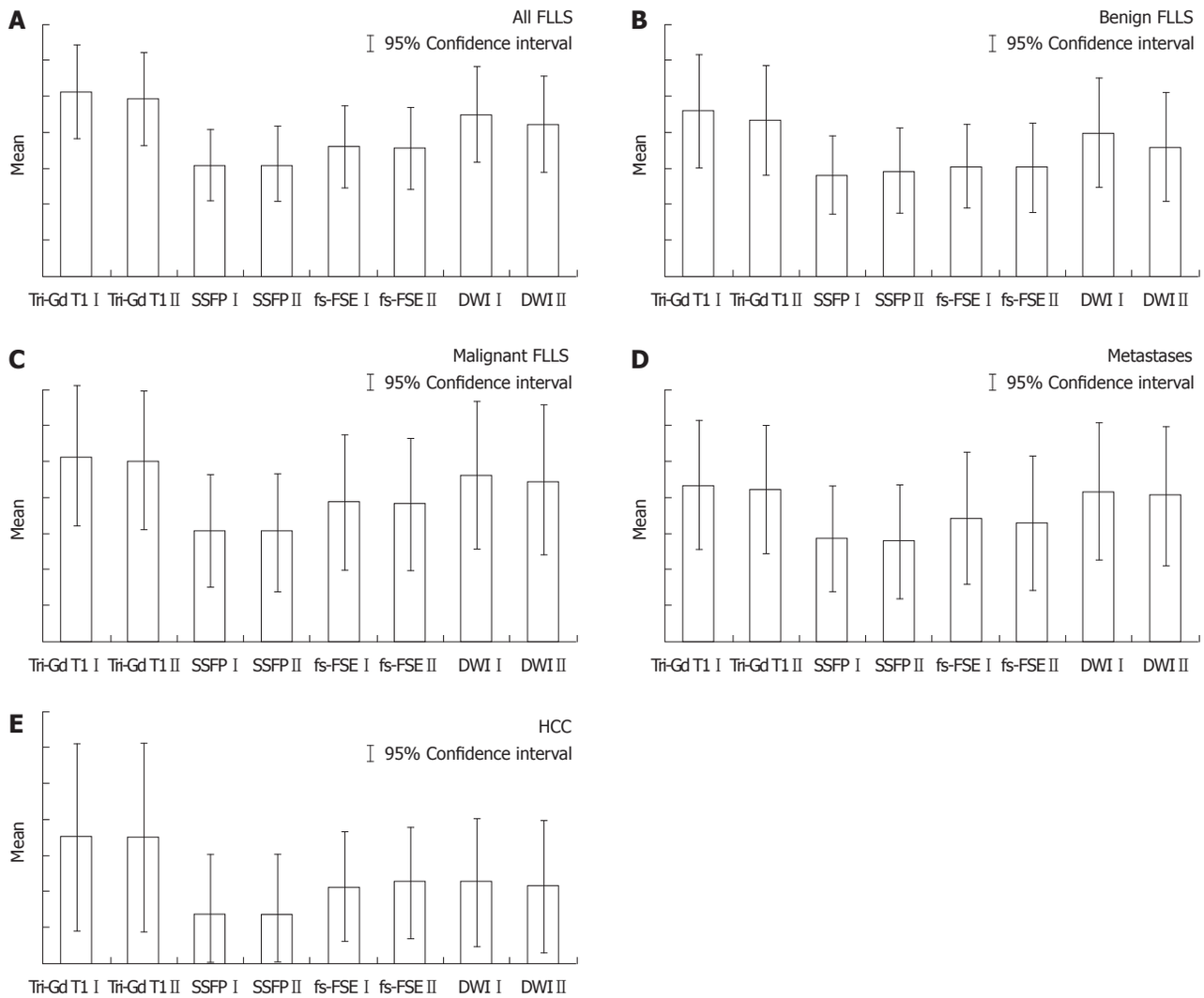

Figure 1 Histograms comparing the different sequences (A-E). Histograms showing the comparison between the mean values of lesions detected among different sequences, for the classes of focal liver lesions (FLLs) [all lesions, benign lesions, malignant lesions, metastases, hepatocellular carcinomas (HCCs)]. I = reader 1; II = reader 2; Tri-Gd T1: Triphasic gadolinium T1-weighted sequence; fs-FSE: Fat suppressed fast spin-echo sequence; SSFP: Steady state free precession; DWI: Diffusion weighted imaging.

= 0.0086 for reader 2 in the comparison with DW SS-EP sequences (Figure 1A).

In the detection of benign FLLs (Figure 1B), DW SS-EP had lower values than 3D FSPGR enhanced acquisition, with $P = 0.011$ and $P = 0.012$ (reader 1 and 2, respectively); in fact - with reference to the detection of benign lesions - reader 1 identified 116/135 of these lesions, whereas reader 2 had a lower score - 105/135; dynamic gadolinium-enhanced acquisitions identified 134 and 127 lesions (reader 1 and reader 2, respectively); mean detection rate was 81.8% for DWI and 96.6% for dynamic enhanced gadolinium T1 weighted FSPGR acquisition.

No statistical differences (Figure 1C-E) were observed by the readers in the detection of malignant lesions ($P = 0.09$ and $P = 0.07$). Detection rates of malignant lesions by diffusion sequences were 83% for reader 1 and 80% for reader 2, whereas enhanced gadolinium 3D FSPGR had higher values - 92.9% and 90.8%, respectively.

With regard to metastases, gadolinium-enhanced 3D FSPGR had a mean score of 102.5 for metastases identified, whereas DWI detected 98.5 metastatic lesions, with a detection rate of 89.9% and 86.4%, respectively; comparing the mean values of metastases observed through the paired samples *t*-test, no statistical difference was found ($P = 0.52$ and $P = 0.56$).

With regard to HCCs, a very slight difference was reported by reader 1 ($P = 0.049$), whereas no difference was found by reader 2 ($P = 0.06$); in our results, diffusion images allowed the identification of 17 and 18 lesions for reader 1 and for reader 2, respectively, with a mean detection rate of 17.5 lesions (62.5%), whereas all HCCs were correctly identified by 3D FSPGR images.

DISCUSSION

In recent years, some studies have emphasized the role of DWI in the characterization and detection of FLLs[5-7,9-12,19-21].

Furthermore, DWI could provide an additional tool in oncological patients, where a correct assessment of the number and localization of FLLs is essential in choosing suitable treatment. In fact, DWI provides better detection of FLLs than other T2-conventional sequences, and our results confirm what has recently been published in the literature. For instance, in a previous study by Bruegel *et al*[10], the sensitivity of DWI was higher than standard breath-hold and respiratory-triggered T2 weighted sequences in the diagnosis of 66 small hepatic metastatic lesions (sensitivity value of 0.85 and 0.26-0.44, respectively)[10]. In a study by Holzapfel *et al*[21], the detection of small FLLs seemed to be significantly increased by respiratory-triggered diffusion sequences, which produced better image quality because of high spatial resolution and an adequate SNR[22]. In the detection of metastases, when DWI was compared to fs-FSE sequences and to SSFP, we found a significantly higher number of lesions identified by both readers using DWI; the highest detection rate - shown by DWI in the detection of FLLs - was probably due to the 'black blood effect' of diffusion-weighted images: this property makes it easier to distinguish small FLLs from hepatic vessels, which may determine false-positive pseudolesions on T2-weighted turbo spin-echo images.

In view of its capability to detect FLLs, DWI has been widely introduced in liver imaging, and many studies have recently emphasized its additional values in liver imaging in order to detect malignant FLLs[13-15]. In this regard, a routine MRI protocol should ideally use all possible strategies, including many un-enhanced scans: in and out-of-phase T1-weighted sequences, T2-weighted FSE sequences - even with spatial fat saturation or different echo-time, white-blood sequences for morphologic assessment of liver anatomy such as steady-state sequences, and SSFSE sequences to emphasize T2-content; dynamic multiphase gadolinium-enhanced acquisitions are necessary to subsequently evaluate FLLs and to study their behavior in the arterial, portal and late phases. For this reason, the role of DWI in a liver MRI protocol should be assessed comparing the diffusion sequences not only to the conventional T2 sequences, but it must also include the dynamic enhanced gadolinium acquisitions.

In a study by Löwenthal *et al*[15] - considering only the detection of benign FLLs - a statistical difference in the comparison between DWI and hepatobiliary phase (MR-late) Gd-EOB-DTPA-enhanced images was reported; no difference was observed between DWI and dynamic (MR-dyn) Gd-EOB-DTPA-enhanced images, unlike the data reported in our comparison. This may be explained by the fact that DWI is less reliable than dynamic enhanced gadolinium FSPGR acquisitions, being much more sensitive to magnetic susceptibility artifacts. For instance, in our study, 6 cases of FNHs were missed by both readers evaluating only the diffusion-weighted images, probably due to their location in the parenchyma of the left lobe, near the gastric area: in this area DWI (Figure 2) could be affected by magnetic susceptibility or motion artifacts related to cardiac and gastric wall.

On analyzing the comparison using the *t*-test, no statistical difference between the number of lesions identified by DWI and dynamic enhanced gadolinium acquisition was observed, and DWI could be considered a valid diagnostic tool in the detection of malignant lesions in a liver study, even if they are characterized by a lower sensitivity in comparison to the dynamic acquisition. The high detection rate using DWI is especially observed in the evaluation of metastases, as confirmed in other studies[14]. The good results obtained using DWI in our study may be explained by the application of respiratory triggering, which produced better image quality because of high spatial resolution and an adequate SNR[12]; use of the respiratory-triggered modality in the diffusion images increases the spatial resolution, but requires a longer time for the acquisition. In addition, the use of low b-value diffusion sequences, acquired by parallel techniques, reduces artifacts such as "blurring" or magnetic susceptibility artifacts, increasing the SNR[10,11].

In a recent study by Kenis *et al*[13], DWI was used in the staging of oncological disease in patients with impaired renal function; in this study, MR showed a significant additional capability in the detection of metastases when considering DWI and gadolinium MRI together[13]. Kenis *et al*[13] analyzed three image sets: unenhanced T1 and T2 acquisitions/gadolinium-enhanced T1, DWI and a combination set; all observers reported high sensitivity values using the combination set of images; as a consequence, diagnostic accuracy increased significantly when DWI was added to Gd-MRI.

DWI is limited in the detection of HCC, with a mean detection rate (62.5%) lower than 3D FSPGR enhanced images (100%). Five HCC lesions missed by both readers were located in a subdiaphragmatic liver segment close to the heart or gastric wall (Figure 3): again, the lower diagnostic accuracy of DWI was probably related to the presence of magnetic susceptibility or motion artifacts in these locations, and even if the introduction of triggered-acquisition increased their image quality, we suggest that the evaluation of these areas could be limited. Similarly, magnetic susceptibility artifacts caused by colonic loop - often located very close to the caudal portion of the right liver - reduces imaging quality on diffusion images, with low signal intensity of parenchyma and loss of liver profile: one metastasis missed by both readers was located in the caudal portion of the IV segment, near to the colonic wall (Figure 4). In addition, lower scores obtained with DWI in our study - regarding the detection of HCCs - may also be explained by the different signal intensity observed in these lesions: in fact, in a recent study by Kim *et al*[14] they were isointense or hyperintense to the liver[14]. In a cirrhotic liver, HCCs may show the same signal intensity as the surrounding parenchyma, involved in a chronic fibrotic process, and as a consequence the detection and characterization of HCCs may be difficult[14].

Although some artifacts may affect the imaging quality of diffusion images, the highest detection rate observed in a liver MRI protocol suggest that they can easily help radiologists in the detection of FLLs, and in particular,

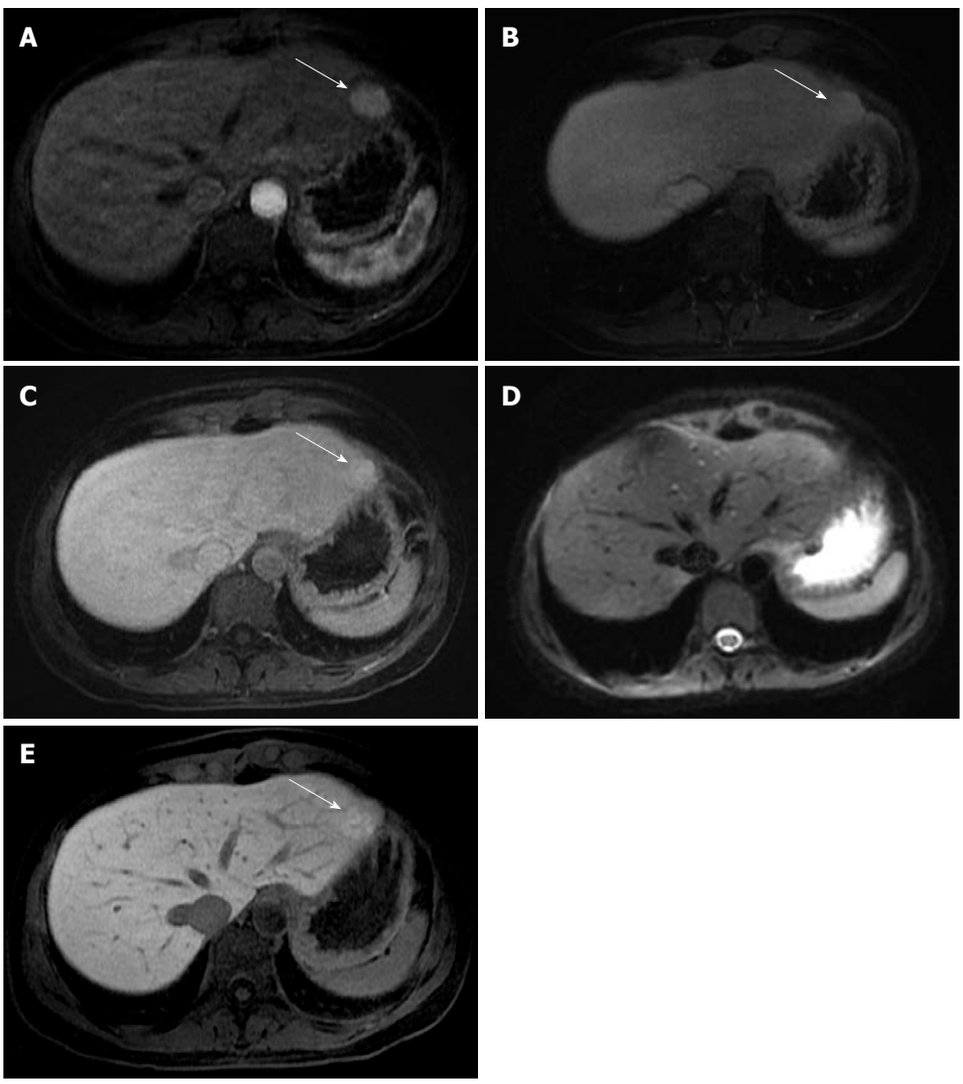

Figure 2 Focal nodular hyperplasia found in the left liver lobe. A: A round-shaped solid lesion (arrow) is depicted in the left liver lobe (in the Ⅱ segment); B, C: The lesion (arrow) appears homogeneously hyperintense in the arterial phase, and remains slightly hyperintense in the portal and in the equilibrium phase; D: The lesion was missed on the diffusion image by both readers, probably due to its location near the gastric wall, along the liver surface; E: In the hepato-specific phase, the lesion (arrow) shows uptake of gadolinium-ethoxybenzyl-diethylenetriamine pentaacetic acid; a diagnosis of focal nodular hyperplasia was suggested due to the dynamic behavior observed after contrast administration.

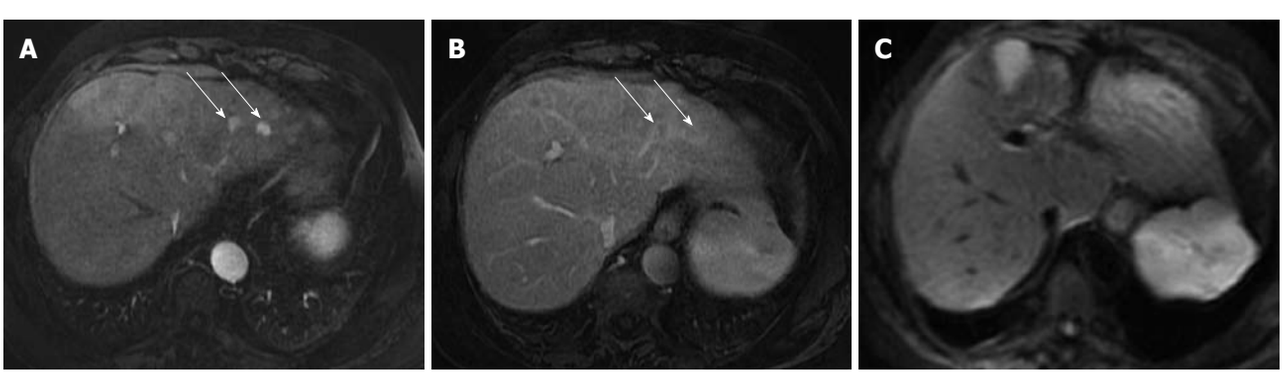

Figure 3 Hepatocellular carcinoma in the left liver lobe. A: Hypervascular lesions depicted (arrows) in the arterial phase; B: Lesions show wash-out in the venous phase (arrows), suggesting the diagnosis of hepatocellular carcinomas; C: On diffusion imaging, acquired at b10 value, lesions were not detected by the readers, due to their location near the gastric wall.

in the evaluation of metastases. These lesions are often reported with a larger size in the diffusion images, in comparison to the measurements observed by enhanced acquisitions. This larger size is better depicted in the

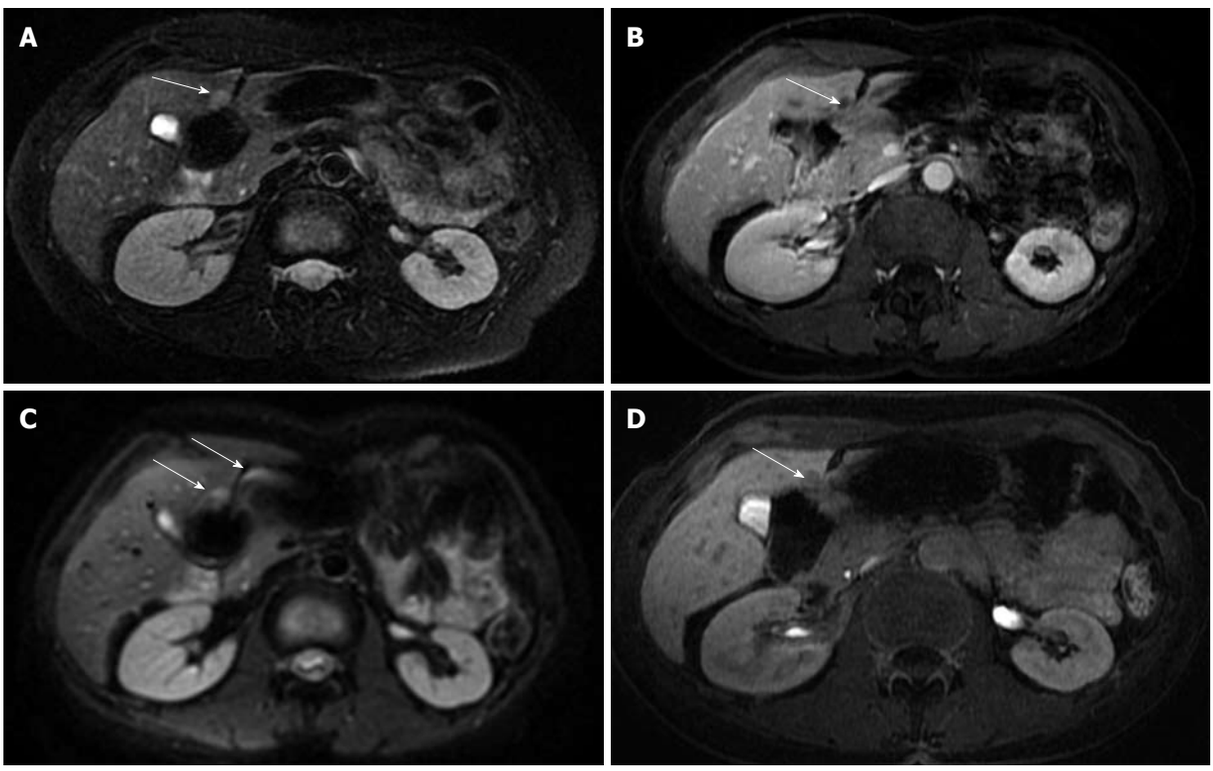

Figure 4 Metastasis in the Ⅳ segment. A: A metastatic lesion in colon carcinoma is depicted in the most caudal area of the Ⅳ liver segment, it was well depicted in the fat-suppressed fast spin-echo T2-weighted sequence (arrow); B: In the gadolinium-enhanced acquisition (arrow); C: The lesion is poorly represented in the diffusion-weighted imaging, covered by magnetic susceptibility artifacts due to the adjacent intestinal loop (arrows); D: Delayed imaging after gadolinium-ethoxybenzyl-diethylenetriamine pentaacetic acid confirmed the metastatic lesion (arrow).

follow-up of oncological patients, where lesions seem to be more reduced than those reported by gradient T1-weighted acquisition.

The main limitations of our work include the small number of histological proofs for FLLs: this may be explained by the fact that we retrospectively analyzed our study population and had many difficulties in collecting the patients' data. In addition, we discarded many exams when the image quality was damaged by artifacts, or in cases of incomplete liver MRI study.

There was no comparison between DW SS-EP and FSPGR images obtained in the hepato-specific phase; this may represent a limitation, considering the high potential value of liver-specific contrast assessed in the literature, especially in the evaluation of HCC[22]. Unfortunately, the number of exams including the hepato-specific phase in our study was not consistent and adequate for statistical analysis.

In conclusion, DWI may be very helpful to radiologists in a liver MRI protocol, increasing the detection of FLLs; considering the data reported in our study, the reliability of DWI is slightly lower than dynamic 3D FSPGR gadolinium-enhanced acquisition, but higher than conventional T2-weighted sequences. Regarding malignant FLLs, no statistical difference was found between DWI and conventional dynamic gadolinium images in our study; nevertheless, we feel contrast administration is mandatory to ensure the absence of malignant liver diseases, especially HCCs.

COMMENTS

Background

The introduction of diffusion weighted imaging (DWI) in liver magnetic resonance imaging (MRI) fuelled high expectations: **in the assessment of diffuse** and focal parenchymal disease, DWI is the latest added value in liver MRI.

Research frontiers

The use of diffusion weighted single-shot echo-planar (DW SS-EP) sequences with low *b*-value is important for the detection of hepatic lesions, especially for small-sized lesions. The acquisition of "black blood" images with DW SS-EP sequences makes it possible to easily differentiate vessels from focal small-sized lesions in the liver. In addition to the use of low *b*-value diffusion sequences, parallel techniques reduce artifacts, such as "blurring" or magnetic susceptibility artifacts, increasing the signal-to-noise ratio.

Innovations and breakthroughs

With regard to the detection all focal liver lesions (FLLs), in this study the authors retrospectively compared DWI with both T2-weighted conventional sequences and three dimensional dynamic gadolinium images. This study brings into focus the ability of DWI to detect FLLs when inserted in a complete standard liver MRI protocol.

Applications

The results suggest that DWI may be adopted as "a standard sequence" in a liver MRI protocol, owing its ability to detect FLLs.

Terminology

DWI is an imaging modality based on the measurement of the "free water" in biological tissues. Water molecules move randomly, in the so-called Brownian motion. Because of the different cellularity and percentage of free water, tissues may produce variable signal intensity, and DWI may help in detecting lesions.

Peer review

In this manuscript, the authors described the usefulness of diffusion-weighted imaging in detection of focal liver lesions. This topic is interesting; however, some revisions are needed to improve your manuscript.

REFERENCES

1 **Prasad SR**, Wang H, Rosas H, Menias CO, Narra VR, Middleton WD, Heiken JP. Fat-containing lesions of the liver: radiologic-pathologic correlation. *Radiographics* **2005; 25**: 321-331

2 **Zech CJ**, Herrmann KA, Reiser MF, Schoenberg SO. MR imaging in patients with suspected liver metastases: value of liver-specific contrast agent Gd-EOB-DTPA. *Magn Reson Med Sci* 2007; **6**: 43-52

3 **Bluemke DA**, Sahani D, Amendola M, Balzer T, Breuer J, Brown JJ, Casalino DD, Davis PL, Francis IR, Krinsky G, Lee FT, Lu D, Paulson EK, Schwartz LH, Siegelman ES, Small WC, Weber TM, Welber A, Shamsi K. Efficacy and safety of MR imaging with liver-specific contrast agent: U.S. multicenter phase III study. *Radiology* 2005; **237**: 89-98

4 **Elsayes KM**, Narra VR, Yin Y, Mukundan G, Lammle M, Brown JJ. Focal hepatic lesions: diagnostic value of enhancement pattern approach with contrast-enhanced 3D gradient-echo MR imaging. *Radiographics* **2005; 25**: 1299-1320

5 **Ichikawa T**, Haradome H, Hachiya J, Nitatori T, Araki T. Diffusion-weighted MR imaging with a single-shot echoplanar sequence: detection and characterization of focal hepatic lesions. *AJR Am J Roentgenol* 1998; **170**: 397-402

6 **Bruegel M**, Rummeny EJ. Hepatic metastases: use of diffusion-weighted echo-planar imaging. *Abdom Imaging* 2010; **35**: 454-461

7 **Taouli B**, Tolia AJ, Losada M, Babb JS, Chan ES, Bannan MA, Tobias H. Diffusion-weighted MRI for quantification of liver fibrosis: preliminary experience. *AJR Am J Roentgenol* 2007; **189**: 799-806

8 **Hussain SM**, De Becker J, Hop WC, Dwarkasing S, Wielopolski PA. Can a single-shot black-blood T2-weighted spin-echo echo-planar imaging sequence with sensitivity encoding replace the respiratory-triggered turbo spin-echo sequence for the liver? An optimization and feasibility study. *J Magn Reson Imaging* 2005; **21**: 219-229

9 **Coenegrachts K**, Delanote J, Ter Beek L, Haspeslagh M, Bipat S, Stoker J, Van Kerkhove F, Steyaert L, Rigauts H, Casselman JW. Improved focal liver lesion detection: comparison of single-shot diffusion-weighted echoplanar and single-shot T2 weighted turbo spin echo techniques. *Br J Radiol* 2007; **80**: 524-531

10 **Bruegel M**, Gaa J, Waldt S, Woertler K, Holzapfel K, Kiefer B, Rummeny EJ. Diagnosis of hepatic metastasis: comparison of respiration-triggered diffusion-weighted echo-planar MRI and five t2-weighted turbo spin-echo sequences. *AJR Am J Roentgenol* 2008; **191**: 1421-1429

11 **Yoshikawa T**, Kawamitsu H, Mitchell DG, Ohno Y, Ku Y, Seo Y, Fujii M, Sugimura K. ADC measurement of abdominal organs and lesions using parallel imaging technique. *AJR Am J Roentgenol* 2006; **187**: 1521-1530

12 **Colagrande S**, Carbone SF, Carusi LM, Cova M, Villari N. Magnetic resonance diffusion-weighted imaging: extraneurological applications. *Radiol Med* 2006; **111**: 392-419

13 **Kenis C**, Deckers F, De Foer B, Van Mieghem F, Van Laere S, Pouillon M. Diagnosis of liver metastases: can diffusion-weighted imaging (DWI) be used as a stand alone sequence? *Eur J Radiol* 2012; **81**: 1016-1023

14 **Kim YK**, Kim CS, Han YM, Lee YH. Detection of liver malignancy with gadoxetic acid-enhanced MRI: is addition of diffusion-weighted MRI beneficial? *Clin Radiol* 2011; **66**: 489-496

15 **Löwenthal D**, Zeile M, Lim WY, Wybranski C, Fischbach F, Wieners G, Pech M, Kropf S, Ricke J, Dudeck O. Detection and characterisation of focal liver lesions in colorectal carcinoma patients: comparison of diffusion-weighted and Gd-EOB-DTPA enhanced MR imaging. *Eur Radiol* 2011; **21**: 832-840

16 **Miller FH**, Hammond N, Siddiqi AJ, Shroff S, Khatri G, Wang Y, Merrick LB, Nikolaidis P. Utility of diffusion-weighted MRI in distinguishing benign and malignant hepatic lesions. *J Magn Reson Imaging* 2010; **32**: 138-147

17 **Horton KM**, Bluemke DA, Hruban RH, Soyer P, Fishman EK. CT and MR imaging of benign hepatic and biliary tumors. *Radiographics* **1999; 19**: 431-451

18 **Kandpal H**, Sharma R, Madhusudhan KS, Kapoor KS. Respiratory-triggered versus breath-hold diffusion-weighted MRI of liver lesions: comparison of image quality and apparent diffusion coefficient values. *AJR Am J Roentgenol* 2009; **192**: 915-922

19 **Coenegrachts K**, Delanote J, Ter Beek L, Haspeslagh M, Bipat S, Stoker J, Steyaert L, Rigauts H. Evaluation of true diffusion, perfusion factor, and apparent diffusion coefficient in non-necrotic liver metastases and uncomplicated liver hemangiomas using black-blood echo planar imaging. *Eur J Radiol* 2009; **69**: 131-138

20 **Parikh T**, Drew SJ, Lee VS, Wong S, Hecht EM, Babb JS, Taouli B. Focal liver lesion detection and characterization with diffusion-weighted MR imaging: comparison with standard breath-hold T2-weighted imaging. *Radiology* 2008; **246**: 812-822

21 **Holzapfel K**, Bruegel M, Eiber M, Ganter C, Schuster T, Heinrich P, Rummeny EJ, Gaa J. Characterization of small (≤10 mm) focal liver lesions: value of respiratory-triggered echo-planar diffusion-weighted MR imaging. *Eur J Radiol* 2010; **76**: 89-95

22 **Ni Y**, Marchal G, Yu J, Mühler A, Lukito G, Baert AL. Prolonged positive contrast enhancement with Gd-EOB-DTPA in experimental liver tumors: potential value in tissue characterization. *J Magn Reson Imaging* **1994; 4**: 355-363

S- Editor Cheng JX **L- Editor** Webster JR **E- Editor** Xiong L

World Journal of Radiology

Online Submissions: http://www.wjgnet.com/esps/
wjr@wjgnet.com
doi:10.4329/wjr.v4.i7.311

World J Radiol 2012 July 28; 4(7): 311-317
ISSN 1949-8470 (online)

BRIEF ARTICLE

Prevalence of unsuspected thyroid nodules in adults on contrast enhanced 16- and 64-MDCT of the chest

Sameer Ahmed, Pamela T Johnson, Karen M Horton, Hong Lai, Atif Zaheer, Saline Tsai, Elliot K Fishman

Sameer Ahmed, Pamela T Johnson, Karen M Horton, Hong Lai, Atif Zaheer, Saline Tsai, Elliot K Fishman, Russell H Morgan Department of Radiology and Radiological Science, Johns Hopkins Hospital, Baltimore, MD 21212, United States

Author contributions: Ahmed S, Horton KM and Fishman EK designed the study; Fishman EK, Zaheer A and Tsai S were involved in data collection and manuscript; Ahmed S, Johnson PT, Lai H were involved in data analysis and manuscript editing; Ahmed S, Horton KM and Johnson PT wrote the manuscript.

Correspondence to: Dr. Pamela T Johnson, Assistant Professor of Radiology, Russell H Morgan Department of Radiology and Radiological Science, Johns Hopkins Hospital, Baltimore, MD 21212, United States. pjohnso5@jhmi.edu

Telephone: +1-410-9559446 Fax: +1-410-6140341
Received: August 6, 2011 Revised: July 1, 2012
Accepted: July 8, 2012
Published online: July 28, 2012

Abstract

AIM: To determine the prevalence of unsuspected thyroid nodules on contrast enhanced 16- and 64-modified discrete cosine transform (MDCT) of the chest, in a population of adult outpatients imaged for indications other than thyroid disease.

METHODS: This retrospective study involved review of intravascular contrast-enhanced MDCT scans of the chest from 3077 consecutive adult outpatients, to identify unsuspected thyroid nodules. Exclusion criteria included history of thyroid cancer, known thyroid nodules or thyroid disease and risk factors for thyroid cancer, as evidenced by their medical records. One of 9 radiologists recorded number of nodules, location and bidirectional measurement of largest nodule, as well as amount of thyroid visualized on the chest computed tomography (CT). Presence of nodule was correlated with age, gender, race and percentage of thyroid imaged.

RESULTS: A total of 2510 (2510/3077 or 81.6%) study subjects were included in the data analysis; among them, one or more nodules were identified in 629 subjects (629/2510 or 25.1%), with 242 (242/629 or 38.5%) having multiple nodules. Patients with nodule(s) were significantly older than those without (64 ± 13 years *vs* 58 ± 14 years, $P < 0.0001$), and female gender was associated with presence of nodule(s) (373/1222 or 30.5% *vs* 256/1288 or 19.9%, $P < 0.0001$). Women were also more likely having multiple nodules (167/373 or 44.8%) compared to men (75/256 or 29.3%, $P < 0.0001$). The majority of nodules (427/629 or 67.9%) were less than 1 cm.

CONCLUSION: This retrospective review revealed a prevalence of 25.1% for unsuspected thyroid nodules on contrast-enhanced chest CT.

Key words: Thyroid nodule; Thyroid cancer; Multidetector cosine transform; Incidental finding; Chest computed tomography

Peer reviewer: Martin A Walter, MD, Institute of Nuclear Medicine, University Hospital, Petersgraben 41, CH-4031 Basel, Switzerland

Ahmed S, Johnson PT, Horton KM, Lai H, Zaheer A, Tsai S, Fishman EK. Prevalence of unsuspected thyroid nodules in adults on contrast enhanced 16- and 64-MDCT of the chest. *World J Radiol* 2012; 4(7): 311-317 Available from: URL: http://www.wjgnet.com/1949-8470/full/v4/i7/311.htm DOI: http://dx.doi.org/10.4329/wjr.v4.i7.311

INTRODUCTION

Thyroid carcinoma is troid cancer results in only approximately 1500 deaths each year, maihe most frequent endocrine cancer, with 33 500 new cases annually in the United States. Thynly due to uncommon, aggressive forms of the disease[1]. The incidence of differentiated thyroid

cancers has increased between 1988 and 2005, likely related to increased detection of small nodules on cross-sectional imaging exams[2]. The highest rate of increase is among primary tumors measuring less than 1.0 cm, nearly all of which are treatable, asymptomatic papillary thyroid cancers[2]. Despite this rise in incidence of thyroid cancer, thyroid cancer-specific mortality has remained stable from 1973 to 2002, due to aggressive treatment of even small incidentally detected lesions. For example, approximately 75% of patients with small papillary thyroid cancers (< 1.0 cm) undergo total thyroidectomy[3]. Overdiagnosis and overtreatment are a rising concern due to the relatively benign nature of these small neoplasms.

The likelihood of thyroid nodules increases with age, iodine deficiency, and history of head and neck radiation[4,5]. The exact prevalence of thyroid nodules varies with the population studied and the methods used for detection. Studies show a prevalence of 2%-6% on palpation, 19%-35% with ultrasound, and as high as 65% in autopsy data[4]. The vast majority of nodules detected employing these methods are diagnosed as benign colloid nodules, cysts or adenomas, while only approximately 5% of nodules are malignant[6].

Identification of incidental thyroid nodules at computed tomography (CT) is an area of growing interest. As chest CT is performed more frequently, especially in the emergency room (ER) setting, incidentally detected thyroid nodules can be a challenge for both ER physicians and radiologists. Two recently published studies have reported that 17% of those imaged with neck CT had an unsuspected thyroid nodule[7]. Improvements in image quality resulting from advances in CT technology have increased the frequency with which these lesions are detected. As smaller lesions are discovered, triage algorithms and management protocols must be defined, to balance identification of malignant or premalignant lesions with additional imaging studies and/or biopsy that prove unnecessary in patients with benign nodules. As a basis for additional research in this area, our study is a focused investigation designed to measure the period prevalence of unsuspected thyroid nodules using high resolution (current state-of-the-art) intravascular contrast enhanced chest modified discrete cosine transform (MDCT) in adult outpatients.

MATERIALS AND METHODS

The institutional review board at Johns Hopkins School of Medicine granted an exemption for this health insurance portability and accountability act compliant retrospective investigation and waived the requirement for informed patient consent.

Subjects

We retrospectively identified all adult patients who underwent contrast enhanced MDCT of the chest at an outpatient center over a 1-year period. The examinations were identified by using an internal coding system for CT scans that included the chest and intravascular contrast. Over the period from April 1, 2008 to April 1, 2009, 3077 adult outpatients were imaged.

To ensure that any nodules discovered were truly unsuspected and previously unknown, we excluded patients with any known thyroid disease or history of head and neck radiation, as evidenced by record review. Exclusion criteria included patients under the age of 18, patients with a known history of either symptomatic thyroid disease or thyroid cysts or masses, indication for CT related to thyroid disease, and patients who underwent prior thyroid surgery. Patients were excluded if no portion of the thyroid was visible on the CT.

CT technique

All CT examinations were performed with a Somatom Sensation 16-MDCT scanner (Siemens Medical Solutions) or Somatom Sensation 64-MDCT. Anatomic coverage was from thoracic inlet to dome of diaphragm. If no portion of the thyroid was visible on the chest CT, the patient was excluded. Depending on the stated indication, the post contrast acquisition was either arterial phase (25-30 s) or venous (50-70 s). If the patient had arterial and venous acquisitions, then the venous was used to perform measurements. Acquisition parameters included detector row configuration of 0.625 mm or 1.25 mm and reconstruction thicknesses ranging from 3 to 5 mm.

Data collection

One of 9 attending radiologists in the division of body CT reviewed each scan, using Ultravisual Software (Emageon) to evaluate the study as axial sections in scroll mode using a soft tissue window. If a patient underwent more than one chest CT examination during the study period, only the first examination was reviewed. The following data were collected for each scan: percentage of the thyroid gland visible on the chest CT, appearance of the gland (normal, enlarged but without nodule, single nodule, multiple nodules without dominant, multiple nodules with dominant). If a nodule (including cyst) was identified, location and size were recorded. Measurements were performed with an electronic caliper measuring tool. Each positive CT was re-reviewed by two experienced attending body CT radiologists in consensus, the purpose being to confirm that the finding represented a true thyroid nodule. Multiplanar reconstructions (MPR) were not reviewed.

All continuous parameters were summarized by means and standard deviations and all categorical parameters were summarized as proportions. To compare between-group differences, the Student's t-test was used for continuous variables, and the χ^2 test was used for categorical variables. The *P*-values reported are two-sided. A P -value < 0.05 indicated statistical significance.

RESULTS

Included were 2510 subjects, among them 1222 (48.7%) were women. The race distribution was 72.8% white (1828/2510), 17.6% black (442/2510), 3.0% Asian

(76/2510), 1.2% Hispanic (29/2510), 3.5% other (88/2510) and 1.9% not reported (47/2510). Mean age was 59.3 years with a range of 18 to 94 years. No association was shown between presence of nodule and race ($P = 0.5612$).

One or more nodules were identified in 629 subjects (629/2510 or 25.1%). More than half of these subjects had only one nodule (61.5%, 387/629), while 38.5% (242/629) had more than one nodule (defined as multiple nodules). The anatomic location of the largest nodule is reported in Table 1. The mean maximum diameter was 8.56 mm, with standard deviation 6.42 mm and range 1.0-62.0 mm. The majority of nodules were less than 1 cm (427/629 or 67.9%), as opposed to 1 cm or greater (202/629 or 32.1%).

The entire thyroid gland was imaged in 55.3% (1389/2510) patients, while more than half of the thyroid gland was imaged in 36.9% (925/2510) patients and less than half in 7.8% (196/2510) patients. The appearance of the gland is reported in Table 2. Of the patients who had the entire thyroid imaged ($n = 1389$), nodules were identified in 352 (25.3%), compared to 277/1121 (24.7%) whose thyroid was only partially imaged. Presence of a nodule was not associated with percentage of thyroid imaged ($P = 0.7165$).

Data on 601 patients provided information on location of nodules. Location of a nodule was more likely mid gland or lower pole than upper pole (Table 3). This was the case for all patients as well as those whose entire thyroid was imaged. However, the pattern of nodule distribution was significantly different between patients who had the entire thyroid imaged and those who had only part of the thyroid imaged. The majority of nodules occurred in the interpolar pole for patients who had only partial thyroid imaged ($P = 0.0008$)

Female gender was associated with presence of nodule(s) (373/1222 or 30.5% *vs* 256/1288 or 19.9%, $P < 0.0001$). Gender were also found to be correlated with presence of multiple nodules, with women more likely having multiple nodules (167/373 or 44.8%) compared to men (75/256 or 29.3%) ($P < 0.0001$).

Age was found to be correlated with number of nodules. Patients with nodule(s) were significantly older than those without (64 ± 13 years *vs* 58 ± 14 years, $P < 0.0001$). There was a significant difference in the mean age of patients with no nodules (mean ± SD: 58 ± 14 years), one nodule (62 ± 13 years) and multiple nodules (66 ± 12 years) ($P < 0.0001$).

Table 1 Location of the 629 nodules identified on chest computed tomography *n* (%)

	Upper pole	Mid gland	Lower pole	Total
Right	72	120	90	282 (45)
Left	47	138	134	319 (51)
Isthmus				28 (5)
	119 (19)	258 (41)	224 (36)	629 (100)

Table 2 Characterization of the thyroid gland on intravascular contrast enhanced computed tomography in 2510 patients

Characterize	Frequency	Percent
No nodule	1790	71.3
Enlarged but no nodule	91	3.6
Solitary nodule	387	15.4
Multiple nodules (no dominant)	143	5.7
Multiple nodules (dominant)	99	3.9

Table 3 Distribution of nodules in patients who had entire thyroid imaged *vs* all patients *n* (%)

Location	Whole thyroid imaged	All patients
Upper pole	81 (24)	119 (20)
Interpolar pole	124 (37)	258 (43)
Lower pole	131 (39)	224 (37)

The pattern of distribution was significantly different; although, interpolar and lower pole location was most common in both groups.

DISCUSSION

The frequency with which thyroid nodules are detected has varied from as low as 2% to as high as 67%[8-10]. Differences in mode of detection certainly account for variability in prevalence. For example, autopsy is more sensitive than ultrasound, which is more sensitive than CT. Incidental lesions are detected least frequently on positron emission tomography (PET) scans. In a study by Carroll *et al*[8] incidental thyroid nodules were detected by ultrasound in 13% (six women and three men) of 67 patients without known thyroid disease, which is at the low end of the detection spectrum. Woestyn *et al*[11] reported on 300 ultrasound examinations in patients without any signs or symptoms of thyroid disease, asymmetry, or enlargement. Approximately 19% of patients (17% of men and 20% of women) presented with small, incidental echoic nodules. However, improvements of ultrasound technology have led to substantial increases in detection of thyroid lesions. In 2006, Bartolotta *et al*[12] demonstrated thyroid nodularity in 33% of 704 patients without known thyroid disease, using high-resolution ultrasonography (HRUS) and real-time spatial compound sonography. Approximately 60% of the nodules were found in women. Ezzat *et al*[9] examined 100 healthy volunteers without history of thyroid disease and ionizing radiation exposure and reported the highest rate of detection using HRUS at 67%. However, 84% of the subjects were female, which likely contributed to an overestimation of nodule prevalence.

Autopsy data on incidental thyroid lesions is limited. An autopsy study by Mortensen *et al*[13] macroscopically examined 821 thyroid glands from patients with no history of thyroid disease and reported a 50% prevalence of thyroid nodules. Approximately 12% contained a single nodule and 38% had multiple nodules.

Incidental thyroid nodules are also detected on FDG PET. In a study of 4525 patients by Cohen *et al*[10], unsuspected thyroid nodules were demonstrated in 2% of

patients. However, these scans were performed for cancer staging which likely introduces selection and population biases. Kang *et al*[14] examined 1330 patients on FDG PET and also reported a prevalence of 2%. This modality is particularly useful for detecting thyroid cancers, with studies reporting sensitivity and specificity of 75%-90% and 90%, respectively[15,16].

A few studies have looked at the prevalence of incidental thyroid nodules on neck CT. In a 2008 study, Yoon *et al*[7] retrospectively reviewed CT scans of the neck in 734 patients without known thyroid disease and reported incidental thyroid nodules in 17% of patients. Their patient population was younger than in our study (mean age 49.8 years compared to our mean age of 59.3 years). This study employed a 16-detector row CT scanner and did not exclude patients with prior history of neck radiation. They also showed that CT features, like calcification, anteroposterior (AP) to transverse (T) diameter ratio, and mean attenuation value, could be used to predict malignancy. This demonstrates the diagnostic value of CT in evaluating thyroid nodules, which may help to avoid extensive ultrasound evaluations.

Youserm *et al*[17] analyzed 123 neck CT scans (HSA or 9800 Quick scanner) and 108 MR images, and reported the prevalence of incidental thyroid nodules at 15%. The lower prevalence probably related to the CT technology, as this study was conducted in 1994. However, this study also did not exclude patients with a history of neck radiation. Given the increased prevalence of thyroid nodules in patients with history of neck radiation[4], we incorporated it in the exclusion criteria. Even though our study evaluated MDCT of the chest, which does not always image the entire thyroid, a prevalence of 25.1% was noted, which is within the range previously reported. Furthermore, there was no difference in the prevalence of those whose entire thyroid was imaged *vs* only a portion of the thyroid included in the acquisition.

The likelihood of having a thyroid nodule and multiple nodules correlated with increasing age, as has been reported previously. Woestyn *et al*[11] found that thyroid nodules were significantly more common on ultrasound scans for patients over the age of 60. Bartolotta *et al*[12] showed that the prevalence of thyroid nodularity on HRUS and real-time spatial compound sonography peaked in the 61- to 70-year-old age group, and then steadily declined. However, this was also the most common age group in their sample. Ezzat *et al*[9] found that there was a tendency toward an increased probability of a thyroid nodule on HRUS with increasing age, but this correlation was not statistically significant. An autopsy based study showed that nodules were significantly more common in women over the age of 40[13]. Both of the previously mentioned CT-based studies did not show any correlation between age and nodule frequency. To our knowledge, our study is the first to show a correlation between age and thyroid nodularity on CT.

Several studies report a higher prevalence of thyroid nodules in females than males[7-9,11,12]. Frequencies range from 20% to 72% in women and 7% to 41% in men. This was also the case in our study, with women more frequently having 1 nodule (16.86% of women *vs* 14.1 % of men) and multiple nodules (13.7% of women and 5.8% of men) ($P < 0.0001$).

The correlation between race and thyroid nodularity still remains unclear. Haselkorn *et al*[18] demonstrated that a greater prevalence of goiter and thyroid nodules accounted for a substantial portion of the higher thyroid cancer incidence rates among Southeast Asian (Filipino, Vietnamese, Thai, Indonesian, Pacific Islander) women living in the United States than among Northern Asian (Chinsese, Japanese, Korean and Asian-Indian) and non-Latino Caucasian women. Our study showed no association with race ($P = 0.5612$).

We also examined the prevalence of solitary and multiple nodules. In our study, one or more nodules were identified in 629 subjects (25.1%). More than half of these subjects had one nodule (61.5%, 387/629), while 242/629 (38.5%) had more than one nodule. Previous studies have examined the relationship between the number of thyroid nodules seen in a patient and the risk of malignancy and thyroid cancer. Sippel *et al*[19] retrospectively reviewed records of 325 patients who underwent thyroidectomy with a fine needle aspiration diagnosis of either follicular neoplasm, Hürthle cell neoplasm, or indeterminate. They showed that the risk of malignancy was lower in patients with multiple nodules as compared to those with a solitary nodule (16% *vs* 28%). Frates *et al*[20] showed that although solitary nodules have a higher per-nodule likelihood of malignancy, the prevalence of thyroid cancer was similar between patients with solitary and multiple nodules. However, that study only considered nodules larger than 10 mm in diameter. These studies suggest that there is a higher risk associated with solitary nodules and approximately two-thirds of thyroid cancers are found in the dominant nodule in patients with multiple nodules[21]. However, non-dominant nodules cannot be ignored because they still comprise a significant portion of carcinomas.

A CT-based study showed that dominant nodules were evenly distributed between lobes, but more commonly detected in the lower pole[22]. In our series, the mid gland was most common (41%), followed by lower pole (36%) for either dominant nodule or solitary nodule. Nearly half (45%) of patients had only a portion of the thyroid imaged, potentially skewing results toward the lower pole. When only those patients whose entire thyroid was imaged are analyzed, the difference between right *vs* left lobe was less pronounced, with 45% in the right lobe and 51% in the left lobe. Our results showed that mean maximum diameter of the largest nodule identified on chest CT was 8.6 mm, and the majority (68%) were less than 1 cm in maximum diameter. The risk of malignancy is difficult to determine using size as a diagnostic criterion. In one study, Papini *et al*[23] correlated sonographic findings with the results of ultrasound-guided FNA biopsy and pathologic staging of resected carcinomas. They examined 494 patients and showed that the prevalence of malignancy was not significantly

different between nodules greater or smaller than 1 cm (9% *vs* 7%). Sahin *et al*[24] examined 207 nodular goiter patients and demonstrated that 21% of nodules smaller than 1 cm and 17% of nodules larger than 1 cm were malignant. However, nodules that are larger than 4 cm may carry a higher risk of malignancy than those smaller than 1 cm[25]. Although the clinical importance of nodule size is still controversial, several studies demonstrate that an AP/T diameter ratio greater than 1.0 is more frequent in malignant than in benign nodules[7,26,27], which suggests that nodule shape may be an important diagnostic indicator. In our study, we measured the AP and T diameter of the largest thyroid nodule found on CT for each patient; however we did not perform long term follow up to determine whether nodules were benign *vs* malignant. Future research collecting follow up data will be useful to determine whether the AP/TRV ratio proves to be a valid indicator of malignancy.

Likely owing to improved resolution resulting from advancements in imaging technology, the prevalence of thyroid nodules on CT and MRI has increased dramatically. Although the risk of cancer is quite low (about 5%), most nodules 1 cm or greater are sampled with ultrasound-guided fine-needle aspiration (FNA) biopsy. This has led to a marked increase in the number of patients with papillary microcarcinomas, which measure less than 10 mm in diameter[28]. Treatment strategies remain controversial In one series, approximately 75% of patients with small papillary thyroid cancers (< 1.0 cm) underwent total thyroidectomy[3], which carries small, but significant risk of complications. Following surgery, many patients are also placed on a lifetime of thyroid replacement therapy. Despite an increase in surgeries to treat these carcinomas, thyroid cancer-specific mortality has not improved[3]. Ito *et al*[29] showed that out of 162 patients with papillary microcarcinomas, more than 70% of tumors either remained stable or decreased in size, even after 5 years or more, suggesting that overtreatment of thyroid disease is a concern, as noted by Black *et al*[30]. Further study to determine the natural history and histologic subtype of the lesions identified will be a great aid in further refining algorithms for cost-effective evaluation and treatment of clinically detectable thyroid nodules.

Management recommendations for thyroid nodules are still under debate because benign nodules are highly prevalent in the population and thyroid carcinoma is relatively uncommon. If we extrapolate from other CT series, we expect that 5% or 32/629 of the nodules that we detected will be cancer. Size has been identified as a discriminatory criteria to guide management. According to guidelines established by the National Comprehensive Cancer Network (NCCN) in 2009[25], solitary nodules measuring greater than 1 cm in diameter in patients with certain risk factors should be further evaluated with measurement of TSH levels, neck ultrasound, and FNA of nodules and clinically suspicious lymph nodes. Risk factors include age below 15 years and above 60 years, male gender, history of head and neck radiation, history of diseases associated with thyroid cancer (eg., Gardner's syndrome, Cowden's syndrome, and Carney Complex), and family history of thyroid cancer. Intranodular hypervascularity, irregular borders, and microcalcification seen on ultrasound are also important factors associated with malignancy[21]. Nodules that are very firm, have exhibited a pattern of rapid growth, and/or are invading other neck structures should be considered for surgery after FNA. NCCN also recommends that unsuspected nodules that measure less than 1 cm in patients without the aforementioned risk factors should be monitored, followed-up clinically as indicated, and a lateral neck ultrasound may be considered. Major sets of guidelines for follow-up and management of incidental thyroid lesions are established by the American Thyroid Association, the British Thyroid Association, and the Society of Radiologists in Ultrasound[21,31,32].

There are certain limitations to our study which should be addressed. First, the retrospective nature of the study is not ideal to obtain a random sample but allowed time efficient review of a large number of cases. Second, since this was a review of all contrast enhanced chest CTs during the selected time period, the data acquisition, contrast administration and reconstruction parameters were not uniform across all subjects. It is possible that more nodules would have been detected if all data sets were reviewed with thin sections or with the addition of MPRs. Third, the entire thyroid was not visible on all patients because the imaging protocol was not standardized to visualize the thyroid. However, there was no significant difference between patients whose entire thyroid was imaged as opposed to partially imaged with respect to percentage of patients who had a nodule, which prompted inclusion of all 2510 patients for analysis. It is also important to note that when the entire thyroid was imaged, the vast majority (76%) of nodules were in the lower and mid-gland regions (Table 3). Scans with partial visualization of the thyroid tended to exclude portions of the upper pole since the protocol was primarily designed for chest imaging. Therefore, the portion of the thyroid with a tendency to be missed on our imaging (i.e., the upper pole) was also the region with the lowest probability of having a lesion. This is likely the reason for insignificant differences in nodule prevalence between patients with fully- and partially-visualized thyroid glands. Nonetheless, our data may slightly underestimate the true prevalence of incidental thyroid nodules.

In patients with multiple scans during the study period we used the first positive CT study rather than choosing one that best visualized the thyroid gland because we wanted to look at truly incidental findings. Thus, by choosing the first study (not optimized for thyroid imaging) our data represents incidental detection of thyroid lesions on routine chest CT imaging.

In conclusion, unsuspected small thyroid nodules are being detected with increased frequency on CT. In this outpatient population the prevalence of unsuspected, asymptomatic nodules identified on contrast enhanced 16- and 64-MDCT of the chest was 25.1%. The presence of a nodule showed a strong correlation with increasing age

as well as female gender, but not race. This study serves to highlight some important characteristics of incidental thyroid lesions on chest CT, including patterns of distribution within the gland and patient demographics. Given that nearly one-quarter of our patients had a positive finding on chest CT, this study also emphasizes the clinical relevance of incidental thyroid lesions and the need for standardized protocols for evaluation and follow up.

ACKNOWLEDGMENTS

We would like to acknowledge the contributions of Rohan Piyasena, MD, Saadet Atay-Rosenthal, MD, Christopher Smith, MD, Bruce Berlanstein, MD, Stanley S Siegelman, MD and Karen B Bleich, MD.

COMMENTS

Background

Identification of incidental thyroid nodules at computed tomography (CT) is an area of growing interest. Incidentally detected thyroid nodules can be a challenge for both referring physicians and radiologists. As smaller lesions are discovered, triage algorithms and management protocols must be defined, to balance identification of malignant or premalignant lesions with additional imaging studies and/or biopsy that prove unnecessary in patients with benign nodules.

Research frontiers

Improvements in image quality resulting from advances in CT technology have increased the frequency with which incidental lesions such as small thyroid nodules are detected. Management of incidental findings is an active area of current radiology research.

Innovations and breakthroughs

The incidence of differentiated thyroid cancer has risen, likely related to increased detection of small nodules on cross-sectional imaging exam. Most are smaller treatable, asymptomatic papillary thyroid cancers. Aggressive treatment of these smaller lesions has held stable the mortality rate.

Applications

As a basis for additional research in this area, our study is a focused investigation designed to measure the period prevalence of unsuspected thyroid nodules using high resolution (current state-of-the-art) intravascular contrast enhanced chest modified discrete cosine transform in adult outpatients.

Peer review

This is a well written manuscript including many patients (more than 3000). It contains, however, not much new information. After exclusions for different reasons 2510 exams are left for this retrospective study. In only 55% (1389) of these cases the whole thyroid has been visualized. In the rest (1121) only part of the thyroid was visible but still these patients are included and reviewed in this study. They should have been excluded as it is impossible to tell the number of nodules, if any, in this group.

REFERENCES

1 **National Cancer Institute.** NCI Cancer Bulliten for February 19, 2008. Available from: URL: http: //www.cancer.gov/ncicancerbulletin/NCI_Cancer_Bulletin_021908/page5
2 **Chen AY**, Jemal A, Ward EM. Increasing incidence of differentiated thyroid cancer in the United States, 1988-2005. *Cancer* 2009; **115**: 3801-3807
3 **Davies L**, Welch HG. Increasing incidence of thyroid cancer in the United States, 1973-2002. *JAMA* 2006; **295**: 2164-2167
4 **Dean DS,** Gharib H. Epidemiology of thyroid nodules. *Best Pract Res Clin Endocrinol Metab* 2008; **22:** 901-911
5 **Guth S**, Theune U, Aberle J, Galach A, Bamberger CM. Very high prevalence of thyroid nodules detected by high frequency (13 MHz) ultrasound examination. *Eur J Clin Invest* 2009; **39**: 699-706
6 **Desser TS**, Kamaya A. Ultrasound of thyroid nodules. *Neuroimaging Clin N Am* 2008; **18**: 463-478, vii
7 **Yoon DY**, Chang SK, Choi CS, Yun EJ, Seo YL, Nam ES, Cho SJ, Rho YS, Ahn HY. The prevalence and significance of incidental thyroid nodules identified on computed tomography. *J Comput Assist Tomogr* 2008; **32**: 810-815
8 **Carroll BA**. Asymptomatic thyroid nodules: incidental sonographic detection. *AJR Am J Roentgenol* 1982; **138**: 499-501
9 **Ezzat S**, Sarti DA, Cain DR, Braunstein GD. Thyroid incidentalomas. Prevalence by palpation and ultrasonography. *Arch Intern Med* 1994; **154**: 1838-1840
10 **Cohen MS**, Arslan N, Dehdashti F, Doherty GM, Lairmore TC, Brunt LM, Moley JF. Risk of malignancy in thyroid incidentalomas identified by fluorodeoxyglucose-positron emission tomography. *Surgery* 2001; **130**: 941-946
11 **Woestyn J**, Afschrift M, Schelstraete K, Vermeulen A. Demonstration of nodules in the normal thyroid by echography. *Br J Radiol* 1985; **58**: 1179-1182
12 **Bartolotta TV**, Midiri M, Runza G, Galia M, Taibbi A, Damiani L, Palermo Patera G, Lagalla R. Incidentally discovered thyroid nodules: incidence, and greyscale and colour Doppler pattern in an adult population screened by real-time compound spatial sonography. *Radiol Med* 2006; **111**: 989-998
13 **Mortensen JD,** Woolner LB, Bennett WA. Gross and microscopic findings in clinically normal thyroid glands. *J Clin Endocrinol Metab* 1955; **15:** 1270-1280
14 **Kang KW,** Kim SK, Kang HS, Lee ES, Sim JS, Lee IG, Jeong SY, Kim SW. Prevalence and risk of cancer of focal thyroid incidentaloma identified by 18F-fluorodeoxyglucose positron emission tomography for metastasis evaluation and cancer screening in healthy subjects. *J Clin Endocrinol Metab* 2003; **88:** 4100-4104
15 **Feine U**, Lietzenmayer R, Hanke JP, Held J, Wöhrle H, Müller-Schauenburg W. Fluorine-18-FDG and iodine-131-iodide uptake in thyroid cancer. *J Nucl Med* 1996; **37**: 1468-1472
16 **Grunwald F,** Kalicke T, Feine U, Lietzenmayer R, Scheidhauer K, Dietlein M, Schober O, Lerch H, Brandt-Mainz K, Burchert W, Hiltermann G, Cremerius U, Biersack HJ. Fluorine-18 fluorodeoxyglucose positron emission tomography in thyroid cancer: results of a multicentre study. *Eur J Nucl Med* 1999; **26:** 1547-1552
17 **Youserm DM**, Huang T, Loevner LA, Langlotz CP. Clinical and economic impact of incidental thyroid lesions found with CT and MR. *AJNR Am J Neuroradiol* 1997; **18**: 1423-1428
18 **Haselkorn T**, Stewart SL, Horn-Ross PL. Why are thyroid cancer rates so high in southeast asian women living in the United States? The bay area thyroid cancer study. *Cancer Epidemiol Biomarkers Prev* 2003; **12**: 144-150
19 **Sippel RS,** Elaraj DM, Khanafshar E, Kebebew E, Duh QY, Clark OH. Does the presence of additional thyroid nodules on ultrasound alter the risk of malignancy in patients with a follicular neoplasm of the thyroid? *Surgery* 2007; **142:** 851-857; discussion 857 e851-852
20 **Frates MC,** Benson CB, Doubilet PM, Kunreuther E, Contreras M, Cibas ES, Orcutt J, Moore FD, Larsen PR, Marqusee E, Alexander EK. Prevalence and distribution of carcinoma in patients with solitary and multiple thyroid nodules on sonography. *J Clin Endocrinol Metab* 2006; **91:** 3411-3417
21 **Frates MC**, Benson CB, Charboneau JW, Cibas ES, Clark OH, Coleman BG, Cronan JJ, Doubilet PM, Evans DB, Goellner JR, Hay ID, Hertzberg BS, Intenzo CM, Jeffrey RB, Langer JE, Larsen PR, Mandel SJ, Middleton WD, Reading CC, Sherman SI, Tessler FN. Management of thyroid nodules detected at US: Society of Radiologists in Ultrasound consensus conference statement. *Radiology* 2005; **237**: 794-800
22 **Shetty SK**, Maher MM, Hahn PF, Halpern EF, Aquino SL. Significance of incidental thyroid lesions detected on CT: correlation among CT, sonography, and pathology. *AJR Am J Roentgenol* 2006; **187**: 1349-1356
23 **Papini E,** Guglielmi R, Bianchini A, Crescenzi A, Taccogna S,

Nardi F, Panunzi C, Rinaldi R, Toscano V, Pacella CM. Risk of malignancy in nonpalpable thyroid nodules: predictive value of ultrasound and color-Doppler features. *J Clin Endocrinol Metab* 2002; **87:** 1941-1946

24 **Sahin M,** Sengul A, Berki Z, Tutuncu NB, Guvener ND. Ultrasound-guided fine-needle aspiration biopsy and ultrasonographic features of infracentimetric nodules in patients with nodular goiter: correlation with pathological findings. *Endocr Pathol* 2006; **17:** 67-74

25 **National Comprehensive Cancer Network.** NCCN Guidelines for Thyroid Carcinoma. 2009. Available from: URL: http://www.nccn.org/about/news/newsinfo.asp?NewsID=209

26 **Kim EK**, Park CS, Chung WY, Oh KK, Kim DI, Lee JT, Yoo HS. New sonographic criteria for recommending fine-needle aspiration biopsy of nonpalpable solid nodules of the thyroid. *AJR Am J Roentgenol* 2002; **178**: 687-691

27 **Cappelli C**, Castellano M, Pirola I, Gandossi E, De Martino E, Cumetti D, Agosti B, Rosei EA. Thyroid nodule shape suggests malignancy. *Eur J Endocrinol* 2006; **155**: 27-31

28 **Lin HW**, Bhattacharyya N. Survival impact of treatment options for papillary microcarcinoma of the thyroid. *Laryngoscope* 2009; **119**: 1983-1987

29 **Ito Y**, Uruno T, Nakano K, Takamura Y, Miya A, Kobayashi K, Yokozawa T, Matsuzuka F, Kuma S, Kuma K, Miyauchi A. An observation trial without surgical treatment in patients with papillary microcarcinoma of the thyroid. *Thyroid* 2003; **13**: 381-387

30 **Black WC**, Welch HG. Advances in diagnostic imaging and overestimations of disease prevalence and the benefits of therapy. *N Engl J Med* 1993; **328**: 1237-1243

31 **Cooper DS**, Doherty GM, Haugen BR, Kloos RT, Lee SL, Mandel SJ, Mazzaferri EL, McIver B, Sherman SI, Tuttle RM. Management guidelines for patients with thyroid nodules and differentiated thyroid cancer. *Thyroid* 2006; **16**: 109-142

32 **British Thyroid Association.** British Thyroid Association guidelines for the management of thyroid cancer. Available from: URL: http://www.british-thyroid-association.org/Guidelines

S- Editor Cheng JX **L- Editor** A **E- Editor** Xiong L

World Journal of Radiology

Online Submissions: http://www.wjgnet.com/esps/
wjr@wjgnet.com
doi:10.4329/wjr.v4.i7.318

World J Radiol 2012 July 28; 4(7): 318-323
ISSN 1949-8470 (online)

BRIEF ARTICLE

Concurrent use of aromatase inhibitors and hypofractionated radiation therapy

Cyrus Chargari, Pablo Castro-Pena, Ivan Toledano, Marc A Bollet, Alexia Savignoni, Paul Cottu, Fatima Laki, François Campana, Patricia De Cremoux, Alain Fourquet, Youlia M Kirova

Cyrus Chargari, Pablo Castro-Pena, Ivan Toledano, Marc A Bollet, François Campana, Patricia De Cremoux, Alain Fourquet, Youlia M Kirova, Department of Radiation Oncology, Institut Curie, 75005 Paris, France
Alexia Savignoni, Department of Biostatistics, Institut Curie, 75005 Paris, France
Paul Cottu, Department of Medical Oncology, Institut Curie 75005 Paris, France
Fatima Laki, Department of Surgery, Institut Curie, 75005 Paris, France
Author contributions: Kirova YM and Savignoni A designed the study; Castro-Pena P, Toledano I, Bollet MA, Savignoni A, Campana F, De Cremoux P, Fourquet A and Kirova YM contributed to acquisition of data; Chargari C, Savignoni A, Campana F, De Cremoux P, Fourquet A and Kirova YM interpreted the data; Chargari C and Kirova YM wrote the paper and revised it; and all authors approved the final version of the version to be published.
Correspondence to: Youlia M Kirova, MD, Department of Radiation Oncology, Institut Curie, 26, rue d'Ulm, 75005 Paris, France. youlia.kirova@curie.net
Telephone: +331-4432-4193 Fax: +331-4432-4616
Received: January 15, 2011 Revised: April 13, 2012
Accepted: April 20, 2012
Published online: July 28, 2012

Abstract

AIM: To retrospectively assess the acute and long-term toxicity using aromatase inhibitors (AI) therapy concurrently with hypofractionated radiotherapy (HFRT) in breast cancer patients.

METHODS: From November 1999 to October 2007, 66 patients were treated with breast HFRT and concurrent AI. In 63 patients (95.5%), HFRT delivered a total dose of 32.5 Gy to the whole breast within 5 wk (five fractions, one fraction per week). Other fractionations were chosen in three patients for the patients' personal convenience. A subsequent boost to the tumor bed was delivered in 35 patients (53.0%). Acute toxicities were scored according to the Common Toxicity Criteria for Adverse Events v3. Late toxicity was defined as any toxicity occurring more than 6 mo after completion of HFRT and was scored according to the Late Effects Normal Tissue Task Force-Subjective, Objective, Management and Analytic scale.

RESULTS: At the end of the HFRT course, 19 patients (28.8%) had no irradiation-related toxicity. Acute grade 1-2 epithelitis was observed in 46 patients (69.7%). One grade 3 toxicity (1.5%) was observed. With a median follow-up of 34 mo (range: 12-94 mo), 31 patients (47%) had no toxicity, and 35 patients (53%) presented with grade 1-2 fibrosis. No grade 3 or greater delayed toxicity was observed.

CONCLUSION: We found that AI was well tolerated when given concurrently with HFRT. All toxicities were mild to moderate, and no treatment disruption was necessary. Further prospective assessment is warranted.

Key words: Breast cancer; Hypofractionated radiotherapy; Skin toxicity; Aromatase inhibitors

Peer reviewers: Ioannis G Valais, PhD, Department of Medical Instrument Technology, Technological Educational Institution of Athens, Ag Spyridonos and Dimitsanis, Egaleo, 12210 Athens, Greece; Volker Rudat, Professor, Department of Radiation Oncology, Saad Specialist Hospital, PO Box 30353, Al Khobar 31952, Saudi Arabia

Chargari C, Castro-Pena P, Toledano I, Bollet MA, Savignoni A, Cottu P, Laki F, Campana F, De Cremoux P, Fourquet A, Kirova YM. Concurrent use of aromatase inhibitors and hypofractionated radiation therapy. *World J Radiol* 2012; 4(7): 318-323 Available from: URL: http://www.wjgnet.com/1949-8470/full/v4/i7/318.htm DOI: http://dx.doi.org/10.4329/wjr.v4.i7.318

INTRODUCTION

Adjuvant endocrine therapy demonstrated clinical benefit in breast cancer patients with tumors that express hormone receptors[1-4]. More particularly, third-generation aromatase inhibitors (AI) demonstrated improved disease-free survival as adjuvant therapy in postmenopausal patients with hormone positive early breast cancer[5-9]. Postoperative endocrine therapy has become standard clinical practice in this population and it is frequently delivered along with adjuvant radiation therapy (RT). However, the preclinical findings that AI might increase radiosensitivity raised concerns about the safety of such association[10].

Retrospective analysis reported that concurrent use of adjuvant normofractionated RT and endocrine therapy using AI did not increase RT-related side effects[11]. More recently, the prospective randomized phase Ⅱ trial Concomitant Hormono-Radiotherapy (CO-HO-RT) study demonstrated that patients receiving conventionally fractionated RT and letrozole did not experience more frequent or more serious skin toxicity[12]. Although this trial provided evidence for the safety of normofractionated RT and AI, no conclusion could be drawn regarding hypofractionated radiotherapy (HFRT) and concurrent AI.

HFRT is frequently proposed as an alternative to standard fractionation in elderly patients treated with a breast conservative strategy[13-15]. In this population, an abbreviated course of radiation therapy is more convenient than standard fractionation. Recently, a randomized trial reported by Whelan *et al*[15] demonstrated that HFRT was not inferior to standard radiation treatment in patients who had undergone breast-conserving surgery for good prognosis breast cancer. Authors found no increase in skin and subcutaneous toxic effects in patients who received accelerated HFRT as compared with those who received the standard regimen. However, since elderly patients are also most likely to receive AI, it would also be clinically relevant to determine whether concurrent HFRT and AI might increase toxicity. Our study is the first to assess the safety of AI therapy concurrently with HFRT.

MATERIALS AND METHODS

Patients' characteristics

We retrospectively reviewed the clinical records of 66 consecutive breast cancer patients who were treated at the Institut Curie, Paris, France, from November 1999 to October 2007 for breast HFRT concurrently with AI. Patients were eligible for analysis only if they had more than 12 mo follow-up after completion of breast HFRT. Patients were treated according to the current protocol available in our Institute for women older than 65 years, presenting with voluminous or pendulous breasts and who wished a breast conservation procedure. Local committees approved the study design. Only one patient was less than 65 years old but she presented with metastatic disease and was judged a candidate for HFRT. At first presentation, the median age of the group was 80.5 years (range: 56-92 years). For all patients, the diagnosis of breast cancer been histologically confirmed by biopsy/surgery of the primary lesion. Patients and tumors' characteristics are reported in Table 1. Regarding associated risk factors, the median body mass index was 26 (range: 16-45), seven patients had type 2 diabetes mellitus, and six patients had active tobacco use.

Table 1 Patients' and tumors' characteristics

Characteristics	
Number of patients	66
Median age in years (range)	80 (56-92)
Stage, *n* (%)	
Ⅰ	28 (42.4)
Ⅱ	23 (34.8)
Ⅲ	10 (18)
Ⅳ	5 (5)
Histological type, *n* (%)	
Invasive ductal carcinoma	54 (81.8)
Invasive lobular carcinoma	11 (16.6)
Other histology	1 (1.6)
Grade, *n* (%)	
1	15 (22.7)
2	38 (57.6)
3	11 (16.6)
NR	2 (3.1)
Mitotic index, *n* (%)	
Low	42 (63.6)
Intermediate	11 (16.7)
High	7 (10.6)
NR	6 (9.1)
Expression of endocrine receptors, % (median)	
ER	100 (60-100)
PgR	100 (60–100)
HER2 status, *n* (%)	
Positive	11 (16.6)
Negative	55 (83.4)

ER: Estrogen receptor; HER2: Human epidermal growth factor receptor 2; *n*: Number of patients; PgR: Progesterone receptor; NR: Not reported..

Treatments' characteristics

Breast conservative surgery (BCS) ± axillary lymph node dissections were performed in 35 patients (53.0%). All of them had received neoadjuvant endocrine therapy, median duration 6 mo (range: 1-12 mo). The remaining patients were not candidates for surgery, due to poor performance status. Following surgery (or following histological confirmation of the diagnosis in patients who had no surgery), AIs were administered daily and was planned for 5 years, either letrozole 2.5 mg daily (n = 16) or anastrozole 1 mg daily (n = 47), or exemestane 25 mg daily (n = 3). Although concurrent endocrine and HFRT was not in our current protocol in 1999-2007, all patients received breast HFRT and concurrent AI because they were referred to our department after having initiated AI therapy, which was not discontinued for HFRT.

HFRT was delivered according to the recommendations of the International Commission on Radiation Units and Measurements report 50 using a high-energy linear

Table 2 Treatment characteristics

Treatments	*n* (%)
Surgery	
Surgery	
Yes (BCS)	35 (53.0)[1]
No	31 (47.0)
Axillary LND	
Yes	17 (25.8)
No	49 (74.2)
Sentinel LN	
Yes	20 (30.3)
No	46 (69.7)
Aromatase inhibitor	
Letrozole	16 (24.2)
Anastrozole	47 (71.2)
Exemestane	3 (4.6)
RT	
Position	
Lateral decubitus	63 (95.4)
Dorsal decubitus	3 (4.6)
Source	
Cobalt 60	57 (86.3)
RX 4 MV	8 (12.2)
RX 6 MV	1 (1.5)
Volume	
Whole breast	66 (100)
Axillary LN	4 (6.1)
Susclavicular LN	3 (4.5)
Boost	35 (4.5)
Protocol for the whole breast	
5 fractions of 6.5 Gy	63 (95)
Other fractionation	3 (5)
Protocol for the boost	
2 fractions of 6.5 Gy	28 (42.4)
1 fraction of 6.5 Gy	5 (7.5)
Other fractionation	2 (3)
Median duration in days (range)	29 (25-52)

[1]Including five patients with neoadjuvant endocrine therapy. BCS: Breast conservative surgery; LN: Lymph node; LND: Lymph node dissection; RT: Radiation therapy.

accelerator or a Cobalt unit[16]. In 63 patients (95.5%), HFRT delivered a total dose of 32.5 Gy to the whole breast within 5 wk (five fractions, one fraction per week). Other fractionations were chosen in three patients because of patients' personal convenience. A subsequent boost to the tumor bed was delivered in 35 patients (53.0%) either because of risk factors for local relapse following BCS or in the setting of exclusive HFRT (Table 2). Axillary lymph node or supraclavicular HFRT could be delivered as 5 weekly fractions of 5.5 Gy in the case of clinical or pathological lymph node involvement. Internal mammary chain (IMC) irradiation was not delivered. A standard technique was used with the patient either in lateral decubitus position (n = 63, 95.4 %) or in dorsal decubitus (n = 3). Treatment characteristics are detailed in Table 2.

Assessment

Weekly examination was performed during HFRT, then every 6 mo after HFRT completion. Local symptomatic therapies could be delivered, at the discretion of the radiation oncologist. Acute skin toxicities were scored according to the Common Toxicity Criteria for Adverse Events v3. Late skin toxicity was defined as any skin toxicity occurring more than 6 mo after completion HFRT and was scored according to the Late Effects Normal Tissue Task Force-Subjective, Objective, Management and Analytic scale[17]. For both acute and late toxicity, the maximal skin reaction was assessed independent of the location within the irradiated breast. Our retrospective design did not allow a thorough assessment of cardiac or lung toxicity, but most patients were treated in the lateral decubitus position. We previously reported that very low doses are delivered to the underlying lung and heart using this technique[18]. Moreover, no IMC irradiation was delivered for minimizing the doses to the heart.

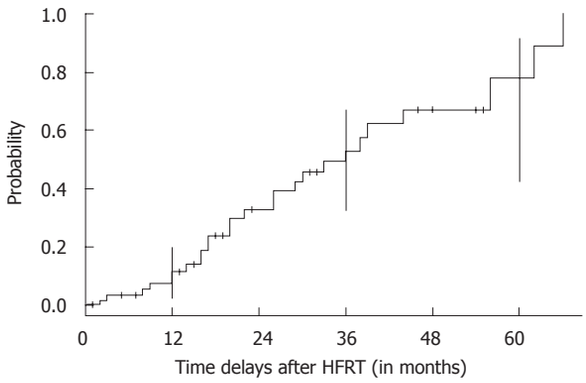

Figure 1 Evolution of the probability of presenting fibrosis according to the time delays after hypofractionated radiotherapy. HFRT: Hypofractionated radiotherapy.

RESULTS

At the end of the HFRT course, acute toxicity was low in most patients. Nineteen patients (28.8%) experienced no toxicity. Acute grade 1 epithelitis was observed in 38 patients (57.6%). Eight patients (12.1%) developed grade 2 epithelitis. One grade 3 skin toxicity (1.5%) was observed. No grade 4 or greater acute skin toxicity was observed. Median delay between HFRT initiating and first skin reaction was 28 d (range: 13-50 d). Median dose to first skin reaction was 31.25 Gy (range: 13-45.5 Gy). No treatment disruption was necessary and no clinical acute lung or cardiac toxicity was reported.

With a median follow-up of 34 mo (range: 12-94 mo), 31 patients (47%) had no delayed skin or subcutaneous toxicity, and 35 patients (53%) presented with grade 1-2 fibrosis. No grade 3 or greater delayed skin toxicity was observed. Figure 1 shows the probability of developing late skin sequelae according to the time delay after breast HFRT. No irradiation-related cardiac or pulmonary delayed toxicity was reported. A multivariate analysis was performed for determining whether fractionation, surgery, or boost delivery could impact on the probability of developing acute or late skin reaction. No significant relation was found between these factors and the cosmetic outcome. Similarly, acute and long-term grade 1 and 2 skin toxicity did not differ among different AIs. Acute and late skin toxicity data are summarized in Table 3.

Table 3 Skin toxicity

Skin toxicity	*n* (%)
Acute toxicity	
Grade 0	19 (28.8)
Grade 1	38 (57.6)
Grade 2	8 (12.1)
Grade 3	1 (1.5)
Grade 4	0 (0)
Long-term toxicity	
Grade 0	31 (47.0)
Grade 1-2	35 (53.0)
Grade 3-4	0 (0)

Acute toxicity is scored according to the Common Toxicity Criteria for Adverse Events v3; long-term toxicity is scored according to the Late Effects Normal Tissue Task Force-Subjective, Objective, Management and Analytic scale.

Seventeen patients (25.5%) discontinued endocrine therapy before completion of treatment for 5 years. Reasons for endocrine therapy discontinuation are detailed in Table 4.

Table 4 Reasons for discontinuating aromatase inhibitors therapy prior to 5 yr adjuvant therapy

Reasons for discontinuation	*n* (%)
Thromboembolic event	4 (6.0)
Progression	3 (4.5)
Patient death	5 (7.5)
Clinical intolerance	5 (7.5)
Total discontinuations	17 (25.5)

DISCUSSION

There is clinical evidence that 5 years of adjuvant AI anastrozole improves recurrence-free survival in postmenopausal early breast cancer patients. Results from the ATAC trial demonstrated that recurrence rates remained significantly lower on anastrozole compared with tamoxifen [HR 0.75 (0.61-0.94), $P = 0.01$][19]. As a matter of fact, AI therapy inhibits the aromatase enzyme function and prevents the conversion of androgens to estrogens. AI therapy has logically become standard adjuvant therapy for postmenopausal women with hormone receptor positive cancers. However, most breast cancer patients also receive adjuvant breast or chest well RT. Up till now, there has been little data available on the rationale for concomitant use of AI in adjuvant RT settings.

The optimal sequence for adjuvant endocrine therapy and RT represents a challenge for the clinician[20]. *In vitro* results by Azria *et al*[10] demonstrated that letrozole sensitizes breast cancer cells to radiation doses ranging from 0 to 4 Gy. Their results suggested possible additive effects for the combined treatment, supporting concurrent use of AI and RT in postsurgical settings for more clinical efficacy. Although this increased sensitivity might theoretically translate into greater toxicity, most data from literature suggest that AI could be safely given concurrently with normofractionated RT.

We have already reported that hormone therapy and RT could be given concurrently to post-menopausal patients with both good efficacy (57% partial responses, 24% partial response and 21% stable disease) and acceptable tolerance[21]. However, only 10% patients had received AI[21]. Ishitobi *et al*[11] assessed the optimal sequence of adjuvant AI and RT. They compared concurrent *vs* sequential treatment for patients with hormone receptor-positive breast cancer treated with BCS. At a median follow-up of 2.9 years, authors found no difference in the breast cancer outcomes and treatment-related complications between the two treatment groups. These retrospective results suggested that both concurrent and sequential use of normofractionated postoperative RT and adjuvant AI therapy were feasible in terms of the breast cancer outcomes and toxicity[11]. Finally, the safety of AI and concurrent adjuvant radiotherapy was prospectively confirmed by the CO-HO-RT study. In this randomized phase Ⅱ study, Azria *et al*[12] found no increase in skin toxicity in breast cancer patients receiving letrozole and concurrent normofractionated breast radiotherapy, delivering 2 Gy per daily fraction. Of importance, concurrent AI did not influence the efficacy of irradiation at a median follow-up of 26 mo.

HFRT could be safe and could be used in post menopausal and or in elderly patients with good local control and acceptable toxicity[13,15]. In some cases these patients are already being treated with IA and the interruption of this treatment is, in some cases, a problem. Therefore the question being asked is interesting and the same time important for everyday practice. While HFRT alone might theoretically increase skin toxicity, no data has been previously reported on AI and concurrent HFRT. Since elderly patients are likely to receive concurrent AI, it is also clinically relevant to determine whether concurrent HFRT and AI could increase toxicity. We found that this association was well tolerated. All skin toxicities were mild to moderate and no treatment disruption was necessary. Multiple known factors influence the severity of acute and late reactions, for example the total dose, beam energy, breast volume, observation time, or type of surgery. Our study population was quite heterogeneous in regard to these factors: 53% of the patients received a boost, 53% underwent surgery, which may significantly influence the severity of fibrosis compared to patients without surgery, 86% of patients were treated with cobalt units, and finally, different AIs were used. We failed to evidence any significant relation between all these factors and the risk of skin toxicity, but our patients' population was probably insufficient for such analysis. Although biased by retrospective analysis and limits inherent to the study design, we found that AI could be safely administered concurrently with HFRT. In the prospective trial by Whelan *et al*[15], 77.9% of patients had an excellent or good global cosmetic outcome. The results presented here are rather comparable for cosmetic outcome. In their prospective trial, the authors reported that poor cosmetic outcome

was reported in only 1.6% of patients. Although any indirect comparison is debatable, we observed no grade 3 or greater late skin toxicity when combining HFRT with AIs. Good tolerance could be obtained using techniques adapted to be less toxic and adapted to patients' anatomy as previously reported[18]. This report was not designed for assessment of potential cardiac or lung toxicity, but our patients were treated in the lateral decubitus position. This technique provides several advantages over more conventional techniques, including total avoidance of cardiac and/or lung irradiation[18]. However, cardiac toxicity may be associated with exposure to radiation doses lower than 4 Gy, suggesting that the theoretical risk of cardiac toxicity should not be underestimated in the setting of adjuvant HFRT[22]. Obviously, our study is limited by biases inherent to the retrospective nature of the analysis. Prospective confirmation will be mandatory.

We found that AI was well tolerated concurrently with HFRT. All toxicities were mild to moderate, and no treatment disruption was necessary. Although retrospective, our study suggests that AI could be given concurrently with HFRT in postmenopausal breast cancer patients without jeopardizing the cosmetic results. Confirmatory prospective assessments are, however, warranted before translating these results into clinical practice.

ACKNOWLEDGMENTS

A part of this work has been presented at the 2010 annual meeting of the American Society for Therapeutic Radiology and Oncology, San Diego, United States, the authors thank Chantal Gautier for her precious help.

COMMENTS

Background

A recent randomized phase Ⅱ trial has demonstrated that conventionally fractionated radiotherapy and aromatase inhibitors could be safely delivered concurrently as adjuvant therapy in breast cancer patients. There is however no data in the literature regarding the use of aromatase inhibitors concurrently with hypofractionated radiotherapy, which is frequently proposed as an alternative to standard fractionation in elderly patients treated with a breast conservative strategy.

Research frontiers

The optimal sequence for adjuvant endocrine therapy and radiation therapy (RT) remains undetermined. *In vitro* data reported that aromatase inhibitors sensitize breast cancer cells to ionizing radiation. This suggested possible additive effects for the combined treatment. This increased sensitivity might translate into greater toxicity.

Innovations and breakthroughs

Although prospective confirmation is warranted, this is the fist study to report how aromatase inhibitors are tolerated when given concurrently with hypofractionated radiotherapy, and how those can affect on cosmetic outcome. Acute high-grade toxicities were reported in 1.5% of patients. With a median follow-up of 34 mo, no grade 3 or greater delayed toxicity was observed.

Applications

This study suggests that treatment with aromatase therapy could safely continued during the irradiation process in patients receiving hypofractionated radiotherapy. However, multiple other factors can influence the severity of acute and late reactions. Those should be carefully considered when choosing the optimal technique for adjuvant radiation therapy.

Terminology

Hypofractionated RT refers to the use of a lower number of fractions, each fraction delivering a higher dose than the standard schedule (> 2 Gy per fraction). It has demonstrated non-inferiority for adjuvant treatment of breast cancer in post-menopausal patients with good local control and acceptable toxicity.

Peer review

The authors report on a retrospective study assessing the acute and late effects of aromatase inhibitor therapy concurrently with hypofractionated radiotherapy in breast cancer patients. They concluded that aromatase inhibitor was well tolerated. While numerous other factors influence the severity of acute and late reactions, the study was not designed to assess cardiac toxicity. Further prospective assessment is therefore recommended.

REFERENCES

1 **Lin NU**, Winer EP. Advances in adjuvant endocrine therapy for postmenopausal women. *J Clin Oncol* 2008; **26**: 798-805
2 **Fisher B**, Costantino J, Redmond C, Poisson R, Bowman D, Couture J, Dimitrov NV, Wolmark N, Wickerham DL, Fisher ER. A randomized clinical trial evaluating tamoxifen in the treatment of patients with node-negative breast cancer who have **estrogen-receptor-positive tumors.** *N Engl J Med* 1989; **320**: 479-484
3 Randomized trial of two versus five years of adjuvant tamoxifen for postmenopausal early stage breast cancer. Swedish Breast Cancer Cooperative Group. *J Natl Cancer Inst* 1996; **88**: 1543-1549
4 **Dalberg K**, Johansson H, Johansson U, Rutqvist LE. A randomized trial of long term adjuvant tamoxifen plus postoperative radiation therapy versus radiation therapy alone for patients with early stage breast carcinoma treated with breast-conserving surgery. Stockholm Breast Cancer Study Group. *Cancer* 1998; **82**: 2204-2211
5 **Thürlimann B**, Keshaviah A, Coates AS, Mouridsen H, Mauriac L, Forbes JF, Paridaens R, Castiglione-Gertsch M, Gelber RD, Rabaglio M, Smith I, Wardley A, Price KN, Goldhirsch A. A comparison of letrozole and tamoxifen in postmenopausal women with early breast cancer. *N Engl J Med* 2005; **353**: 2747-2757
6 **Kaufmann M**, Jonat W, Hilfrich J, Eidtmann H, Gademann G, Zuna I, von Minckwitz G. Improved overall survival in postmenopausal women with early breast cancer after anastrozole initiated after treatment with tamoxifen compared with continued tamoxifen: the ARNO 95 Study. *J Clin Oncol* 2007; **25**: 2664-2670
7 **Boccardo F**, Rubagotti A, Puntoni M, Guglielmini P, Amoroso D, Fini A, Paladini G, Mesiti M, Romeo D, Rinaldini M, Scali S, Porpiglia M, Benedetto C, Restuccia N, Buzzi F, Franchi R, Massidda B, Distante V, Amadori D, Sismondi P. Switching to anastrozole versus continued tamoxifen treatment of early breast cancer: preliminary results of the Italian Tamoxifen Anastrozole Trial. *J Clin Oncol* 2005; **23**: 5138-5147
8 **Howell A**, Cuzick J, Baum M, Buzdar A, Dowsett M, Forbes JF, Hoctin-Boes G, Houghton J, Locker GY, Tobias JS. Results of the ATAC (Arimidex, Tamoxifen, Alone or in Combination) trial after completion of 5 years' adjuvant treatment for breast cancer. *Lancet* 2005; **365**: 60-62
9 **Jakesz R**, Jonat W, Gnant M, Mittlboeck M, Greil R, Tausch C, Hilfrich J, Kwasny W, Menzel C, Samonigg H, Seifert M, Gademann G, Kaufmann M, Wolfgang J. Switching of postmenopausal women with endocrine-responsive early breast cancer to anastrozole after 2 years' adjuvant tamoxifen: combined results of ABCSG trial 8 and ARNO 95 trial. *Lancet* 2005; **366**: 455-462
10 **Azria D**, Larbouret C, Cunat S, Ozsahin M, Gourgou S, Martineau P, Evans DB, Romieu G, Pujol P, Pèlegrin A. Letrozole sensitizes breast cancer cells to ionizing radiation. *Breast Cancer Res* 2005; **7**: R156-R163
11 **Ishitobi M**, Komoike Y, Motomura K, Koyama H, Nishiyama K, Inaji H. Retrospective analysis of concurrent vs. sequential administration of radiotherapy and hormone

therapy using aromatase inhibitor for hormone receptor-positive postmenopausal breast cancer. *Anticancer Res* 2009; **29**: 4791-4794

12 **Azria D**, Belkacemi Y, Romieu G, Gourgou S, Gutowski M, Zaman K, Moscardo CL, Lemanski C, Coelho M, Rosenstein B, Fenoglietto P, Crompton NE, Ozsahin M. Concurrent or sequential adjuvant letrozole and radiotherapy after conservative surgery for early-stage breast cancer (CO-HO-RT): a phase 2 randomised trial. *Lancet Oncol* 2010; **11**: 258-265

13 **Kirova YM**, Campana F, Savignoni A, Laki F, Muresan M, Dendale R, Bollet MA, Salmon RJ, Fourquet A. Breast-conserving treatment in the elderly: long-term results of adjuvant hypofractionated and normofractionated radiotherapy. *Int J Radiat Oncol Biol Phys* 2009; **75**: 76-81

14 **Chargari C**, Kirova YM, Laki F, Savignoni A, Dorval T, Dendale R, Bollet MA, Fourquet A, Campana F. The impact of the loco-regional treatment in elderly breast cancer patients: hypo-fractionated exclusive radiotherapy, single institution long-term results. *Breast* 2010; **19**: 413-416

15 **Whelan TJ**, Pignol JP, Levine MN, Julian JA, MacKenzie R, Parpia S, Shelley W, Grimard L, Bowen J, Lukka H, Perera F, Fyles A, Schneider K, Gulavita S, Freeman C. Long-term results of hypofractionated radiation therapy for breast cancer. *N Engl J Med* 2010; **362**: 513-520

16 **International Commission on Radiation Units and Measurements.** ICRU report 50: Prescribing, recording, and reporting photon beam therapy. Bethesda: ICRU, 1999

17 **Pavy JJ**, Denekamp J, Letschert J, Littbrand B, Mornex F, Bernier J, Gonzales-Gonzales D, Horiot JC, Bolla M, Bartelink H. EORTC Late Effects Working Group. Late effects toxicity scoring: the SOMA scale. *Radiother Oncol* 1995; **35**: 11-15

18 **Campana F**, Kirova YM, Rosenwald JC, Dendale R, Vilcoq JR, Dreyfus H, Fourquet A. Breast radiotherapy in the lateral decubitus position: A technique to prevent lung and heart irradiation. *Int J Radiat Oncol Biol Phys* 2005; **61**: 1348-1354

19 **Buzdar A**, Howell A, Cuzick J, Wale C, Distler W, Hoctin-Boes G, Houghton J, Locker GY, Nabholtz JM. Comprehensive side-effect profile of anastrozole and tamoxifen as adjuvant treatment for early-stage breast cancer: long-term safety analysis of the ATAC trial. *Lancet Oncol* 2006; **7**: 633-643

20 **Chargari C**, Toillon RA, Macdermed D, Castadot P, Magné N. Concurrent hormone and radiation therapy in patients with breast cancer: what is the rationale? *Lancet Oncol* 2009; **10**: 53-60

21 **Bollet MA**, Kirova YM, Antoni G, Pierga JY, Sigal-Zafrani B, Laki F, Campana F, Dendale R, Salmon R, Cottu P, Fourquet A. Responses to concurrent radiotherapy and hormonetherapy and outcome for large breast cancers in post-menopausal women. *Radiother Oncol* 2007; **85**: 336-345

22 **Darby SC**, McGale P, Taylor CW, Peto R. Long-term mortality from heart disease and lung cancer after radiotherapy for early breast cancer: prospective cohort study of about 300,000 women in US SEER cancer registries. *Lancet Oncol* 2005; **6**: 557-565

S- Editor Cheng JX **L- Editor** O'Neill M **E- Editor** Xiong L

World Journal of Radiology

Online Submissions: http://www.wjgnet.com/esps/
wjr@wjgnet.com
doi:10.4329/wjr.v4.i7.324

World J Radiol 2012 July 28; 4(7): 324-327
ISSN 1949-8470 (online)

BRIEF ARTICLE

Sixty-four MDCT achieves higher contrast in pancreas with optimization of scan time delay

Tina Stuber, Hans-Jürgen Brambs, Wolfgang Freund, Markus S Juchems

Tina Stuber, Hans-Jürgen Brambs, Wolfgang Freund, Markus S Juchems, Department of Diagnostic and Interventional Radiology, University Hospitals Ulm, Steinhövelstr. 9, 89075 Ulm, Germany

Author contributions: Stuber T contributed to the interpretation of data and writing of the manuscript; Brambs HJ helped with data analysis; Freund W helped with data analysis and manuscript correction; Juchems MS designed the study and contributed to the writing of the manuscript.

Correspondence to: Markus S Juchems, MD, Associate Professor, Vice-chairman, Department of Diagnostic and Interventional Radiology, University Hospitals Ulm, Steinhövelstr. 9, D-89075 Ulm, Germany. markus.juchems@uni-ulm.de

Telephone: +49-731-50061151 Fax: +49-731-50061004
Received: November 9, 2011 Revised: June 16, 2012
Accepted: June 23, 2012
Published online: July 28, 2012

Abstract

AIM: To compare different multidetector computed tomography (MDCT) protocols to optimize pancreatic contrast enhancement.

METHODS: Forty consecutive patients underwent contrast-enhanced biphasic MDCT (arterial and portal-venous phase) using a 64-slice MDCT. In 20 patients, the scan protocol was adapted from a previously used 40-channel MDCT scanner with arterial phase scanning initiated 11.1 s after a threshold of 150 HU was reached in the descending aorta, using automatic bolus tracking (Protocol 1). The 11.1-s delay was changed to 15 s in the other 20 patients to reflect the shorter scanning times on the 64-channel MDCT compared to the previous 40-channel system (Protocol 2). HU values were measured in the head and tail of the pancreas in the arterial and portal-venous phase.

RESULTS: Using an 11.1-s delay, 74.2 HU (head) were measured on average in the arterial phase and 111.2 HU (head) were measured using a 15-s delay (P < 0.0001). For the pancreatic tail, the average attenuation level was 76.73 HU (11.1 s) and 99.89 HU (15 s) respectively (P = 0.0002). HU values were also significantly higher in the portal-venous phase [pancreatic head: 70.5 HU (11.1 s) *vs* 84.0 HU (15 s) (P = 0.0014); pancreatic tail: 67.45 HU (11.1 s) and 77.18 HU (15 s) using Protocol 2 (P = 0.0071)].

CONCLUSION: Sixty-four MDCT may yield a higher contrast in pancreatic study with (appropriate) optimization of scan delay time.

Key words: Computed tomography; Pancreas; Scan delay; Protocol; Contrast enhancement

Peer reviewers: Dr. Kazushi Kishi, Wakayama Medical University, Wakayama City 641-8510, Japan; Dr. Charikleia Triantopoulou, Konstantopouleion Hospital, 3-5, Agias Olgas street, Athens 14233 Nea Ionia, Greece

Stuber T, Brambs HJ, Freund W, Juchems MS. Sixty-four MDCT achieves higher contrast in pancreas with optimization of scan time delay. *World J Radiol* 2012; 4(7): 324-327 Available from: URL: http://www.wjgnet.com/1949-8470/full/v4/i7/324.htm DOI: http://dx.doi.org/10.4329/wjr.v4.i7.324

INTRODUCTION

Contrast-enhanced multidetector computed tomography (MDCT) for pancreatic imaging is widely accepted, especially for detection and preoperative staging of pancreatic adenocarcinoma, as well as for diagnosis and follow-up examinations of patients with pancreatitis. Scanning protocols are usually multiphasic with acquirement of arterial and portal-venous phases of contrast material (CM) enhancement.

Several studies[1-3] have been conducted to evaluate the

appropriate scan timing to achieve optimal CM enhancement. To the best of our knowledge, the data published to date have evaluated CM enhancement of pancreatic parenchyma with scan protocols for MDCT scanners with up to 16 detector rows. The purpose of our study was to compare different MDCT protocols for a 64-slice MDCT scanner to achieve a better pancreatic contrast enhancement protocol.

MATERIALS AND METHODS

Forty consecutive patients underwent biphasic pancreatic examination with a 64-channel MDCT (Brilliance 64; Philips Medizin-Systeme, Hamburg, Germany). The patient group consisted of 22 female and 18 male patients, aged 36-92 years, with a mean age of 68.8 years. Indications for abdominal CT were as follows: follow-up after abdominal tumor [gastrointestinal stromal tumor (GIST): n = 10; cholangiocellular carcinoma (CCC): n = 12]; exclusion of abdominal tumor (CCC: n = 5; GIST: n = 1, carcinoid: n = 1); exclusion of gastrointestinal bleeding: n = 6; exclusion of pancreatitis: n = 2; exclusion of intraductal papillary neoplasia: n = 3.

Written consent was obtained from each patient or patient's legal representative before CT examination. Exclusion criteria included general contraindications for CT including pregnancy and allergy to CM, as well as known pancreatic tumor and pancreatitis.

Arterial and portal-venous phase images were obtained after intravenous administration of CM (400 mg/mL iomeprol, Imeron 400; Bracco, Milano, Italy) using a power injector (Injektron CT2; Medtron AG, Saarbrücken, Germany) at a dose of 1.2 mL/kg body weight and a rate of 4 mL/s followed by a saline chaser.

In 20 patients, the scan protocol was adapted from a previously used 40-channel MDCT scanner with arterial phase scanning initiated 11.1 s after a threshold of 150 HU was reached in the descending aorta using automatic bolus tracking (Protocol 1). The delay was changed to 15 s in the other 20 patients to reflect the shorter scanning times on the 64-channel MDCT compared to the previous 40-channel system (Protocol 2). The delay of the portal-venous phase acquisition was set to 60 s after onset of arterial phase. For all scans, the scanner parameters were set as follows: arterial phase (120 kv, 200-300 mAs, collimation 64 × 0.625, pitch: 0.9, reconstructed slice thickness: 0.8 mm), portal-venous phase (120 kv, 180-250 mAs, collimation 64 × 0.625, pitch: 0.9, reconstructed slice thickness: 2 mm). CT images were reviewed digitally on a dedicated PACS workstation (Impax 4.5; AGFA Healthcare, Köln, Germany). Attenuation levels were measured in the head and tail of the pancreas in the arterial and portal-venous phase by an attending radiologist with 8 years of experience in reading abdominal CT. The size of the measurement region ranged from 0.45 to 0.55 cm^2. Focal lesions within the pancreatic tissue were excluded from measurement areas. The differences between the groups were investigated by an exploratory unpaired t test. $P < 0.01$ was considered statistically significant.

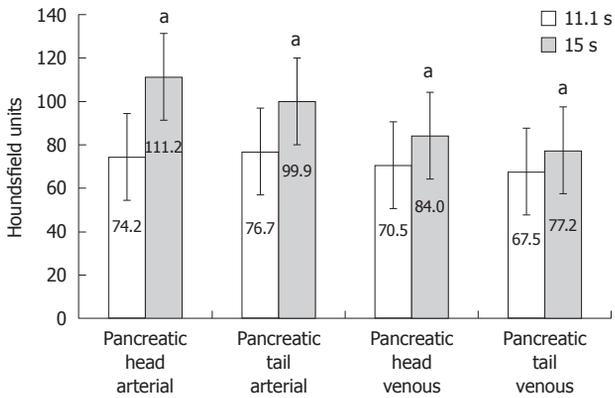

Figure 1 Influence of multidetector computed tomography scan delay on mean attenuation levels of pancreatic parenchyma. $^aP < 0.05$.

RESULTS

In the arterial phase, the mean attenuation level in the pancreatic head was 74.2 ± 14.3 (mean ± SD) HU using the 11.1-s delay compared to 111.2 ± 19.9 HU with scan Protocol 2 (P = 0.0001). Attenuation levels ranged from 49.8 to 98.1 HU (11.1 s) and 81.3 to 148.4 HU (15 s). Attenuation measured in the pancreatic tail parenchyma ranged from 54.5 to 98.8 HU (11.1 s) and 73.0 to 139.9 (Protocol 2) with an average parenchymal attenuation level of 76.73 ± 13.8 HU (11.1 s) and 99.89 ± 20.6 HU (15 s) (P = 0.0002).

HU values were also significantly higher (P = 0.0014) in the pancreatic head using the longer scan delay (Figure 1). Mean attenuation levels were 70.5 ± 11.3 HU (11.1 s) *vs* 84.0 HU (15 s). Contrast density within the pancreatic head ranged from 49.5 to 91.6 HU (Protocol 1) and 63.0 to 111.9 HU (15 s). In the pancreatic tail parenchyma, the average enhancement was 67.45 ± 7.7 HU (11.1 s) compared to 77.18 ± 13.2 HU (15 s) using Protocol 2 (P = 0.0071). The range of attenuation in the pancreatic tail was 51.1-83.2 HU (11.s) and 53.6-100.2 HU (15 s). Figure 2 give examples of attenuation levels of pancreatic parenchyma in arterial-phase imaging with a 15-s scan delay.

DISCUSSION

MDCT is an excellent tool for diagnostic work-up of patients with pancreatic diseases, especially of patients suffering from pancreatic tumors. The role of CT in the assessment of pancreatic diseases has gained more impact since multi-channel CT became widely available[4].

Bae[5] investigated the peak aortic contrast enhancement in a porcine model in 2003 and showed a linear increase in enhancement with duration of CM injection. Since then, examination protocols and scan delay have been subject to several studies. In 2001, McNulty *et al*[6] demonstrated for a four-channel MDCT that the mean attenuation level of normal pancreatic parenchyma was higher in the pancreatic parenchymal phase than in arterial or portal-venous phase imaging. The mean CM enhancement was 122 compared to 70 and 109 HU, respectively. The delay for the pancreatic parenchymal

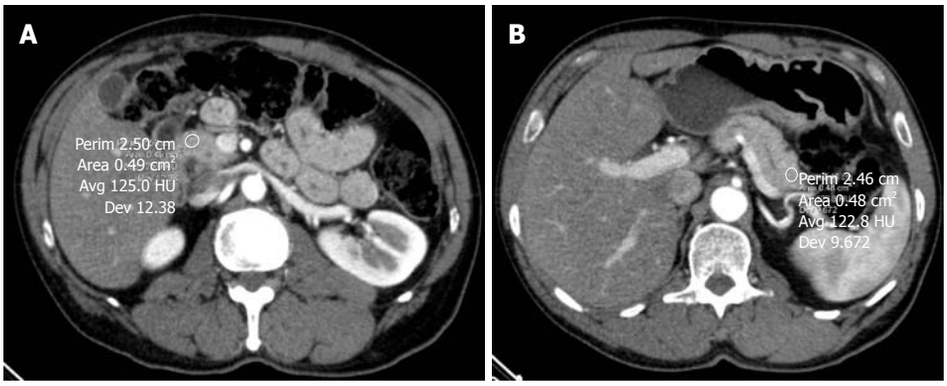

Figure 2 Axial arterial phase multidetector computed tomography image in a 58-year-old male patient with weight loss. A:The scan delay for multidetector computed tomography examination was 15 s. The mean attenuation level was 125.0 HU in the pancreatic head; B: Within the parenchyma of the pancreatic tail, the mean attenuation value was 122.8 HU.

phase was 35 s after the onset of CM injection. In 2006, Goshima *et al*[7] examined the enhancement of pancreatic tissue with scan delays ranging from 25 to 80 s after injection of CM, with a fixed duration of 30 s. The CT scanner used in this study was an eight-channel MDCT. The peak enhancement was obtained after a 40-s delay with intense attenuation levels of pancreatic parenchyma ranging from 82.1 to 85.2 HU with delays of 35-45 s. Kondo *et al*[8] published data for eight-channel MDCT pancreatic imaging showing the most intensive enhancement of the pancreatic parenchyma 15-20 s after triggering of bolus tracking with attenuation levels of 84-85 HU. Ichikawa *et al*[9] reported a delay of 40 s after injection of CM for the pancreatic parenchymal phase. Images were acquired with a 16-channel MDCT scanner after administration of 100 mL CM. Horton *et al*[10] described a scan protocol for a 64-channel MDCT scanner in an educational exhibit on MDCT appearance of pancreatic islet cell tumors.

In our study, we found significant differences in attenuation levels of pancreatic parenchyma between the scan protocols with an 11-s *vs* 15-s delay for the start of the arterial phase. HU values in the portal-venous phase were also significantly higher using Protocol 2 instead of Protocol 1. Our findings suggest that higher pancreatic parenchymal attenuation and therefore increased tumor-to-pancreas contrast can be obtained by optimizing scan protocols when using faster MDCT scanners.

One of the limitations of our study was the relatively small number of 40 patients and the fact that we only used one manufacturer's 64-channel MDCT scanner. The attenuation levels of pancreatic parenchyma may differ with different types of MDCT generations or scanners. Birnbaum *et al*[11] assessed intra- and interscanner variability using an anthropomorphic body CT phantom, showing that there are significant differences of CT attenuation levels between different MDCT scanner generations as well as between different manufacturers' scanners. Further studies should investigate the influence of scan delays for pancreatic imaging with different manufacturer's scanners.

Sixty-four MDCT may achieve higher contrast in pancreatic studies, with appropriate optimization of scan delay time.

COMMENTS

Background

Scanning protocols for pancreatic imaging with multidetector row computed tomography (MDCT) are usually multiphasic with acquisition of arterial and portal-venous phases of contrast material (CM) enhancement. Due to the faster scanning speed, a redesign of scanning protocols is required.

Research frontiers

Pancreatic parenchyma can contain benign or malignant lesions that should be classified by pancreatic imaging in order to prevent unnecessary operations. Achievement of optimal CM enhancement is mandatory for evaluation of pancreatic lesions. CT scanners of newer generations consist of more detector rows, allowing faster scanning of patients and thinner imaging slices.

Innovations and breakthroughs

Optimized contrast between normal pancreatic parenchyma and pathological changes can be achieved by adaptation of examination protocols to the faster scanning speed of MDCT. **Data published to date evaluate CM enhancement of** pancreatic parenchyma with scan protocols for MDCT scanners with up to 16 detector rows. The **authors of the present study evaluated scanning protocols** of 40- and 64-channel MDCT scanners and found significant differences in contrast attenuation of pancreatic parenchyma between the scan protocol with an 11-s *vs* 15-s **delay for the start of the arterial phase. The findings suggest** that higher pancreatic parenchymal attenuation and therefore increased tumor-to-pancreas contrast can be obtained by optimizing scan protocols when using faster MDCT scanners.

Applications

The study results suggest that 64 MDCT may achieve higher contrast in pancreatic studies with appropriate optimization of scan delay time. This may help to optimize pancreatic imaging.

Peer review

It is an interesting paper, **but it should be revised before publication.**

REFERENCES

1 **Hollett MD**, Jorgensen MJ, Jeffrey RB. Quantitative evaluation of pancreatic enhancement during dual-phase helical CT. *Radiology* 1995; **195**: 359-361
2 **Bonaldi VM**, Bret PM, Atri M, Garcia P, Reinhold C. A comparison of two injection protocols using helical and dynamic acquisitions in CT examinations of the pancreas. *AJR Am J Roentgenol* 1996; **167**: 49-55
3 **Graf O**, Boland GW, Warshaw AL, Fernandez-del-Castillo C, Hahn PF, Mueller PR. Arterial versus portal venous helical CT for revealing pancreatic adenocarcinoma: conspicuity of tumor and critical vascular anatomy. *AJR Am J Roentgenol* 1997; **169**: 119-123
4 **Tamm EP**, Balachandran A, Bhosale P, Szklaruk J. Update on 3D and multiplanar MDCT in the assessment of biliary and pancreatic pathology. *Abdom Imaging* 2009; **34**: 64-74

5 **Bae KT**. Peak contrast enhancement in CT and MR angiography: when does it occur and why? Pharmacokinetic study in a porcine model. *Radiology* 2003; **227**: 809-816
6 **McNulty NJ**, Francis IR, Platt JF, Cohan RH, Korobkin M, Gebremariam A. Multi--detector row helical CT of the pancreas: effect of contrast-enhanced multiphasic imaging on enhancement of the pancreas, peripancreatic vasculature, and pancreatic adenocarcinoma. *Radiology* 2001; **220**: 97-102
7 **Goshima S**, Kanematsu M, Kondo H, Yokoyama R, Miyoshi T, Kato H, Tsuge Y, Shiratori Y, Hoshi H, Onozuka M, Moriyama N, Bae KT. Pancreas: optimal scan delay for contrast-enhanced multi-detector row CT. *Radiology* 2006; **241**: 167-174
8 **Kondo H**, Kanematsu M, Goshima S, Miyoshi T, Shiratori Y, Onozuka M, Moriyama N, Bae KT. MDCT of the pancreas: optimizing scanning delay with a bolus-tracking technique for pancreatic, peripancreatic vascular, and hepatic contrast enhancement. *AJR Am J Roentgenol* 2007; **188**: 751-756
9 **Ichikawa T**, Erturk SM, Sou H, Nakajima H, Tsukamoto T, Motosugi U, Araki T. MDCT of pancreatic adenocarcinoma: optimal imaging phases and multiplanar reformatted imaging. *AJR Am J Roentgenol* 2006; **187**: 1513-1520
10 **Horton KM**, Hruban RH, Yeo C, Fishman EK. Multi-detector row CT of pancreatic islet cell tumors. *Radiographics* 2006; **26**: 453-464
11 **Birnbaum BA**, Hindman N, Lee J, Babb JS. Multi-detector row CT attenuation measurements: assessment of intra- and interscanner variability with an anthropomorphic body CT phantom. *Radiology* 2007; **242**: 109-119

S- Editor Cheng JX **L- Editor** Kerr C **E- Editor** Zheng XM

World Journal of Radiology

Online Submissions: http://www.wjgnet.com/esps/
wjr@wjgnet.com
doi:10.4329/wjr.v4.i7.328

World J Radiol 2012 July 28; 4(7): 328-334
ISSN 1949-8470 (online)

BRIEF ARTICLE

Evaluation of a handheld creatinine measurement device for real-time determination of serum creatinine in radiology departments

Stefan Haneder, Alexandra Gutfleisch, Claudia Meier, Joachim Brade, Dieter Hannak, Stefan O Schoenberg, Christoph R Becker, Henrik J Michaely

Stefan Haneder, Alexandra Gutfleisch, Claudia Meier, Stefan O Schoenberg, Henrik J Michaely, Institute of Clinical Radiology and Nuclear Medicine, University Medical Centre Mannheim, University of Heidelberg, 68167 Mannheim, Germany
Joachim Brade, Institute for Clinical Statistics, University Medical Centre Mannheim, University of Heidelberg, 68167 Mannheim, Germany
Dieter Hannak, Institute of Clinical Chemistry, University Medical Centre Mannheim, University of Heidelberg, 68167 Mannheim, Germany
Christoph R Becker, Institute of Clinical Radiology, Hospital Munich-Grosshadern, University of Munich, 81377 Munich, Germany
Author contributions: Haneder S, Gutfleisch A, Schoenberg SO, Becker CR and Michaely HJ participated in the study; and all authors contributed to supportive work.
Correspondence to: Stefan Haneder, MD, Institute of Clinical Radiology and Nuclear Medicine, University Medical Centre Mannheim, Heidelberg University, Thoedor-Kutzer-Ufer 1-3, 68167 Mannheim, Germany. stefan.haneder@umm.de
Telephone: +49-621-3832067 Fax: +49-621-3831910
Received: May 14, 2012 Revised: July 5, 2012
Accepted: July 12, 2012
Published online: July 28, 2012

Abstract

AIM: To assess the feasibility/accuracy of a commercial handheld device in the context of increased demand for point-of-care serum creatinine (SCr) determination.

METHODS: In this institutional review board-approved, prospective study, 401 patients referred for contrast-enhanced computed tomography were included at two centres. Capillary (c)SCr was determined using two devices A+B and venous (v)SCr was determined in the centre's laboratory. Method comparison statistics for both centres and for vSCr<>1.2 mg/dL, receiver operating characteristic analysis, negative predictive values (NPV), sensitivity and specificity were calculated pre-/post-curve offset correction with vSCr.

RESULTS: Pearson's coefficients for cSCr *vs* vSCr were: centre 1-A:0.93/B:0.92; centre 2-A:0.85/B:0.82 (all $P < 0.0001$). Overall correlation was better for vSCr > 1.2 mg/dL. The area under the receiver operating characteristic curves showed a high accuracy for cSCr, but the device underestimated SCr, which was confirmed by Bland-Altman plot. Addition of the offset correction factor to the original data from centre 1 resulted in an improvement in sensitivity for detecting patients at risk (> 1.2 mg/dL), whilst maintaining acceptable specificity and improving NPV.

CONCLUSION: This study showed the feasibility of SCr determination using the evaluated handheld device in a routine clinical setting. The device showed high sensitivity and high NPV, but may significantly underestimate SCr without offset correction to local laboratories.

Key words: Contrast-medium-induced nephropathy; Nephrogenic systemic fibrosis; Point of care testing; Serum creatinine determination; StatSensor

Peer reviewer: Dr. Kazushi Kishi, Department of Radiology, Wakayama Medical University, Kimiidera 811-1, Wakayama 641-8510, Japan

Haneder S, Gutfleisch A, Meier C, Brade J, Hannak D, Schoenberg SO, Becker CR, Michaely HJ. Evaluation of a handheld creatinine measurement device for real-time determination of serum creatinine in radiology departments. *World J Radiol* 2012; 4(7): 328-334 Available from: URL: http://www.wjgnet.com/1949-8470/full/v4/i7/328.htm DOI: http://dx.doi.org/10.4329/wjr.v4.i7.328

INTRODUCTION

Contrast-medium-induced nephropathy (CIN)[1] and nephrogenic systemic fibrosis (NSF)[2] are two potentially life-threatening complications of iodinated contrast agents and gadolinium-based contrast agents (GBCA), respectively, which have attracted increasing attention over the last few years. In particular, patients with impaired renal function are at a high risk of developing CIN or NSF. Serum creatinine (SCr) is an important surrogate parameter for renal function and thus offers an opportunity for risk stratification by detecting patients at risk. The new European Medicines Agency guidelines also require mandatory SCr testing for some GBCA[3].

CIN occurs, especially in patients with heavily impaired renal function, after the application of iodinated contrast agents, e.g., in computed tomography (CT) or catheter angiography and leads to a significant increase in mortality and morbidity[4]. CIN is defined as a temporary percentage increase in SCr of more than 25% or as an absolute increase in SCr of more than 0.5 mg/dL in the first 24 h and up to 5 d after contrast medium application. The incidence of CIN in the general population is estimated to be 1%-2%, whereas up to 70% of patients with severe chronic kidney disease are at risk of developing clinically significant CIN[5]. A direct relationship with increased length of hospitalisation, cost and long-term morbidity has been reported. For those patients who require dialysis, a 30% in-hospital mortality rate and 80% 2-year mortality rate can be expected[6]. The first step in the prevention of CIN is therefore to identify patients at risk.

NSF is a rare systemic fibrosing disorder that was first described in the literature in 2000[2]. Currently, there are at least 500 recorded cases worldwide. The first cases were observed in 1997. Occurring almost exclusively in patients with heavily impaired renal function, NSF shows a very heterogeneous clinical appearance ranging from indurations of the skin as a hallmark of the disease to rare and potentially fatal cardiac fibrosis[7,8]. The reported 24-mo mortality rate of NSF was found to be between 20% and 48%. A causative relationship between GBCA and NSF has not been proven but seems likely at this time[9]. There is no consistent successful treatment for NSF.

Consequently, the determination of renal function before contrast-enhanced CT or magnetic resonance imaging (MRI) examinations or interventions is mandatory. A surrogate parameter for renal function in widespread use is SCr in conjunction with the modification of diet in renal disease (MDRD) formula to assess the estimated glomerular filtration rate (eGFR)[10]. Clinical laboratories can provide SCr values within approximately one hour, which is sufficient for scheduled examinations, e.g., inpatients, but insufficient for outpatients and emergency patients. Furthermore, routine blood sampling from outpatients seems inappropriate due to invasiveness, disruption of the workflow, waiting time and additional expense. The immediate availability of SCr values for patients in radiology with a non-specific history concerning potentially impaired renal function should foster patient safety and an improved workflow in radiology. Recently, a new handheld device for the determination of SCr and estimation of the eGFR, called StatSensor™ Creatinine (NovaBiomedical, Waltham, MA, United States) has become commercially available[11,12]. The aim of this study was to assess the feasibility of its broad clinical application in a radiology department and the accuracy of SCr measurements and estimation of the GFR in daily point-of-care testing compared with standard laboratory diagnostics.

MATERIALS AND METHODS

Ethic statement and patients

After approval of the local Institutional Review Board and informed written consent was obtained, 401 consecutive patients scheduled for contrast-enhanced CT were included in this prospective study performed at two large university hospitals: the Institute of Clinical Radiology and Nuclear Medicine, University Medical Centre Mannheim (referred to as centre 1) and the Institute of Clinical Radiology-Grosshadern, Munich (referred to as centre 2). Two hundred and one consecutive patients were included in centre 1 (127 male, 74 female; mean age = 62 ± 15 years; mean weight = 77.3 ± 18.1 kg) and 200 consecutive patients were included in centre 2 (127 male, 73 female, mean age = 62 ± 13 years; mean weight = 77.7 ± 14.9 kg).

Blood sampling

For the purpose of the determination and comparison of SCr values, three different SCr measurements were performed for each patient: two capillary (cSCr - StatSensor™) and one venous blood sample (vSCr - laboratory reference). The capillary blood (3-6 μL) was obtained by a small lancet puncture in the fingertip. The two capillary samples were performed as point-of-care testing, using two different handheld StatSensor™ devices (referred to as A and B) in each study centre, to allow measurement of interdevice agreement. As the patients already had venous access for GBCA administration, this access was used to draw blood for the venous blood sample (5 mL). SCr of the venous blood samples (vSCr) was determined by the local hospital laboratory.

Methods of creatinine determination and correction

The laboratory gold standard for SCr measurement is the Jaffé method, a colorimetric assay, which measures the reaction between creatinine and picric acid and can be accomplished using commercially available autoanalysers. The laboratories at the study centres were equipped with the following autoanalysers based on a device-specific modified Jaffé method: Siemens Dimension RXL (Siemens Healthcare, Erlangen, Germany) at centre 1 and Olympus AU2700 (Olympus, Tokio, Japan) at centre 2.

The technology of the creatinine handheld device is based on a different, enzymatic amperometric pathway:

first creatinine is hydrolysed in creatine (catalysed by the enzyme creatinine amidohydrolase) and then hydrolysed to sarcosine (catalysed by amidinohydrolase). The oxidation of sarcosine (catalysed by sarcosine oxidase) produces hydrogen peroxide which oxidises the terminal indicator (Fe^{3+}) at the working electrode to produce a current. This current, measured electrochemically, is proportional to the creatinine concentration in the sample. This method was standardised by Nova Biomedical against a laboratory enzymatic method (Vitros Kodak DT60; Ortho-Clinical Diagnostics, Rochester, NY, United States)[13]. The handheld device (360 g, 15.3 mm × 82.5 mm × 46 mm; Nova Biomedical, Boston, MA, United States) allows the measurement of SCr level within a range of 0.3-12 mg/dL and calculation of the GFR in about 30 s. Therefore, a small capillary blood sample of a few microlitres is sufficient.

Because of the lack of standardisation between the methodologies for creatinine determination in the laboratories and the thereby likely bias of the results, a re-evaluation of the obtained data was planned for centre 1. To evaluate, and if applicable, correct this bias a follow-up assessment was undertaken to calculate and implement a curve offset for the handheld device in order to standardise with the Siemens Dimension RXL used in the clinical laboratory at centre 1. Therefore, a method correlation and curve offset were calculated using the original data from centre 1 generated from the patient evaluation. The curve offset implemented was then added as a correction factor to the original data and the data re-analysed.

Statistical analysis

For statistical analyses, SAS 9.1 (Cary, NC, United States) and Microsoft Excel 2007 (Redmond, WA, United States) were used. The normal distribution of the data was confirmed beforehand by a Kolmogorov-Smirnov test. Descriptive statistical analyses of the creatinine determinations were performed including means and standard deviations for cSCR, vSCr and the differences. Throughout the entire analysis, statistical significance was assumed at $P < 0.05$. Further statistical analyses were subdivided into different parts. First, the correlations between the two determination methods (cSCr *vs* vSCr) were assessed with regard to statistical significance by Pearson's correlation coefficients (r). Subgroup-wise analyses (stratified by centre, creatinine level and gender) were also performed. The cut-off for patients with a normal creatinine level was vSCr = 1.2 mg/dL (laboratory reference); higher values were considered to indicate renal impairment. Additionally, the correlation between cSCr and vSCr was assessed by linear regression. The linear regression is presented figuratively as a scatter plot, regression equation and correlation coefficient. Second, the agreement between the two methods was analysed. Therefore, to visualise the agreement, Bland-Altman plots were performed. The Bland-Altman plot shows the deviation between the two methods with different SCr levels. The red line indicates the average value of the differences between the two methods; the two yellow lines form the 95% reference range. Furthermore, paired t-tests and the corresponding mean difference confidence interval approach were used to assess deviations in the location of the two methods; the test procedure of Maloney and Rastogi was used for comparison of precision in paired data. Third, to estimate the accuracy of cSCr measured by the handheld device, receiver operating characteristics (ROC) analyses were performed. Fourth, to test the congruence of cSCr determination between the two handheld devices used (A/B), Pearson's correlation coefficients and the test of Maloney and Rastogi were performed. In order to correct the bias between the two methods, the patient data from centre 1 were re-assessed after implementation of a curve offset correction. Slope and y-axis offset correction factors were computed. After applying the offset correction factor, the correlation and agreement between the two methods and the agreement between the two devices were re-analysed. Finally, before and after implementing the curve offset, sensitivity, specificity, positive and negative predictive values (PPV and NPV) were calculated for the cut-off level of 1.2 mg/dL.

RESULTS

All measurements were performed successfully. The means, standard deviations of cSCr (StatSensor™), vSCr (laboratory reference) and the differences between these two methods, for the two devices and for both centres before and after offset correction are summarised in Table 1. In a comparison of the two methods, the handheld device underestimated SCr compared with the laboratory reference in both study centres, which was confirmed by the Bland-Altman plot (Figure 1D). In centre 1, the Pearson correlation coefficient of cSCr *vs* cSCr was higher than in centre 2: $r = 0.93$ for handheld device A ($P < 0.0001$) in centre 1, $r = 0.92$ for handheld device B ($P < 0.0001$) (mean correlation coefficient at centre 1: $r = 0.93$), centre 2 $r = 0.85$ for handheld device A ($P < 0.0001$) and $r = 0.82$ ($P < 0.0001$) for handheld device B (mean correlation coefficient at centre 2: $r = 0.84$). The stratification with regard to gender revealed a slightly higher correlation for male patients (Table 2). The subgroup-wise analysis as a mean for both centres for a vSCr > 1.2 mg/dL showed a better correlation (device A 0.91, $P < 0.0001$ and device B 0.90, $P < 0.0001$) compared with vSCr values < 1.2 mg/dL (device A 0.66, $P < 0.0001$ and device B 0.59, $P < 0.0001$). The results of the linear regression corresponded to the Pearson correlation and are presented figuratively in Figure 1A for both centres and stratified for vSCr >< 1.2 mg/dL (Figure 1B, C). In the inter-method agreement, paired tests showed significant differences between cSCr and vSCr ($P < 0.0001$) in both centres (Table 2). Furthermore, the comparison of the precision of both methods showed significant differences ($P < 0.0001$, Table 1). The AUC values (area under the curve) of the ROC analysis for cSCr (centre 1: 0.915 (device A), 0.926 (device B) and centre 2: 0.919 [device A), 0.911 (device B)] demonstrated a high accuracy. The

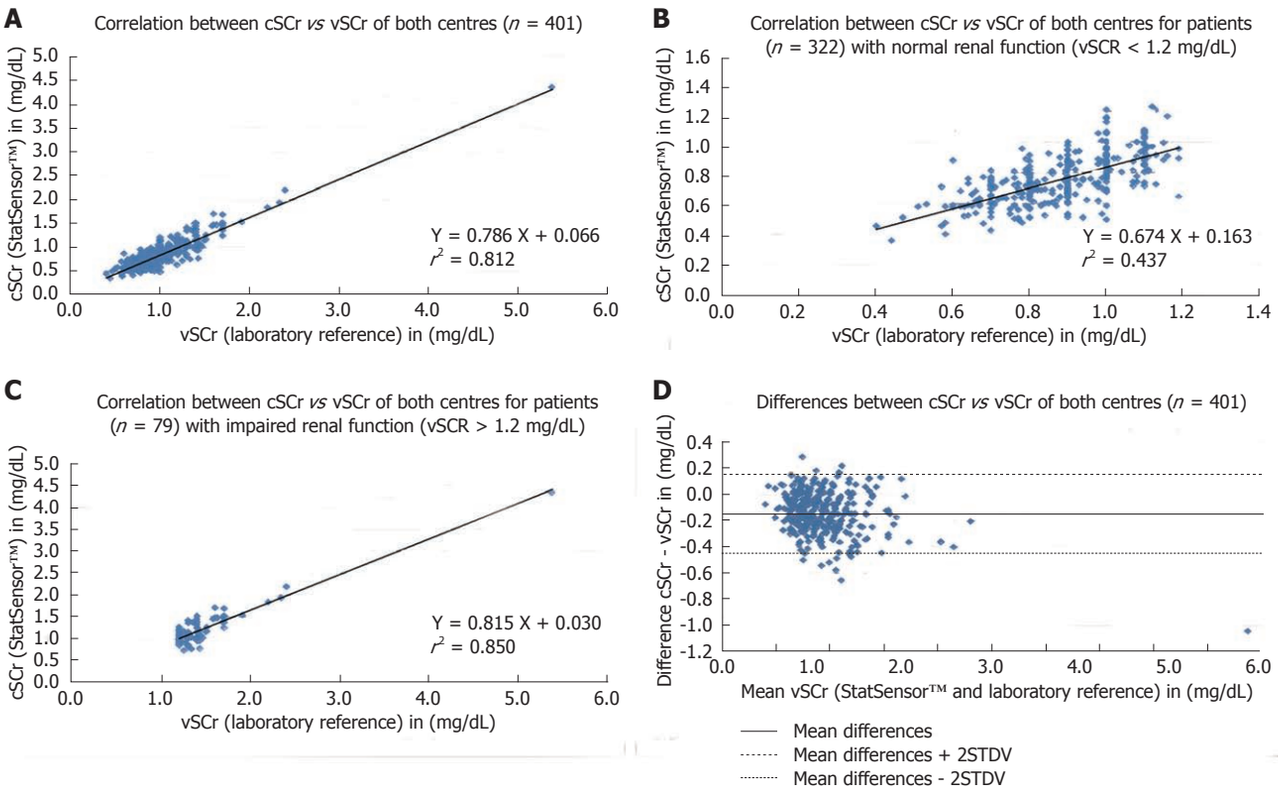

Figure 1 Scatter plots, regression equations and correlation coefficients for the correlation for capillary point-of-care serum creatinine *vs* venous point-of-care serum creatinine for both centres (A), for creatinine values below (B) and above (C) the cut-off-level of 1.2 mg/dL (venous point-of-care serum creatinine). The Bland-Altman plot for the differences between capillary point-of-care serum creatinine (cSCr) and venous point-of-care serum creatinine (vSCr) for both centres (D).

Table 1 Means, standard deviations, calculated difference between the measured serum creatinine level (mg/dL) using StatSensor™ creatinine and the laboratory reference, Pearson's correlation coefficients, paired *t*-test and Maloney-Rastogi test, subdivided by study centre, pre- and post-offset correction

			Centre 1	Centre 2	Mean (centre 1 + 2)	Pearson correlation coefficient	*P* value (paired *t*-test)	*P* value (Maloney-Rastogi-test)
StatSensor™								
cSCr	Pre offset	Device A	0.80 ± 0.34	0.89 ± 0.27	0.85 ± 0.31	Inter-device evaluation (Device A *vs* B)		
		Device B	0.81 ± 0.34	0.89 ± 0.26	0.85 ± 0.30	Center 1 = 0.97	Center 1 = 0.404	Center 1 = 0.480
		Difference between Device A *vs* B	-0.01 ± 0.09	0.00 ± 0.09		Center 2 = 0.95	Center 2 = 0.689	Center 2 = 0.521
		Mean (Device A + B)	0.80 ± 0.34	0.89 ± 0.26	0.85 ± 0.31			
	Post offset	Device A	0.97 ± 0.50					
		Device B	0.96 ± 0.50					
Laboratory reference								
vSCr			0.96 ± 0.42	1.02 ± 0.26	0.99 ± 0.35	Inter-method evaluation (cSCr *vs* vSCr)		
Difference								
cSCr - vSCr	Pre offset	Mean (Device A + B)	-0.16 ± 0.16[a]	-0.14 ± 0.15[b]	-0.15 ± 0.15[c]		< 0.0001[a,b,c]	< 0.0001[a,c]; 0.9962[b]
		Device A	-0.16 ± 0.16			0.93	< 0.0001	< 0.0001
		Device B	-0.15 ± 0.17			0.92	< 0.0001	< 0.0001
	Post offset	Device A	0.01 ± 0.19			0.93	0.638	< 0.0001
		Device B	0.00 ± 0.20			0.92	0.955	< 0.0001

cSCr: Capillary serum creatinine; vSCr: Venous serum creatinine.

inter-device agreement in both study centres was excellent ($P < 0.0001$, Table 1).

Re-assessment of the data from centre 1 revealed the following results. For device A, a slope correction factor of 1.45 and of 1.46 for device B was calculated. The y-axis correction factor was 0.193 (device A) and 0.215

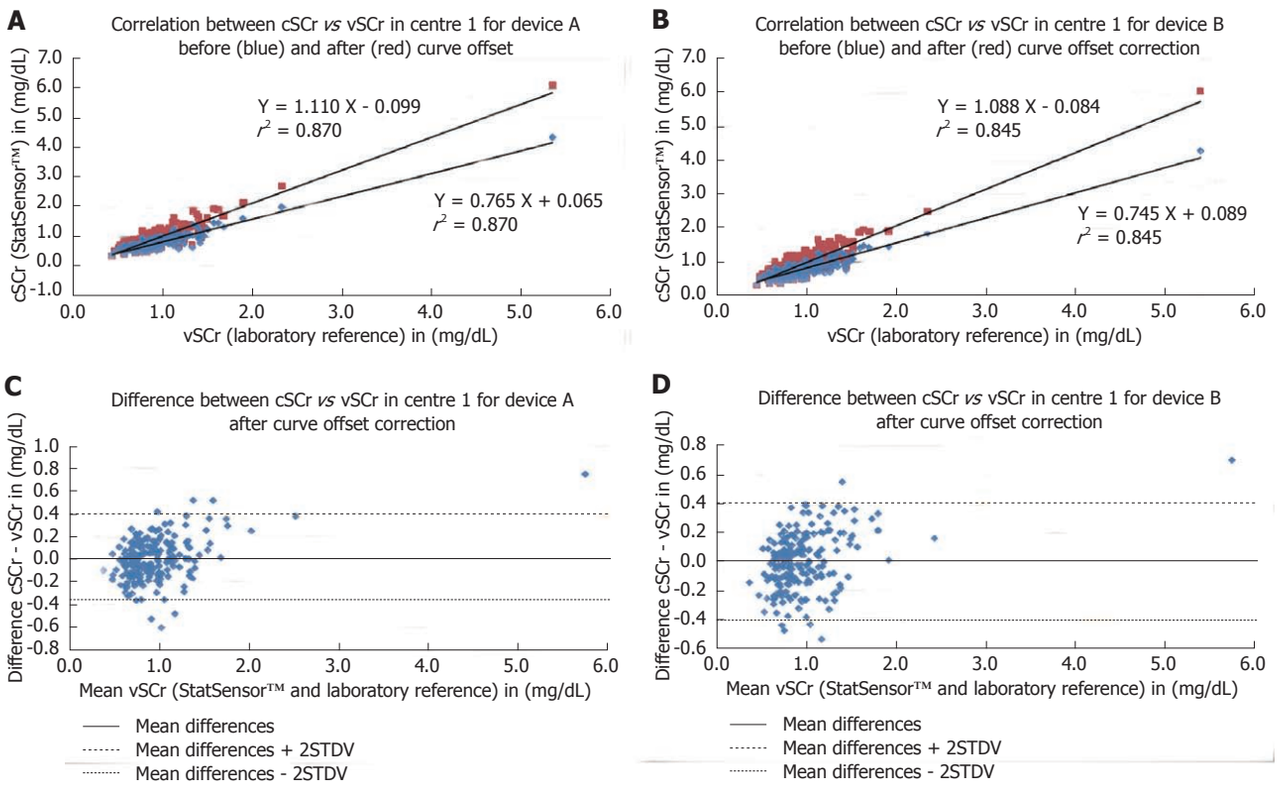

Figure 2 Scatter plots, regression equations and correlation coefficients for the correlation for capillary point-of-care serum creatinine *vs* venous point-of-care serum creatinine for centres 1 and device A (A) and device B (B), each before and after implementation of the offset correction. C: The Bland-Altman plot for the differences between capillary point-of-care serum creatinine (cSCr) and venous point-of-care serum creatinine (vSCr) for centre 1 and device A after curve offset correction; D: The Bland-Altman plot for the differences between cSCr *vs* vSCr for centre 1 and device B after curve offset correction.

Table 2 Pearson's correlation coefficients for creatinine values measured using the laboratory reference (venous serum creatinine) and StatSensor™ creatinine, subdivided by study centre, renal function and gender

vSCr (laboratory) *vs*	cSCr (StatSensor™)		Overall
	Device A	Device B	
Study centre			
Centre 1	0.93	0.92	0.93
Centre 2	0.85	0.82	0.84
Overall	0.90	0.88	0.89
Renal function			
vSCr < 1.2 mg/dL	0.66	0.59	0.63
vSCr > 1.2 mg/dL	0.91	0.90	0.91
Gender			
Male	0.91	0.89	0.90
Female	0.81	0.78	0.80

cSCr: Capillary serum creatinine; vSCr: Venous serum creatinine.

(device B). Consequently, the correlation for vSCr *vs* cSCr for both devices improved after implementation of the offset correction. The regression graph showed an approximation to the graph with the equation y = x (Figure 2A, B). After applying the offset correction, no change in the correlation coefficient for device A and B (Figure 2A, B) was observed, but a minimisation of the percentage bias between the two methods was achieved (Table 3). The previous significant differences in the paired *t*-test for the agreement between the two methods were non-significant after the offset correction (Table 4). No significant changes were found for the Pearson correlation coefficient and the Maloney-Rastogi testing. Addition of the offset correction factor to the original data from centre 1 resulted in an improvement in the sensitivity (device A: 35.48% to 80.65%; device B: 41.94% to 70.97%) for detecting patients at risk (> 1.2 mg/dL), whilst maintaining acceptable specificity (device A: 99.41% to 98.26%; device B: 99.41% to 94.12%). Furthermore, the NPV improved (device A: 89.42% to 96.57%; device B: 90.37% to 94.67%).

DISCUSSION

Chronic renal disease is a widespread problem, which can lead to potential life-threatening complications (CIN/NSF) after the administration of iodinated contrast agents, e.g., in the framework of CT or cardiology procedures and of GBCA in MRI. Particularly, in emergency and out-patients who often lack available laboratory values and clinical history, an estimation of the glomerular filtration rate from SCr level would be helpful. In such clinical situations requiring rapid decision-making based on renal function, a rapid SCr determination could identify patients at risk and lead to a different treatment procedure. For the prevention of CIN and of NSF, the assessment of renal function is recommended or rather mandatory[3,14,15], due to the limited treatment options. Our study showed the feasibility of creatinine

Table 3 Results of the re-analysed data from centre 1 (n = 201), shown pre- and post-implementation of the curve offset, separated for the two devicespre- and post-offset correction

	Device	Slope	Intercept (mg/dL)	r^2	Mean difference (mg/dL) (method-difference)	STDV of differences (method-difference)	% bias
Pre offset	A	0.765	0.065	0.870	-0.16	0.16	-15.54
	B	0.745	0.089	0.845	-0.16	0.17	-14.76
Post offset	A	1.110	-0.099	0.870	0.01	0.19	0.39
	B	1.088	-0.084	0.845	0.00	0.20	-0.02

The results are given as slope, intercept, mean difference, standard deviation and percentage bias.

Table 4 Sensitivity, specificity, positive predictive value, negative predictive value and mean values for the cut-off value of 1.2 mg/dL, of the re-analysed data from centre 1 (n = 201), shown pre- and post-implementation of the curve offset, separated for the two devices (%)

	Device	Sensitivity	Specificity	PPV	NPV
Pre offset	A	35.48	99.41	91.67	89.42
	B	41.94	99.41	92.86	90.37
Post offset	A	80.65	98.26	89.29	95.57
	B	70.97	94.12	68.75	94.67
	Mean (A + B)	77.42	94.71	72.37	95.83

PPV: Positive predictive values; NPV: Negative predictive values.

determination using the new handheld device (StatSensor ™) in a routine clinical setting in the radiology departments of two large university hospitals. The comparison demonstrated a significant correlation between the capillary measurements of the handheld device StatSensor™ and the venous laboratory reference method. In centre 1, the correlation was slightly higher than in centre 2 (r = 0.93 *vs* r = 0.84), which can potentially be explained by the two different laboratory autoanalysers and/or by the different handheld devices used. The method correlation in both centres was apparently better for normal renal function (vSCr ⩾ 1.2 mg/dL; r = 0.91) compared with impaired renal function (r = 0.63). This inaccuracy for lower SCr values was recently described for the Jaffé method[16]. StatSensor™ yielded significantly lower values throughout and significant differences were found in the agreement between the two methods. Nevertheless, the measurements of the StatSensorc seem to be reliable because the inter-device agreement was excellent. After implementation of the curve offset correction, the data for centre 1 were re-analysed and showed a significantly improved correlation between the two methods. No statistically significant differences with the paired t-test were observed, however, significant differences in the precision (Maloney and Rastogi-test) remained. In addition to minimisation of bias, the NPV and PPV improved and were higher than the laboratory reference. Although maintaining high specificity, the curve offset correction led to high sensitivity and NPV for patients at risk (> 1.2 mg/dL). Due to the higher sensitivity and NPV, the discrimination between normal and impaired renal function improved.

To date, only a small number of studies have evaluated the accuracy of the new handheld device[11,12,17,18], however, similar results have been described, although Aumatell *et al*[17] and Korpi-Steiner *et al*[18] used an enzymatic reference method and venous full blood for StatSensor™. To our knowledge, our study is the first to use a colorimetric reference laboratory method. However, negative differences between SCr determinations using StatSensor™ compared with the enzymatic laboratory reference were also described in our study. Schnabl *et al*[11] also observed a good correlation for whole blood creatinine compared with laboratory plasma measurements (r^2 = 0.933), but described a negative proportional bias. In an in vitro study, high levels of creatine and urea falsely elevated creatinine measurement. The evaluation of StatSensor™ by Shephard *et al*[12] compared with an enzymatic laboratory reference in 100 patients confirmed our results of a statistically significant underestimation of SCr. These authors also used an alignment with the laboratory results. They found that for eGFRs above or below 60 mL/min, 100% and 87% of the results, respectively, agreed with the laboratory eGFR (79% and 96% post-alignment). Similar to our results, Shephard *et al*[12] concluded that the handheld device will identify most patients with an eGFR < 60 mL/min, but there will be many false undereGFR results that require laboratory validation.

Potential limitations of this study were, as mentioned above, the different autoanalysers used in the two study centres, which may partially explain the different results. A further problem was the lack of standardisation between the methods, which hampered comparability. The general limitations of SCr evaluation (e.g., late rise from about 50% renal function) are widely known and are not discussed here. The standardisation could be improved by calculating the GFR using the MDRD formula[10]. The differences between the laboratory reference method and the handheld device could be based on the known bias of the colorimetric Jaffé method *vs* enzymatic methods, which result in systematically higher creatinine values due to non-creatinine chromogens[19,20]. However, corresponding to this bias it seems to be mandatory to analyse potential interfering substances using the StatSensor™ in a larger patient population. Furthermore, to achieve a higher validity for the decision-making cut-off range of creatinine values, a larger collective should be included in a further study. In our study, the number of patients at risk with elevated creatinine values was relatively small

for adequate evaluation. Finally, the curve offset correction significantly improved the results, but did not actually represent the real performance of the StatSensor™ handheld device.

In conclusion the StatSensor™ seems to be a rapid, cost-effective method for the determination of SCr with a high sensitivity and NPV. This could contribute to improving the workflow in a radiology department, especially in patients with an unknown history of renal diseases. The high sensitivity and NPV predict the differentiation between normal *vs* impaired renal function. However, without offset correction to the local specific laboratory, StatSensor™ may significantly underestimate SCr and should be corrected technically.

COMMENTS

Background

Contrast-medium-induced nephropathy (CIN) and nephrogenic systemic fibrosis (NSF) are two potentially life-threatening complications of iodinated contrast agents and gadolinium-based contrast agents (GBCA). According to increased requests over the last few years, the demand for point-of-care serum creatinine (SCr) determination in radiology departments has increased.

Research frontiers

Before implementing a decision-making, commercially available handheld device (StatSensor™) into clinical practice, the feasibility and accuracy of the device need to be tested in a large collective in the daily routine of a radiology department. This study showed the feasibility of serum creatinine (SCr) determination using this handheld device in a routine clinical setting. The device showed high sensitivity and high negative predictive value, but may significantly underestimate SCr without offset correction to local laboratories.

Innovations and breakthroughs

Recent reports have highlighted the importance of possible point-of-care determination of SCr in radiology departments. To the knowledge, the study is the first to compare StatSensor™ with a colorimetric reference laboratory method. The method correlation was apparently better for normal renal function than for impaired renal function. StatSensor™ yielded significantly lower values throughout and significant differences were found in the agreement between the methods. Nevertheless, the measurements using StatSensor™ seem to be reliable as the inter-device agreement was excellent. After implementation of the curve offset correction, the data showed a significant improvement in the correlation between the two methods.

Applications

By knowing the strengths and the potential pitfalls in the determination of SCr using the handheld device (StatSensor™), this may represent a future strategy for point-of-care testing of patients undergoing contrast-enhanced computed tomography (CT) or magnetic resonance imaging (MRI).

Terminology

CIN and CT are two complications of iodinated contrast agents and GBCA (MRI). Both are associated with impaired kidney function, and therefore the a priori determination of SCr is crucial in patients at risk.

Peer review

This is an interesting and critical report. It is a well written scientific paper.

REFERENCES

1 **Mehran R**, Nikolsky E. Contrast-induced nephropathy: definition, epidemiology, and patients at risk. *Kidney Int Suppl* 2006; (100): S11-S15

2 **Cowper SE**, Robin HS, Steinberg SM, Su LD, Gupta S, LeBoit PE. Scleromyxoedema-like cutaneous diseases in renal-dialysis patients. *Lancet* 2000; **356**: 1000-1001

3 **European Medicines Agency.** Questions and answers on the review of gadolinium-containing contrast agents. 2010. Available from: URL: http://www.emea.europa.eu/docs/en_GB/document_library/Referrals_document/gadolinium_31/WC500015635.pdf

4 **McCullough PA**, Adam A, Becker CR, Davidson C, Lameire N, Stacul F, Tumlin J. Epidemiology and prognostic implications of contrast-induced nephropathy. *Am J Cardiol* 2006; **98**: 5K-13K

5 **Hou SH**, Bushinsky DA, Wish JB, Cohen JJ, Harrington JT. Hospital-acquired renal insufficiency: a prospective study. *Am J Med* 1983; **74**: 243-248

6 **McCullough PA**, Sandberg KR. Epidemiology of contrast-induced nephropathy. *Rev Cardiovasc Med* 2003; **4** Suppl 5: S3-S9

7 **Shellock FG**, Spinazzi A. MRI safety update 2008: part 1, MRI contrast agents and nephrogenic systemic fibrosis. *AJR Am J Roentgenol* 2008; **191**: 1129-1139

8 **Cowper SE**, Rabach M, Girardi M. Clinical and histological findings in nephrogenic systemic fibrosis. *Eur J Radiol* 2008; **66**: 191-199

9 **Cowper SE**. Nephrogenic systemic fibrosis: a review and exploration of the role of gadolinium. *Adv Dermatol* 2007; **23**: 131-154

10 **Levey AS**, Bosch JP, Lewis JB, Greene T, Rogers N, Roth D. A more accurate method to estimate glomerular filtration rate from serum creatinine: a new prediction equation. Modification of Diet in Renal Disease Study Group. *Ann Intern Med* 1999; **130**: 461-470

11 **Schnabl KL**, Bagherpoor S, Diker P, Cursio C, Dubois J, Yip PM. Evaluation of the analytical performance of the Nova StatSensor creatinine meter and reagent strip technology for whole blood testing. *Clin Biochem* 2010; **43**: 1026-1029

12 **Shephard M**, Peake M, Corso O, Shephard A, Mazzachi B, Spaeth B, Barbara J, Mathew T. Assessment of the Nova StatSensor whole blood point-of-care creatinine analyzer for the measurement of kidney function in screening for chronic kidney disease. *Clin Chem Lab Med* 2010; **48**: 1113-1119

13 **Rao LV**, Jakubiak F, Sidwell JS, Winkelman JW, Snyder ML. Accuracy evaluation of a new glucometer with automated hematocrit measurement and correction. *Clin Chim Acta* 2005; **356**: 178-183

14 **Cowper SE**. Nephrogenic systemic fibrosis: an overview. *J Am Coll Radiol* 2008; **5**: 23-28

15 **Schweiger MJ**, Chambers CE, Davidson CJ, Blankenship J, Bhalla NP, Block PC, Dervan JP, Gasperetti C, Gerber L, Kleiman NS, Krone RJ, Phillips WJ, Siegel RM, Uretsky BF, Laskey WK. Prevention of contrast induced nephropathy: recommendations for the high risk patient undergoing cardiovascular procedures. *Catheter Cardiovasc Interv* 2007; **69**: 135-140

16 **Panteghini M**. Enzymatic assays for creatinine: time for action. *Clin Chem Lab Med* 2008; **46**: 567-572

17 **Aumatell A,** Sharpe D, Reed W. Validation of the StatSensor Creatinine Meter for Testing Blood Before Contrast Computed Tomography Studies. *Point of Care* 2000; **9:** 25-31

18 **Korpi-Steiner NL**, Williamson EE, Karon BS. Comparison of three whole blood creatinine methods for estimation of glomerular filtration rate before radiographic contrast administration. *Am J Clin Pathol* 2009; **132**: 920-926

19 **Apple F**, Bandt C, Prosch A, Erlandson G, Holmstrom V, Scholen J, Googins M. Creatinine clearance: enzymatic vs Jaffé determinations of creatinine in plasma and urine. *Clin Chem* 1986; **32**: 388-390

20 **Badiou S**, Dupuy AM, Descomps B, Cristolead JP. Comparison between the enzymatic vitros assay for creatinine determination and three other methods adapted on the Olympus analyzer. *J Clin Lab Anal* 2003; **17**: 235-240

S- Editor Cheng JX **L- Editor** Webster JR **E- Editor** Xiong L

World Journal of Radiology

Online Submissions: http://www.wjgnet.com/esps/
wjr@wjgnet.com
doi:10.4329/wjr.v4.i7.335

World J Radiol 2012 July 28; 4(7): 335-340
ISSN 1949-8470 (online)

CASE REPORT

Bipolar radiofrequency ablation of tibialchondroblastomas: A report of three cases

Prathiba Rajalakshmi, Deep N Srivastava, Shishir Rastogi, Pramod Kumar Julka, Sushma Bhatnagar, Shivanand Gamanagatti

Prathiba Rajalakshmi, Deep N Srivastava, Shivanand Gamanagatti, Department of Radiodiagnosis, All India Institute of Medical Sciences, New Delhi 110029, India
Shishir Rastogi, Department of Orthopedics, All India Institute of Medical Sciences, New Delhi 110029, India
Pramod Kumar Julka, Department of Radiotherapy, All India Institute of Medical Sciences, New Delhi 110029, India
Sushma Bhatnagar, Department of Anaesthesiology, All India Institute of Medical Sciences, New Delhi 110029, India
Author contributions: Prathiba P analysed the data and prepared the manuscript; Srivastava DN performed the work; Rastogi S and Julka PK made clinical contributions; Bhatnagar S analysed the data; and Gamanagatti S performed the work and preparedthe manuscript.
Correspondence to: Dr. Shivanand Gamanagatti, MD, Associate Professor, Department of Radiodiagnosis, All India Institute of Medical Sciences, New Delhi 110029, India. shiv223@rediffmail.com
Telephone: +91-11-26864851 Fax: +91-11-26862663
Received: April 13, 2012 Revised: May 19, 2012
Accepted: May 26, 2012
Published online: July 28, 2012

Abstract

Chondroblastoma is a rare benign cartilaginous neoplasm of bone. The recurrence rate is high and complications are frequent following open curettage with bone grafting which is the standard treatment forchondroblastomas. We performed radiofrequency ablation in three cases of tibialchondroblastoma using the bipolar system. One patient experienced residual pain for which repeat ablation was performed. No other complications were observed during follow-up. Radiofrequency ablation may offer an effective alternative for the treatment of selected cases of chondroblastoma. The lesion characteristics which are likely to influence treatment outcome and the advantages offered by the bipolar system are discussed.

Key words: Bipolar; Chondroblastoma; Radiofrequency ablation

Peer reviewers: Adnan Kabaalioglu, MD, Professor, Department of Radiology, Akdeniz University Hospital, Antalya 07059, Turkey; John L Nosher, MD, Clinical Professor, Chairman, Department of Radiology, University of Medicine and Dentistry of New Jersey-Robert Wood Johnson Medical School, 1 Robert Wood Johnson Place, PO Box 19, Medical Education Bldg., Room 404, New Brunswick, NJ 08903-0019, United States

Prathiba R, Srivastava DN, Rastogi S, Julka PK, Bhatnagar S, Gamanagatti S. Bipolar radiofrequency ablation of tibialchondroblastomas: A report of three cases. *World J Radiol* 2012; 4(7): 335-340 Available from: URL: http://www.wjgnet.com/1949-8470/full/v4/i7/335.htm DOI: http://dx.doi.org/10.4329/wjr.v4.i7.335

INTRODUCTION

Chondroblastomas are uncommon bone tumours of cartilaginous origin, accounting for less than 1% of all primary bone tumours. They are commonly seen in children and young adults, usually before the age of epiphyseal closure and are classically located in the epiphysis and apophysis of long bones[1]. Affected individuals usually present with pain and restriction of movement of the adjacent joint. Surgical curettage with or without bone grafting/cementing has been the treatment of choice for chondroblastomas and the risk of recurrence following surgery is high ranging from 10% to 35%[2]. Considering the epiphyseal location of the lesions, the risk of damage to articular cartilage and the growth plate with subsequent development of premature degenerative changes and limb shortening, respectively, is high[3].

Due to its minimally invasive nature and high success rates, radiofrequency (RF) ablation has become the treatment of choice for osteoid osteoma and is being increasingly used as palliative treatment for bone metastasis. It

is also being evaluated in other benign bone tumours and recently, a few studies have described its effectiveness in the treatment of chondroblastomas[3-6]. In this article, we report three cases of chondroblastoma treated using the bipolar RF ablation system.

The study was approved by our institutional ethics committee. The decision to proceed with RF ablation over open surgery was taken in consensus with the orthopaedic surgeons taking into account the lesion size, location and potential surgical morbidity.

CASE REPORT

Case 1

A 14-year-old male presented with pain in the left knee for the past 18 mo which was partially relieved with analgesics. The Visual Analogue Scale (VAS) score was 7. Radiograph and computed tomography (CT) images of the left knee revealed a 1.6 cm × 1.4 cm × 1.0 cm geographic lytic lesion with sclerotic margins in the left tibial epiphysis. There was associated thinning of the articular bone. The growth plate was open and the lesion was abutting the physis without breaching it. The lesion was hypointense on T1W images and heterogeneously hyperintense on T2W images with associated bone marrow oedema and mild joint effusion. A diagnosis of chondroblastoma was presumed based on the clinical profile and the characteristic location and imaging appearance of the lesion.

RF ablation was performed under general anaesthesia and CT guidance (Somatom Sensation 40 slice CT scanner, Siemens, Erlangen, Germany). Thin axial sections were acquired for precise localisation of the lesion. An 11 G bone biopsy needle set (Osteo Site, COOK Medical, Bloomington, United States) and a hammer were used to gain lesion access. An 18 G bipolar RF applicator with a 15 mm exposed tip (CelonProSurge Micro, Celon AG Medical Instruments, Teltow, Germany) and a bipolar/multipolar RF power generator (CelonLab POWER, Celon AG Medical Instruments, Teltow, Germany) were used for the ablation procedure. Since a bipolar RF system was used, grounding pads were not required for heat dispersion. As recommended by the manufacturers, pulsed RF energy was applied at a power setting of 5 W until a total energy of 0.90 KJ was deposited. As claimed by the manufacturers, the RF electrode produced an ablation zone of approximately 10 mm in diameter. Repeat ablation was performed after repositioning the needle so as to encompass the entire lesion. No immediate complications were observed. Analgesics and antibiotics were prescribed and the patient was discharged the next day. Since the lesion was located along a weight-bearing surface, the patient was instructed to restrain from strenuous/weight-bearing activities for 1-2 mo. A core biopsy specimen of the lesion obtained at the time of the procedure showed histopathological features consistent with chondroblastoma.

The patient experienced complete pain relief 1-2 d after the procedure (VAS = 0) and remained asymptomatic during the follow-up period (18 mo). Follow-up imaging (radiograph and CT) obtained at 6 mo showed increased matrix ossification with no significant change in lesion size. No delayed complications were observed. The pre-procedural, procedural and follow-up CT images of the patient are presented in Figure 1.

Case 2

A 12-year-old female presented with severe pain in the left knee for the past year (VAS = 8) which was partially relieved with analgesics. Plain radiograph and CT images of the left knee showed a geographic lytic lesion with sclerotic margins of approximately 2.5 cm × 2.1 cm × 2.0 cm in size in the proximal epiphysis of the left tibia. The growth plate was open and breached and the lesion extended into the metaphysis. The overlying subchondral bone was significantly thinned. A diagnosis of chondroblastoma was presumed considering the clinical and imaging presentation which was confirmed histopathologically from the core biopsy specimen obtained during the procedure. RF ablation was performed in a similar manner to that in case 1 under general anaesthesia using an18G RF probe with a 15 mm active tip. A total of 3 ablations were performed at different needle positions to ensure adequate lesion coverage. The patient experienced complete pain relief (VAS = 0) 1-2 d after the procedure and remained asymptomatic during follow-up (17 mo). No further analgesic intake was required. No complications were observed. Pre-procedural and procedural images of the patient are shown in Figure 2.

Case 3

A 55-year-old female presented with severe pain and restriction of movement of the right knee joint for the past 2 years. The pain was increasing in severity over time and the VAS score at the time of presentation was 8. Radiograph and CT images of the right knee showed a 2.5 cm × 1.5 cm × 1.8 cm geographic lytic lesion with sclerotic margins in the proximal epiphysis of the right tibia. The lesion was hypointense on T1W images, homogeneously hyperintense on T2W images with associated mild joint effusion. There was thinning of the overlying subchondral bone. Although the age of the patient was atypical for chondroblastoma, the epiphyseal location of the lesion and its typical CT appearance favoured a diagnosis of chondroblastoma over other bone pathologies occurring in this location and RF ablation was chosen as the treatment option.

RF ablation was performed in a similar manner to that in the previous cases under general anaesthesia using the 18 G RF probe with a 15 mm exposed tip, and a total of 3 ablations were performed to adequately cover the lesion. Core biopsy of the lesion performed during the procedure confirmed the diagnosis of chondroblastoma. The patient continued to experience similar pain of reduced intensity (VAS 4-6) following the procedure. Follow-up CT imaging showed no obvious change in lesion appearance or the development of complications

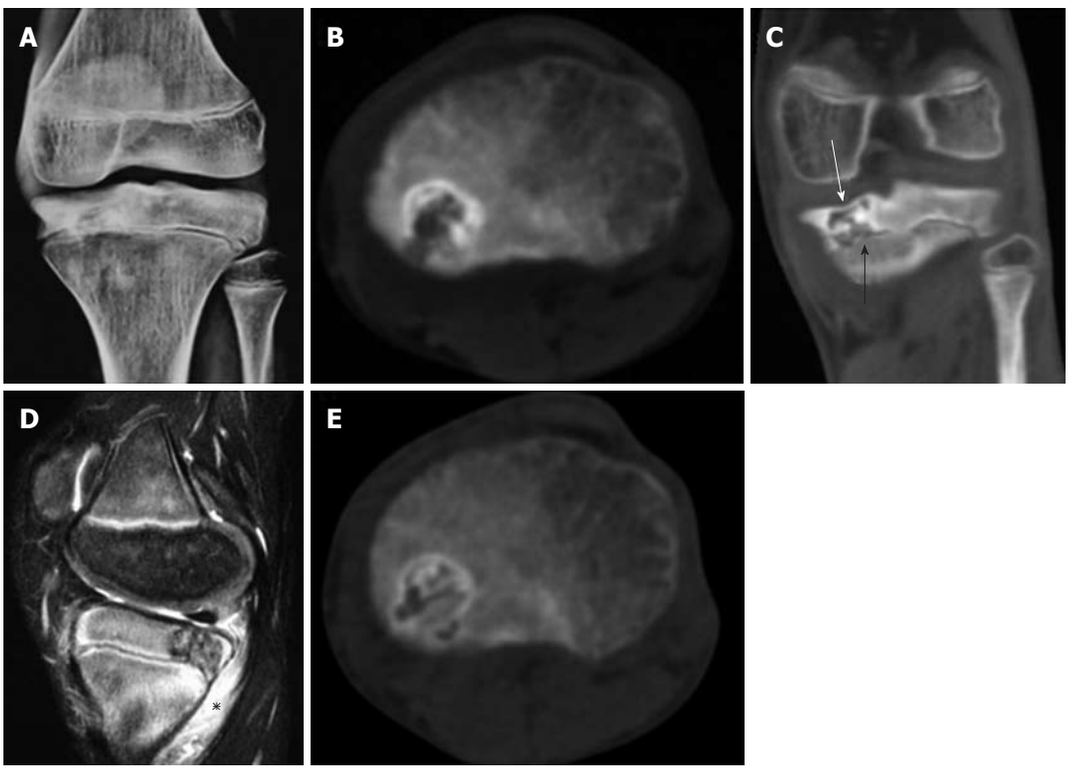

Figure 1 Chondroblastoma of the left tibia in a 14-year-old male. A, B: Plain radiograph and non-contrast computed tomography (NCCT) axial image show a geographic lytic lesion with sclerotic margins and foci of matrix calcification in the medial tibial epiphysis; C: NCCT coronal image shows thinning of the subchondral bone superiorly (white arrow) and extension of the lesion to thephyseal plate inferiorly (black arrow) which is non-fused; D: Sagittal short-tau inversion-recovery magnetic resonance (MR) image showing heterogeneous signal intensity of the lesion with surrounding bone marrow and soft tissue oedema (asterisk); E: Follow-up CT image after 6 mo showing increased mineralization of the matrix with no appreciable change in lesion size.

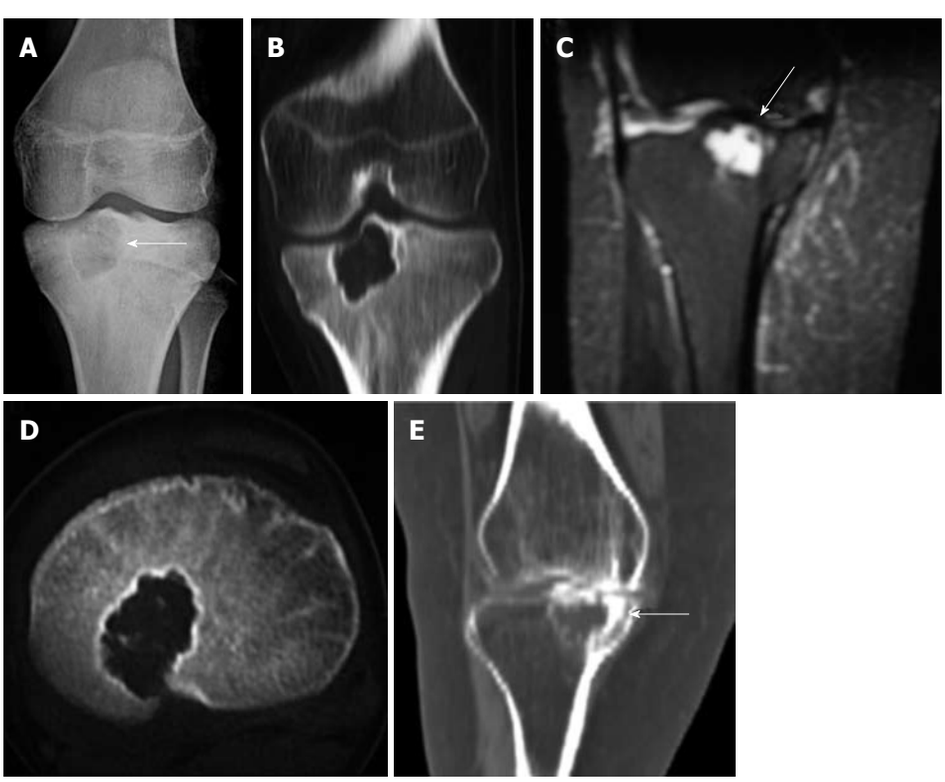

Figure 2 Chondroblastoma of the left tibia in a 13-year-old female. A, B: Frontal radiograph and axial computed tomography (CT) image of the left knee showing a geographic lytic lesion with sclerotic margins (arrow) involving the proximal epiphysis of the tibia; C: Coronal non-contrast computed resonance image showing the lesion with thinning of the subchondral bone superiorly (arrow) and extension of the lesion into the metaphysis inferiorly; D: CT image obtained at the time of the procedure showing the radiofrequency electrode placed in the lesion. Access tracks from a prior biopsy are also seen; E: Follow-up image after 6 mo showing increased mineralizaion of the matrix with no appreciable change in lesion size.

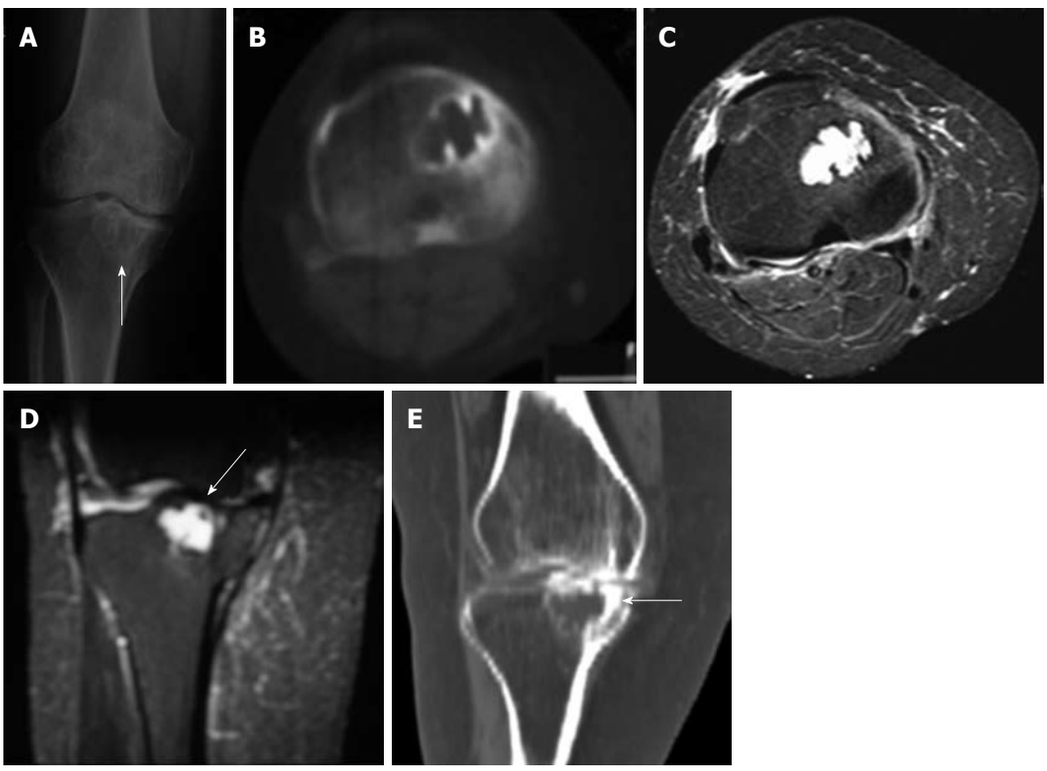

Figure 3 Chondroblastoma of the right tibia in a 55-year-old female. A: Frontal radiograph of the right knee showing an ill-defined lytic lesion in the proximal epiphysis of the right tibia (arrow); B: Unenhanced axial computed tomography (CT) image shows to a better advantage the geographic lytic lesion with sclerotic margins. No matrix mineralization is seen; C, D: Axial and coronal short-tau inversion-recovery magnetic resonance image images showing that the lesion is homogeneously hyperintense and reaching upto the subarticular region causing thinning of the overlying subchondral bone (arrow); E: Follow-up CT image obtained after the second radiofrequency session showing increased peripheral sclerosis of the lesion (arrow) with no significant change in lesion size.

Table 1 Summary of patient and procedure details

S.No	Parameter	Patient 1	Patient 2	Patient 3
1	Age/sex	14/M	12/F	55/F
2	Pre-procedure VAS score	7	8	8
3	Location	Proximal tibia-Lt	Proximal tibia-Lt	Proximal tibia-Rt
4	Lesion dimension	1.6 cm x 1.4 cm x 1.0 cm	2.5 cm x 2.1 cm x 2.0 cm	2.5 cm x 1.5 cm x 1.8 cm
5	Sub-chondral bone thinning	Present	Present	Present
6	Growth plate	Open-lesion abutting physis	Open-breached	Closed
7	Number of procedures	1	1	2
8	Number of ablations per procedure	2	3	3
9	Follow-up period	18 mo	17 mo	21 mo
10	Complications	None	None	Recurrence
11	Post procedure VAS 1 wk, 1 mo, 3 mo	2,0,0	0,0,0	4,6,0
12	Post procedure analgesic intake	None	None	None

S. No: Serial Number; VAS: Visual Analogue Scale; M: Male; F: Female.

related to the procedure. A diagnosis of residual disease was made, and repeat RFA was carried out. A second RF ablation was performed 3 mo after the first procedure in a similar manner under general anaesthesia using an18 G RF probe with a 15 mm active tip. A total of 3 ablations were performed at different needle positions. The patient experienced complete pain relief (VAS 0) following the procedure. No complications were observed during follow-up (21 mo). Follow-up imaging (radiograph and CT) performed after the second RF procedure showed increased peripheral sclerosis of the lesion with no obvious change in lesion size. Procedural and follow-up images of the patient are shown in Figure 3.

Patient and procedure details are summarised in Table 1.

DISCUSSION

Chondroblastomas are rare benign cartilaginous tumours commonlyoccurring in children and young adults between 10 and 20 years of age. They characteristically involve the epiphysis and apophysis of long bones with the proximal femur, proximal tibia and proximal humerus being the

most commonly affected sites[7]. They are highly prone to recurrence following surgery due to difficult anatomical locations, inadequate tumour removal, or tumour aggressiveness[8]. Surgery is also associated with a risk of damage to articular cartilage and physeal plate leading to premature degenerative changes and limb length discrepancies,respectively[3,9].

RF ablation is a focal form of thermal ablation in which the deposited energy causes ionic oscillation, frictional heating and coagulation necrosis of the tissues[10]. In the musculoskeletal system, RF ablation is widely used in benign bone lesions such as osteoid osteoma and in bone metastasis due to high success rates, reduced surgical risks and early postoperative recovery[11,12]. A few recent studies have proved the effectiveness of RF ablation in the treatment of selected cases of chondroblastomas and have shown high success rates and minimal associated complications[3-6]. To the best of our knowledge, RF ablation of chondroblastomas using bipolar RF applicators has not been reported previously.

The bipolar RF system is considered a safer form of treatment compared to the monopolar system, since placement of grounding pads is eliminated, precluding the risk of skin burns. Additionally, the applied RF energy is confined to the treatment area in the bipolar system in contrast to the monopolarsystem where the energy streams out through the body in all directions, increasing the body temperature by 1-2 ℃. For the same reason, metallic implants are a contraindication to the use of the monopolar system since they may be included in the electrical circuit leading to undesirable effects[13]. The bipolar system is also considered a more efficient form of treatment than the monopolar system. Since current flow is restricted to the probe tip, the bipolar system allows the use of higher current densities resulting in more uniform heating of tissues and the production of larger volumes of ablation[14]. Burdío *et al*[15] and several other authors[14,16] have established the precise and uniform nature of ablation produced by the bipolar system *in vivo*/animal studies. This may offer an additional advantage in the management of chondroblastomas, considering their critical location close to articular cartilage and joints.

The average size of the three lesions in the present study was 2.2 cm (longest dimension). All three lesions were located in weight-bearing surfaces (proximal tibial epiphysis) and there was associated thinning of the subchondral bone in all three patients. Considering the critical location of the lesions and the associated subchondral bone thinning, there was a risk of mechanical failure and articular surface damage following the procedure. We did not experience any complications regarding articular surface damage (collapse, osteonecrosis or chondrolysis) in the follow-up period. Intact cortical bone is a thermal and electrical insulator. Therefore, small chondroblastomas with an intact surrounding shell of bone carry a reduced risk of collateral thermal damage[4]. However, in large lesions, such as those treated in our study with expansion and cortical thinning, the insulating properties are greatly reduced with a substantial risk for articular cartilage damage. We believe that a restricted and precise zone of ablation produced by the bipolar system reduced the risk of collateral damage to surrounding structures. However, a larger study with a longer follow-up is required to confirm this. In the study by Rybak *et al*[3], the largest lesion in the study developed articular collapse which they attributed to the presence of a residual viable tumour. In the study by Tins *et al*[4], two of the four cases developed articular collapse. This was attributed to the use of multi-tined expandable electrodes which produced larger volumes of coagulation and carried an increased risk of damage to the surrounding structures. Large lesion size with thinning/breach of subchondral bone, location along a weight-bearing surface and the use of probes which produce larger coagulation zones increase the risk of articular surface damage following RF treatment[3].

Petsas *et al*[5] performed RF ablation of two large femoral head chondroblastomas (average size 2.7 cm) using multi-tined probes followed by apposition of bone grafts. Neither of the patients developed articular failure since the procedures were coupled with bone augmentation procedures. Both patients experienced clinical success.

Since chondroblastomas are epiphyseal tumours occurring in the younger population, there is risk of damage to the physis both during surgery and RF ablation. In fact, RF ablation is being evaluated in animal models as a method of producing epiphysiodesis for the treatment of limb length discrepancy and angular deformity[17]. Two patients (patients 1 and 2) in our study had an open growth plate and one of them had a physeal breach with extension of the lesion into the metaphysis. We did not observe any limb length discrepancy (on physical examination) during follow-up in either patient (17 and 18 mo). However, longer periods of follow-up are required to assess the occurrence of growth plate damage and limb length discrepancy, if any. The presence of a rim of bone between the lesion and the physis reduces the risk of damage to the physis[3].

One of our patients (patient 3) experienced residual pain following the procedure which was likely due to incomplete tumour ablation. Repeat RF ablation was performed after which she was asymptomatic at follow-up. Chondroblastomas have a high recurrence rate ranging from 10% to 35% following surgery,and cases have been reported to recura decade aftersurgery[18]. Hence, a larger study with a longer follow-up would be required to assess the risk of recurrence following RF ablation.

The average VAS score of the patients before the RF procedure was 7.7 (range: 7-8). All three patients experienced complete pain relief (VAS 0) in the initial few days following successful RF treatment requiring no further analgesic intake.

To conclude, RF ablation allows successful treatment of small chondroblastomas. Larger lesions carry a risk of damage to articular cartilage/growth plate and mechanical failure following RF treatment. The bipolar system

may allow treatment of larger lesions with a relatively reduced risk of damage to surrounding structures compared to the monopolar system. However, a larger study with longer follow-up is required to establish the long-term outcome of this treatment.

REFERENCES

1 **Yochum TR,** Rowe LJ. Essentials of Skeletal Radiology. 3rd ed. Hagerstown, MD: Lippincott Williams and Wilkins, 2005: 1280-1283
2 **Ramappa AJ**, Lee FY, Tang P, Carlson JR, Gebhardt MC, Mankin HJ. Chondroblastoma of bone. *J Bone Joint Surg Am* 2000; **82**-A: 1140-1145
3 **Rybak LD**, Rosenthal DI, Wittig JC. Chondroblastoma: radiofrequency ablation--alternative to surgical resection in selected cases. *Radiology* 2009; **251**: 599-604
4 **Tins B**, Cassar-Pullicino V, McCall I, Cool P, Williams D, Mangham D. Radiofrequency ablation of chondroblastoma using a multi-tined expandable electrode system: initial results. *Eur Radiol* 2006; **16**: 804-810
5 **Petsas T**, Megas P, Papathanassiou Z. Radiofrequency ablation of two femoral head chondroblastomas. *Eur J Radiol* 2007; **63**: 63-67
6 **Christie-Large M**, Evans N, Davies AM, James SL. Radiofrequency ablation of chondroblastoma: procedure technique, clinical and MR imaging follow up of four cases. *Skeletal Radiol* 2008; **37**: 1011-1017
7 **Sepah YJ**, Umer M, Minhas K, Hafeez K. Chondroblastoma of the cuboid with an associated aneurysmal bone cyst: a case report. *J Med Case Rep* 2007; **1**: 135
8 **Garin IE**, Wang EH. Chondroblastoma. *J Orthop Surg* (Hong Kong) 2008; **16**: 84-87
9 **Masui F**, Ushigome S, Kamitani K, Asanuma K, Fujii K. Chondroblastoma: a study of 11 cases. *Eur J Surg Oncol* 2002; **28**: 869-874
10 **Goldberg SN**. Radiofrequency tumor ablation: principles and techniques. *Eur J Ultrasound* 2001; **13**: 129-147
11 **Rosenthal DI**, Hornicek FJ, Torriani M, Gebhardt MC, Mankin HJ. Osteoid osteoma: percutaneous treatment with radiofrequency energy. *Radiology* 2003; **229**: 171-175
12 **Callstrom MR**, Charboneau JW, Goetz MP, Rubin J, Wong GY, Sloan JA, Novotny PJ, Lewis BD, Welch TJ, Farrell MA, Maus TP, Lee RA, Reading CC, Petersen IA, Pickett DD. Painful metastases involving bone: feasibility of percutaneous CT- and US-guided radio-frequency ablation. *Radiology* 2002; **224**: 87-97
13 **Mahnken AH**, Tacke JA, Wildberger JE, Günther RW. Radiofrequency ablation of osteoid osteoma: initial results with a bipolar ablation device. *J Vasc Interv Radiol* 2006; **17**: 1465-1470
14 **Nakada SY**, Jerde TJ, Warner TF, Wright AS, Haemmerich D, Mahvi DM, Lee FT. Bipolar radiofrequency ablation of the kidney: comparison with monopolar radiofrequency ablation. *J Endourol* 2003; **17**: 927-933
15 **Burdío F**, Güemes A, Burdío JM, Navarro A, Sousa R, Castiella T, Cruz I, Burzaco O, Guirao X, Lozano R. Large hepatic ablation with bipolar saline-enhanced radiofrequency: an experimental study in in vivo porcine liver with a novel approach. *J Surg Res* 2003; **110**: 193-201
16 **Yi B**, Somasundar P, Espat NJ. Novel laparoscopic bipolar radiofrequency energy technology for expedited hepatic tumour ablation. *HPB* (Oxford) 2009; **11**: 135-139
17 **Kunkel MG**, Dahlin DC, Young HH. Benign chondroblastoma. *J Bone Joint Surg Am* 1956; **38**-A: 817-826
18 **Ghanem I**, El Hage S, Diab M, Saliba E, Khazzaka A, Aftimos G, Dagher F, Kharrat K. Radiofrequency application to the growth plate in the rabbit: a new potential approach to epiphysiodesis. *J Pediatr Orthop* 2009; **29**: 629-635

S- Editor Cheng JX **L- Editor** Webster JR **E- Editor** Xiong L

World Journal of Radiology

Online Submissions: http://www.wjgnet.com/esps/
wjr@wjgnet.com
doi:10.4329/wjr.v4.i7.341

World J Radiol 2012 July 28; 4(7): 341-344
ISSN 1949-8470 (online)

CASE REPORT

Multiple occipital defects caused by arachnoid granulations: Emphasis on T2 mapping

Chao-Xuan Lu, Yong Du, Xiao-Xue Xu, Yang Li, Han-Feng Yang, Shao-Qiang Deng, Dong-Mei Xiao, Bing Li, Yun-Hong Tian

Chao-Xuan Lu, Yong Du, Xiao-Xue Xu, Yang Li, Han-Feng Yang, Shao-Qiang Deng, Dong-Mei Xiao, Bing Li, Yun-Hong Tian, Sichuan Key Laboratory of Medical Imaging, Department of Radiology, Affiliated Hospital of North Sichuan Medical College, Nanchong 637000, Sichuan Province, China

Author contributions: Lu CX and Yang HF contributed equally to this work; Lu CX, Yang HF, Du Y and Xu XX collected information about the patient; Lu CX, Yang HF, Deng SQ, Xiao DM, Li B and Tian YH collected data; Lu CX, Yang HF, Du Y, Xu XX and Li Y analyzed the data; Lu CX and Yang HF wrote the paper.

Correspondence to: Han-Feng Yang, MD, Sichuan Key Laboratory of Medical Imaging, Department of Radiology, Affiliated Hospital of North Sichuan Medical College, 63 Wenhua Road, Nanchong 637000, Sichuan Province, China. yhf5nc@yahoo.com

Telephone: +86-13890816795 Fax: +86-817-2222568
Received: February 25, 2012 Revised: June 23, 2012
Accepted: June 30, 2012
Published online: July 28, 2012

Abstract

A 56-year-old man presented with a 6-mo history of headache. Although neurological and laboratory examinations were normal, computed tomography (CT) scan was performed which revealed multiple occipital osteolytic lesions, which were suspected to be multiple myeloma. Subsequently nuclear magnetic resonance imaging (MRI) showed that these lesions presented with a cerebrospinal fluid (CSF)-like signal intensity, no diffusional restriction and intrinsic mass-like enhancement on conventional sequences were seen. T2 relaxation time was similar to that of CSF in the ventricles and adjacent subarachnoid space on T2-mapping. Single photon emission CT with ^{99m}Tc-Methyl diphosphonate was performed which revealed no increased radiotracing accumulation. Finally, these lesions were diagnosed as mutiple arachnoid granulations (AGs). The headache was treated symptomatically with medical therapy. On follow up examination after 6 mo no evidence of tumor was detected. This report aimed to illustrate the appearance and differentiation of occipital defects caused by multiple AGs on CT and MRI, with emphasis on the findings from T2 mapping.

Key words: Arachnoid granulation; Occipital defect; Magnetic resonance imaging; Computed tomography; T2-mapping

Peer reviewers: Farideh Nejat, MD, MPH, Department of Neurosurgery, Children's Hospital Medical Center, Tehran University of Medical Sciences, Gharib Street, Mail Box 14155-7854, Tehran, Iran; Rivka R Colen, MD, Department of Radiology, Brigham and Womens Hospital, 75 Francis St, Boston, MA 02115, United States

Lu CX, Du Y, Xu XX, Li Y, Yang HF, Deng SQ, Xiao DM, Li B, Tian YH. Multiple occipital defects caused by arachnoid granulations: Emphasis on T2 mapping. *World J Radiol* 2012; 4(7): 341-344 Available from: URL: http://www.wjgnet.com/1949-8470/full/v4/i7/341.htm DOI: http://dx.doi.org/10.4329/wjr.v4.i7.341

INTRODUCTION

Arachnoid granulations (AGs) are tufts of arachnoid membrane invaginated into the dural sinuses through which cerebrospinal fluid (CSF) enters the venous system. The lesions are primarily located in the parasagittal region along the superior sagittal sinus[1], which is occasionally seen at the transverse sinus. Normally dural venous sinus AGs typically range from 2 to 8 mm in size, but may grow enough to expand the dural sinuses, and even the inner table, diploic space and outer table of the skull[2].

Although AGs can also produce bone defects[3], due to their infrequency, multiple AGs leading to osteolytic

lesions within the occipital area have been incompletely characterized and could be responsible for diagnostic confusion, and sometimes represent a diagnostic challenge even for experienced radiologists. Identification of normal AGs within the occipital region may reduce the erroneous diagnosis of a malignant pathologic process. This case report described the imaging features of such AGs that allow differentiation from pathology on computed tomography (CT), standard magnetic resonance imaging (MRI), and T2-mapping, which may help many radiologists, especially young doctors, reduce the misdiagnosis rate of AGs.

CASE REPORT

A 56-year-old man with a 6-mo history of headache was referred to our hospital. Neurological and general physical examinations were normal. Nonenhanced CT of the brain was performed which revealed multiple osteolytic lesions in the occipital area (Figure 1), with sharp but slightly irregular margins; no bone spicules or calcifications were present. The lesions were suspected to be multiple myeloma. On laboratory examination, there was no evidence of systemic myelomatous changes or anemia and urine analysis was completely normal with no evidence of Bence-Jones protein and excretion of immunoglobulin elements. The screening tests for tumor markers were negative. Subsequently MRI showed that signal intensity within the bone erosions was isointense to CSF, hypointense relative to the brain on T1-weighted image (T1WI) (Figure 2A), hyperintense relative to the brain on T2-weighted image (T2WI), with a banded lower signal most likely representing the intra-AGs collagenous connective tissue (Figure 2B and C), complete suppression on fluid attenuated inversion recovery (FLAIR) (Figure 2D), no restricted diffusion on diffusion-weighted imaging (DWI) (Figure 2E) and no mass-like enhancement on contrast-enhanced T1WI (Figure 2F). The three-dimensional fast imaging employing steady state acquisition (3D FIESTA) showed that the adjacent subarachnoid space communicated with the AGs (Figure 3A). T2 relaxation time was similar to that of CSF in the ventricles and adjacent subarachnoid space on T2-mapping (Figure 3B and C). For further investigation to detect possible metastases, single photon emission CT (SPECT) with ^{99m}Tc-Methyl diphosphonate (^{99m}Tc-MDP) was performed which revealed no increased radiotracing accumulation (Figure 3D). On the basis of these findings, the erosions were identified as multiple AGs and the headache was managed with symptomatic treatment. The patient has been followed up for 6 mo without change.

DISCUSSION

CSF is synthesized and produced by the choroid plexus in the lateral, third, and fourth ventricles where it circulates to the subarachnoid space and eventually returns to the venous blood *via* the AGs. Histologically, AGs are composed of dense collagenous connective tissue admixed with clusters of arachnoid cells and a network of delicate vascular space filled with CSF from the contiguous subarachnoid space. This cell layer was continuous with the underlying arachnoid membrane[4].

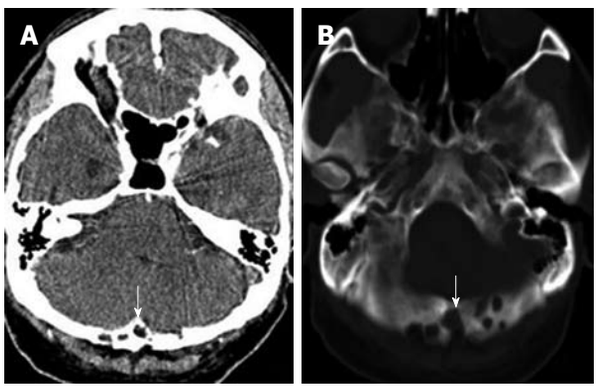

Figure 1 Multiple arachnoid granulations (arrows) in a 56-year-old man. Axial noncontrast computed tomography on soft-tissue windows (A) and bone windows (B) showed occipital multiple osteolytic lesions adjacent to the transverse sinus.

AGs are growths of arachnoid membrane into the dural sinuses which have a wide variability in the site, number, size and morphology[5]. Occasionally, these extend partly up to the inner table of the skull as so called foveolae granulations, and even expand into the diploic space and eventually involve the outer table, mimicking malignant osteolytic lesions. It was thought that some AGs hypertrophy was in response to increasing CSF volume and pressure[6]. The most common site for AGs is at the superior sagittal sinus[5,7]. The occipital and temporal bone defects caused by AGs in the transverse sinus and sigmoid sinus, respectively, were rarely reported[2,8]. In this case, multiple AGs which led to occipital bone defects were located at the transverse sinus, and varied in diameter with a range of 5 to 17 mm, and showed expansion into the outer table.

The clinical significance of AGs is uncertain. Most cases are usually asymptomatic and there are incidental findings on imaging studies, while some giant AGs may cause dural venous sinus pressure gradients and headache[2]. In this case, the headache might be closely associated with multiple AGs.

AGs were identified on skull radiography as smoothly marginated impressions in the inner table of the calvarium. Typically, regardless of size AGs were commonly diagnosed by identifying intra-AG fluid which was revealed as CSF-like attenuation on CT and parallel CSF signal intensity on all MRI sequences, which was a conventional diagnostic criterion for AGs[2]. Haroun *et al*[5] thought that the identification of AGs could be facilitated by their characteristic appearances: rounded or oval shape, well-defined outlines and homogenous intensity; the presence of an adjacent cortical vein can be considered as an additional supportive element. Trimble *et al*[2] found that AGs may be complex structures whose contents do not

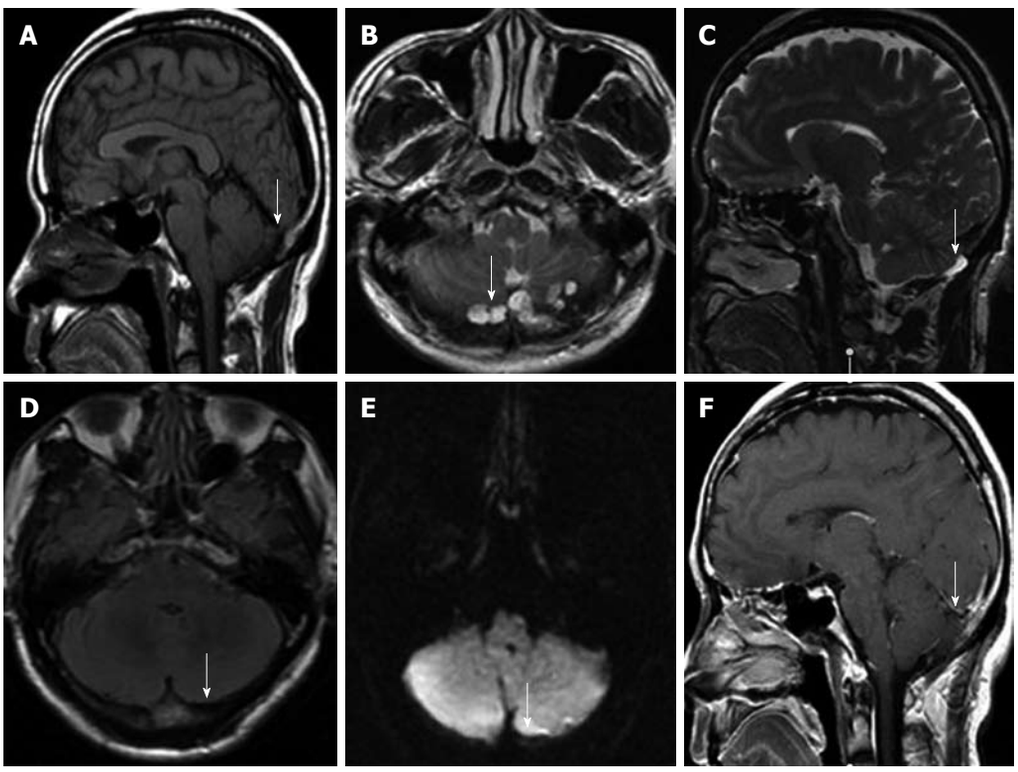

Figure 2 Multiple arachnoid granulations (arrows) in a 56-year-old man. A-C: Sagittal T1-weighted image (T1WI) (A) showed hypointensity relative to the brain, axial (B) and sagittal (C) T2-weighted image showed hyperintensity relative to the brain, with a banded lower signal most likely representing the intra-arachnoid granulations (AGs) collagenous connective tissue; D: Axial fluid attenuated inversion recovery image demonstrated complete suppression of intra-AG fluid; E, F: Axial diffusion-weighted imaging (E) showed no restricted diffusion. Sagittal postcontrast T1WI (F) showed no gadolinium enhancement.

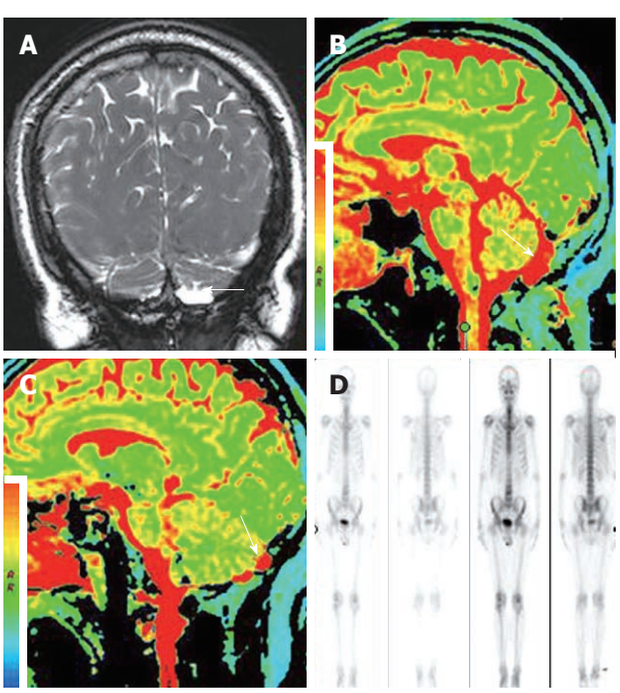

Figure 3 Multiple arachnoid granulations (arrow) in a 56-year-old man. A: Coronal three-dimensional fast imaging employing steady state acquisition showed that the subarachnoid cavity communicated with a large arachnoid granulation (AG); B, C: Sagittal T2-mapping demonstrated T2 relaxation times of intra-AG contents paralleled that of cerebrospinal fluid in the ventricles and adjacent subarachnoid spaces; D: Single photon emission computed tomography with ^{99m}Tc-Methyl diphosphonate revealed no increased radiotracer accumulation.

invariably parallel CSF signal intensity. In this case, AGs presented as occipital erosions with CSF-like attenuation and a lobulated surface on nonenhanced CT, hypointense relative to the brain on T1WI, isointense to CSF on T2WI and 3D FIESTA, with linear hypointense components which may represent the internal fibrous structure of AGs, complete suppression on FLAIR, no restricted diffusion on DWI, and no gadolinium enhancement on postcontrast T1WI. In addition, the intra-AG fluid signal intensity was assessed quantitatively and compared with CSF in the ventricles and adjacent subarachnoid space on T2-mapping. T2 relaxation time of intra-AG contents paralleled that of CSF.

Differentiation should be primarily made from multiple myeloma and metastatic tumor. In addition, arachnoid cysts, dermoids and epidermoid also should be excluded. The key MRI features of AGs were very well-defined CSF-like signal intensity protuberances. No enhancement or aggressive appearance like typical neoplasms, such as multiple myeloma and metastatic tumor, no fat signal intensity or attenuation to suggest dermoid, and no restricted diffusion to suggest epidermoid were present[7]. For narrowing the differential diagnosis, SPECT with ^{99m}Tc-MDP was performed in order to functionally characterize the lesion[9]. In this case, no uptake of ^{99m}Tc-MDP which was explained by the hypovascularity and low metabolic activity was observed. In this case, despite lack of biopsy-proved results, additional supports for AGs such as CT imaging, conventional MRI sequences, quantitative T2

relaxation time analysis, exclusive methods for diagnosis of other diseases such as SPECT, laboratory tests, and 6-mo follow-up were performed. All of these strongly supported the presence of AGs.

In conclusion, multiple AGs can occur in the transverse sinus and lead to occipital osteolytic lesions which may be mistaken for other pathology due to rare presentation of AGs. A careful analysis of MR imaging characteristics especially quantitative T2 relaxation time paralleling that of CSF should lead to the correct diagnosis.

REFERENCES

1 **Kan P**, Stevens EA, Couldwell WT. Incidental giant arachnoid granulation. *AJNR Am J Neuroradiol* 2006; **27**: 1491-1492

2 **Trimble CR**, Harnsberger HR, Castillo M, Brant-Zawadzki M, Osborn AG. "Giant" arachnoid granulations just like CSF?: NOT!! *AJNR Am J Neuroradiol* 2010; **31**: 1724-1728

3 **VandeVyver V**, Lemmerling M, De Foer B, Casselman J, Verstraete K. Arachnoid granulations of the posterior temporal bone wall: imaging appearance and differential diagnosis. *AJNR Am J Neuroradiol* 2007; **28**: 610-612

4 **Haybaeck J**, Silye R, Soffer D. Dural arachnoid granulations and "giant" arachnoid granulations. *Surg Radiol Anat* 2008; **30**: 417-421

5 **Haroun AA**, Mahafza WS, Al Najar MS. Arachnoid granulations in the cerebral dural sinuses as demonstrated by contrast-enhanced 3D magnetic resonance venography. *Surg Radiol Anat* 2007; **29**: 323-328

6 **Choi HJ**, Cho CW, Kim YS, Cha JH. Giant arachnoid granulation misdiagnosed as transverse sinus thrombosis. *J Korean Neurosurg Soc* 2008; **43**: 48-50

7 **Leach JL**, Meyer K, Jones BV, Tomsick TA. Large arachnoid granulations involving the dorsal superior sagittal sinus: findings on MR imaging and MR venography. *AJNR Am J Neuroradiol* 2008; **29**: 1335-1339

8 **Lee MH**, Kim HJ, Lee IH, Kim ST, Jeon P, Kim KH. Prevalence and appearance of the posterior wall defects of the temporal bone caused by presumed arachnoid granulations and their clinical significance: CT findings. *AJNR Am J Neuroradiol* 2008; **29**: 1704-1707

9 **Alexiou GA**, Fotopoulos AD, Papadopoulos A, Kyritsis AP, Polyzoidis KS, Tsiouris S. Evaluation of brain tumor recurrence by (99m)Tc-tetrofosmin SPECT: a prospective pilot study. *Ann Nucl Med* 2007; **21**: 293-298

S- Editor Cheng JX **L- Editor** O'Neill M **E- Editor** Zheng XM

World Journal of Radiology

Online Submissions: http://www.wjgnet.com/1949-8470office
wjr@wjgnet.com
www.wjgnet.com

World J Radiol 2012 July 28; 4(7): I
ISSN 1949-8470 (online)

Acknowledgments to reviewers of *World Journal of Radiology*

Many reviewers have contributed their expertise and time to the peer review, a critical process to ensure the quality of *World Journal of Radiology*. The editors and authors of the articles submitted to the journal are grateful to the following reviewers for evaluating the articles (including those published in this issue and those rejected for this issue) during the last editing time period.

Dr. Kazushi Kishi, Wakayama Medical University, Wakayama City 641-8510, Japan

Roberto Miraglia, MD, Department of Diagnostic and Interventional Radiology, Mediterranean Institute for Transplantation and Advanced Specialized Therapies (IsMeTT), Via Tricomi 1, 90100 Palermo, Italy

Yasunori Minami, MD, PhD, Division of Gastroenterology and Hepatology, Department of Internal Medicine, 377-2 Ohno-higashi, Osaka-sayama, Osaka 589-8511, Japan

Yicheng Ni, MD, PhD, Professor, Biomedical Imaging, Interventional Therapy and Contrast Media Research, Department of Radiology, University Hospitals, KU Leuven, Herestraat 49, B-3000 Leuven, Belgium

Volker Rudat, Professor, Department of Radiation Oncology, Saad Specialist Hospital, PO Box 30353, Al Khobar 31952, Saudi Arabia

Zhonghua Sun, MD, PhD, Associate Professor, Discipline of Medical Imaging, Department of Imaging and Applied Physics, Curtin University of Technology, GPO Box U 1987, Perth, Western Australia 6845, Australia

Dr. Charikleia Triantopoulou, Konstantopouleion Hospital, 3-5, Agias Olgas street, Athens 14233 N. Ionia, Greece

Ioannis G Valais, PhD, Department of Medical Instrument Technology, Technological Educational Institution of Athens, Ag Spyridonos and Dimitsanis, Egaleo, 12210 Athens, Greece

Martin A Walter, MD, Institute of Nuclear Medicine, University Hospital, Petersgraben 41, CH-4031 Basel, Switzerland

WJR World Journal of Radiology

Online Submissions: http://www.wjgnet.com/esps/
wjr@wjgnet.com
www.wjgnet.com

World J Radiol 2012 July 28; 4(7): I
ISSN 1949-8470 (online)

Events Calendar 2012

January 3-7, 2012
Imaging at Bachelor Gulch
Beaver Creek, CO 81620,
United States

January 12-14, 2012
IROS 2012: Interventionell
Radiologischen Olbert Symposium
Salzburg, Austria

January 26-29, 2012
American Society of Neuroimaging
2012 35th Annual Meeting
Miami, FL 33169, United States

February 9-11, 2012
JIM joint interventional meeting
2012
Rome, Italy

February 13-16, 2012
Emergency Radiology
Palm Beach, FL 33480, United States

February 16-19, 2012
ASSR 2012 Annual Symposium
Miami Beach, FL 33169,
United States

February 19-23, 2012
Internal Derangements of Joints:
Advanced and Intensive MR
Imaging/With a Special Symposium
on Ankle and Foot
Coronado, CA 92118, United States

February 21-24, 2012
MRI in Practice
Oslo, Norway

March 1-5, 2012
ECR 2012
Vienna, Austria

March 7-10, 2012
ISCD's 18th Annual Meeting
Los Angeles, CA 90001,
United States

March 7-11, 2012
7th Annual Fundamentals of
Musculoskeletal Ultrasound
San Diego, CA 92111, United States

March 25-30, 2012
Diseases of the Brain, Head and
Neck Spine
Davos, Switzerland
April 13-15, 2012
ACR 35th National Conference on
Breast Cancer
Hollywood, FL 33019, United States

April 22-24, 2012
Euroson 2012
Madrid, Spain

April 24-27, 2012
MRI in Practice
Aalst, Belgium

April 25-28, 2012
ECIO 2012 - Third European
Conference on Interventional
Oncology
Florence, Italy

May 15-18, 2012
EURO PCR
Paris, France

May 19-23, 2012
ECTS 2012
Stockholm, Sweden

May 28-June 01, 2012
The International Congress of
Pediatric Radiology
Athens Greece

June 7-9, 2012
ASCI 2012 6th Congress of Asian
Society of Cardiovascular Imaging
Bangkok, Thailand

June 14-16, 2012
ICCIR 2012 – International
Conference on Complications in
Interventional Radiology
Poertschach, Austria

June 16-19, 2012
2nd IDKD Hong Kong 2012,
Diseases of the Abdomen and Pelvis
Hong Kong, China

June 17-20, 2012
14th Annual International
Symposium on Multidetector-Row
CT
San Francisco, CA **94103,**
United States

June 27-30, 2012
CARS 2012
Pisa, Italy

July 1-3, 2012
16th Symposium Mammographicum
Harrogate, United Kingdom

July 19-22, 2012
Society of Cardiovascular Computed
Tomography 6th Annual Scientific
Meeting
Baltimore, Maryland

August 30-2, 2012
14th Asian Oceanian Congress of
Radiology
Sydney, Australia

September 6-8, 2012
Update in Abdominal and
Urogenital Imaging
Bruges, Belgium

September 12-15, 2012
ISS 2012
Rome, Italy

September 13-15, 2012
4th ESMINT Congress
Nice, France

September 13-16, 2012
18th Annual Symposium ESUR
Edinburgh, United Kingdom

September 15-19, 2012
CIRSE 2012
Lisbon, Portugal

September 20-23, 2012
2012 SDMS Annual Conference
Seattle, WA 98113, United States

September 24-27, 2012
MRI in Practice
Ballerup, Denmark

October 4-6, 2012
ESMRMB congress 2012 29th Annual
Scientific Meeting
Lisbon, Portugal

October 12-13, 2012
EUSOBI Annual Scientific Meeting
2012
Barcelona, Spain

October 26-28, 2012
22th Annual Meeting of the Society
of Radiologists in Ultrasound
Baltimore, MD 21213, United States

November 10-14, 2012
13th congress of WFITN
Buenos Aires, Agentina

November 14-17, 2012
BSIR Annual Meeting 2012
Bournemouth, United Kingdom

November 27- December 03, 2012
IEEE Nuclear Science Symposium
and Medical Imaging Conference
Anaheim, CA 92805, United States

December 2-4, 2012
ICI 2012 - Innovations in
Cardiovascular Interventions
Meeting
Tel Aviv, Israel

December 4-8, 2012
34rd San Antonio Breast Cancer
Symposium,
San Antonio, TX 78258 ,
United States

WJR World Journal of Radiology

Online Submissions: http://www.wjgnet.com/esps/
wjr@wjgnet.com
www.wjgnet.com

World J Radiol 2012 July 28; 4(7): I-V
ISSN 1949-8470 (online)

INSTRUCTIONS TO AUTHORS

GENERAL INFORMATION

World Journal of Radiology (*World J Radiol*, *WJR*, online ISSN 1949-8470, DOI: 10.4329), is a monthly, open-access (OA), peer-reviewed journal supported by an editorial board of 319 experts in Radiology from 40 countries.

The biggest advantage of the OA model is that it provides free, full-text articles in PDF and other formats for experts and the public without registration, which eliminates the obstacle that traditional journals possess and usually delays the speed of the propagation and communication of scientific research results. The open access model has been proven to be a true approach that may achieve the ultimate goal of the journals, i.e. the maximization of the value to the readers, authors and society.

Maximization of personal benefits

The role of academic journals is to exhibit the scientific levels of a country, a university, a center, a department, and even a scientist, and build an important bridge for communication between scientists and the public. As we all know, the significance of the publication of scientific articles lies not only in disseminating and communicating innovative scientific achievements and academic views, as well as promoting the application of scientific achievements, but also in formally recognizing the "priority" and "copyright" of innovative achievements published, as well as evaluating research performance and academic levels. So, to realize these desired attributes of *WJR* and create a well-recognized journal, the following four types of personal benefits should be maximized. The maximization of personal benefits refers to the pursuit of the maximum personal benefits in a well-considered optimal manner without violation of the laws, ethical rules and the benefits of others. (1) Maximization of the benefits of editorial board members: The primary task of editorial board members is to give a peer review of an unpublished scientific article via online office system to evaluate its innovativeness, scientific and practical values and determine whether it should be published or not. During peer review, editorial board members can also obtain cutting-edge information in that field at first hand. As leaders in their field, they have priority to be invited to write articles and publish commentary articles. We will put peer reviewers' names and affiliations along with the article they reviewed in the journal to acknowledge their contribution; (2) Maximization of the benefits of authors: Since *WJR* is an open-access journal, readers around the world can immediately download and read, free of charge, high-quality, peer-reviewed articles from *WJR* official website, thereby realizing the goals and significance of the communication between authors and peers as well as public reading; (3) Maximization of the benefits of readers: Readers can read or use, free of charge, high-quality peer-reviewed articles without any limits, and cite the arguments, viewpoints, concepts, theories, methods, results, conclusion or facts and data of pertinent literature so as to validate the innovativeness, scientific and practical values of their own research achievements, thus ensuring that their articles have novel arguments or viewpoints, solid evidence and correct conclusion; and (4) Maximization of the benefits of employees: It is an iron law that a first-class journal is unable to exist without first-class editors, and only first-class editors can create a first-class academic journal. We insist on strengthening our team cultivation and construction so that every employee, in an open, fair and transparent environment, could contribute their wisdom to edit and publish high-quality articles, thereby realizing the maximization of the personal benefits of editorial board members, authors and readers, and yielding the greatest social and economic benefits.

Aims and scope

The major task of *WJR* is to rapidly report the most recent improvement in the research of medical imaging and radiation therapy by the radiologists. *WJR* accepts papers on the following aspects related to radiology: Abdominal radiology, women health radiology, cardiovascular radiology, chest radiology, genitourinary radiology, neuroradiology, head and neck radiology, interventional radiology, musculoskeletal radiology, molecular imaging, pediatric radiology, experimental radiology, radiological technology, nuclear medicine, PACS and radiology informatics, and ultrasound. We also encourage papers that cover all other areas of radiology as well as basic research.

Columns

The columns in the issues of *WJR* will include: (1) Editorial: To introduce and comment on major advances and developments in the field; (2) Frontier: To review representative achievements, comment on the state of current research, and propose directions for future research; (3) Topic Highlight: This column consists of three formats, including (A) 10 invited review articles on a hot topic, (B) a commentary on common issues of this hot topic, and (C) a commentary on the 10 individual articles; (4) Observation: To update the development of old and new questions, highlight unsolved problems, and provide strategies on how to solve the questions; (5) Guidelines for Basic Research: To provide guidelines for basic research; (6) Guidelines for Clinical Practice: To provide guidelines for clinical diagnosis and treatment; (7) Review: To review systemically progress and unresolved problems in the field, comment on the state of current research, and make suggestions for future work; (8) Original Articles: To report innovative and original findings in radiology; (9) Brief Articles: To briefly report the novel and innovative findings in radiology; (10) Case Report: To report a rare or typical case; (11) Letters to the Editor: To discuss and make reply to the contributions published in *WJR*, or to introduce and comment on a controversial issue of general interest; (12) Book Reviews: To introduce and comment on quality monographs of radiology; and (13) Guidelines: To introduce consensuses and guidelines reached by international and national academic authorities worldwide on the research in radiology.

Name of journal

World Journal of Radiology

ISSN

ISSN 1949-8470 (online)

Editor-in-Chief

Editorial Office

World Journal of Radiology
Editorial Department: Room 903, Building D,
Ocean International Center, No. 62 Dongsihuan Zhonglu,
Chaoyang District, Beijing 100025, China

E-mail: wjr@wjgnet.com
http://www.wjgnet.com
Telephone: +86-10-59080039
Fax: +86-10-85381893

Indexed and Abstracted in
PubMed Central, PubMed, Digital Object Identifier, and Directory of Open Access Journals.

Published by
Baishideng Publishing Group Co., Limited.

SPECIAL STATEMENT

All articles published in this journal represent the viewpoints of the authors except where indicated otherwise.

Biostatistical editing
Statisital review is performed after peer review. We invite an expert in Biomedical Statistics from to evaluate the statistical method used in the paper, including *t*-test (group or paired comparisons), chi-squared test, Ridit, probit, logit, regression (linear, curvilinear, or stepwise), correlation, analysis of variance, analysis of covariance, *etc*. The reviewing points include: (1) Statistical methods should be described when they are used to verify the results; (2) Whether the statistical techniques are suitable or correct; (3) Only homogeneous data can be averaged. Standard deviations are preferred to standard errors. Give the number of observations and subjects (*n*). Losses in observations, such as drop-outs from the study should be reported; (4) Values such as ED50, LD50, IC50 should have their 95% confidence limits calculated and compared by weighted probit analysis (Bliss and Finney); and (5) The word 'significantly' should be replaced by its synonyms (if it indicates extent) or the *P* value (if it indicates statistical significance).

Conflict-of-interest statement
In the interests of transparency and to help reviewers assess any potential bias, *WJR* requires authors of all papers to declare any competing commercial, personal, political, intellectual, or religious interests in relation to the submitted work. Referees are also asked to indicate any potential conflict they might have reviewing a particular paper. Before submitting, authors are suggested to read "Uniform Requirements for Manuscripts Submitted to Biomedical Journals: Ethical Considerations in the Conduct and Reporting of Research: Conflicts of Interest" from International Committee of Medical Journal Editors (ICMJE), which is available at: http://www.icmje.org/ethical_4conflicts.html.

Sample wording: [Name of individual] has received fees for serving as a speaker, a consultant and an advisory board member for [names of organizations], and has received research funding from [names of organization]. [Name of individual] is an employee of [name of organization]. [Name of individual] owns stocks and shares in [name of organization]. [Name of individual] owns patent [patent identification and brief description].

Statement of informed consent
Manuscripts should contain a statement to the effect that all human studies have been reviewed by the appropriate ethics committee or it should be stated clearly in the text that all persons gave their informed consent prior to their inclusion in the study. Details that might disclose the identity of the subjects under study should be omitted. Authors should also draw attention to the Code of Ethics of the World Medical Association (Declaration of Helsinki, 1964, as revised in 2004).

Statement of human and animal rights
When reporting the results from experiments, authors should follow the highest standards and the trial should conform to Good Clinical Practice (for example, US Food and Drug Administration Good Clinical Practice in FDA-Regulated Clinical Trials; UK Medicines Research Council Guidelines for Good Clinical Practice in Clinical Trials) and/or the World Medical Association Declaration of Helsinki. Generally, we suggest authors follow the lead investigator's national standard. If doubt exists whether the research was conducted in accordance with the above standards, the authors must explain the rationale for their approach and demonstrate that the institutional review body explicitly approved the doubtful aspects of the study.

Before submitting, authors should make their study approved by the relevant research ethics committee or institutional review board. If human participants were involved, manuscripts must be accompanied by a statement that the experiments were undertaken with the understanding and appropriate informed consent of each. Any personal item or information will not be published without explicit consents from the involved patients. If experimental animals were used, the materials and methods (experimental procedures) section must clearly indicate that appropriate measures were taken to minimize pain or discomfort, and details of animal care should be provided.

SUBMISSION OF MANUSCRIPTS

Manuscripts should be typed in 1.5 line spacing and 12 pt. Book Antiqua with ample margins. Number all pages consecutively, and start each of the following sections on a new page: Title Page, Abstract, Introduction, Materials and Methods, Results, Discussion, Acknowledgements, References, Tables, Figures, and Figure Legends. Neither the editors nor the publisher are responsible for the opinions expressed by contributors. Manuscripts formally accepted for publication become the permanent property of Baishideng Publishing Group Co., Limited, and may not be reproduced by any means, in whole or in part, without the written permission of both the authors and the publisher. We reserve the right to copy-edit and put onto our website accepted manuscripts. Authors should follow the relevant guidelines for the care and use of laboratory animals of their institution or national animal welfare committee. For the sake of transparency in regard to the performance and reporting of clinical trials, we endorse the policy of the ICMJE to refuse to publish papers on clinical trial results if the trial was not recorded in a publicly-accessible registry at its outset. The only register now available, to our knowledge, is http://www.clinicaltrials.gov sponsored by the United States National Library of Medicine and we encourage all potential contributors to register with it. However, in the case that other registers become available you will be duly notified. A letter of recommendation from each author's organization should be provided with the contributed article to ensure the privacy and secrecy of research is protected.

Authors should retain one copy of the text, tables, photographs and illustrations because rejected manuscripts will not be returned to the author(s) and the editors will not be responsible for loss or damage to photographs and illustrations sustained during mailing.

Online submissions
Manuscripts should be submitted through the Online Submission System at: http://www.wjgnet.com/esps/. Authors are highly recommended to consult the ONLINE INSTRUCTIONS TO AUTHORS (http://www.wjgnet.com/1949-8470/g_info_20100316162358.htm) before attempting to submit online. For assistance, authors encountering problems with the Online Submission System may send an email describing the problem to wjr@wjgnet.com, or by telephone: +86-10-85381892. If you submit your manuscript online, do not make a postal contribution. Repeated online submission for the same manuscript is strictly prohibited.

MANUSCRIPT PREPARATION

All contributions should be written in English. All articles must be submitted using word-processing software. All submissions must be typed in 1.5 line spacing and 12 pt. Book Antiqua with ample margins. Style should conform to our house format. Required information for each of the manuscript sections is as follows:

Title page
Title: Title should be less than 12 words.

Running title: A short running title of less than 6 words should be provided.

Authorship: Authorship credit should be in accordance with the standard proposed by International Committee of Medical Journal Editors, based on (1) substantial contributions to conception and design, acquisition of data, or analysis and interpretation of data; (2) drafting the article or revising it critically for important intellectual content; and (3) final approval of the version to be published. Authors should meet conditions 1, 2, and 3.

Institution: Author names should be given first, then the complete name of institution, city, province and postcode. For example, Xu-Chen Zhang, Li-Xin Mei, Department of Pathology, Chengde Medical College, Chengde 067000, Hebei Province, China. One author may be represented from two institutions, for example, George Sgourakis, Department of General, Visceral, and Transplantation Surgery, Essen 45122, Germany; George Sgourakis, 2nd Surgical Department, Korgialenio-Benakio Red Cross Hospital, Athens 15451, Greece

Author contributions: The format of this section should be: Author contributions: Wang CL and Liang L contributed equally to this work; Wang CL, Liang L, Fu JF, Zou CC, Hong F and Wu XM designed the research; Wang CL, Zou CC, Hong F and Wu XM performed the research; Xue JZ and Lu JR contributed new reagents/analytic tools; Wang CL, Liang L and Fu JF analyzed the data; and Wang CL, Liang L and Fu JF wrote the paper.

Supportive foundations: The complete name and number of supportive foundations should be provided, e.g., Supported by National Natural Science Foundation of China, No. 30224801

Correspondence to: Only one corresponding address should be provided. Author names should be given first, then author title, affiliation, the complete name of institution, city, postcode, province, country, and email. All the letters in the email should be in lower case. A space interval should be inserted between country name and email address. For example, Montgomery Bissell, MD, Professor of Medicine, Chief, Liver Center, Gastroenterology Division, University of California, Box 0538, San Francisco, CA 94143, United States. montgomery.bissell@ucsf.edu

Telephone and fax: Telephone and fax should consist of +, country number, district number and telephone or fax number, e.g., Telephone: +86-10-85381892 Fax: +86-10-85381893

Peer reviewers: All articles received are subject to peer review. Normally, three experts are invited for each article. Decision for acceptance is made only when at least two experts recommend an article for publication. Reviewers for accepted manuscripts are acknowledged in each manuscript, and reviewers of articles which were not accepted will be acknowledged at the end of each issue. To ensure the quality of the articles published in *WJR*, reviewers of accepted manuscripts will be announced by publishing the name, title/position and institution of the reviewer in the footnote accompanying the printed article. For example, reviewers: Professor Jing-Yuan Fang, Shanghai Institute of Digestive Disease, Shanghai, Affiliated Renji Hospital, Medical Faculty, Shanghai Jiaotong University, Shanghai, China; Professor Xin-Wei Han, Department of Radiology, The First Affiliated Hospital, Zhengzhou University, Zhengzhou, Henan Province, China; and Professor Anren Kuang, Department of Nuclear Medicine, Huaxi Hospital, Sichuan University, Chengdu, Sichuan Province, China.

Abstract

There are unstructured abstracts (no more than 256 words) and structured abstracts (no more than 480). The specific requirements for structured abstracts are as follows:

An informative, structured abstracts of no more than 480 words should accompany each manuscript. Abstracts for original contributions should be structured into the following sections. AIM (no more than 20 words): Only the purpose should be included. Please write the aim as the form of "To investigate/study/…; MATERIALS AND METHODS (no more than 140 words); RESULTS (no more than 294 words): You should present *P* values where appropriate and must provide relevant data to illustrate how they were obtained, e.g. 6.92 ± 3.86 *vs* 3.61 ± 1.67, $P < 0.001$; CONCLUSION (no more than 26 words).

Key words

Please list 5-10 key words, selected mainly from *Index Medicus*, which reflect the content of the study.

Text

For articles of these sections, original articles and brief articles, the main text should be structured into the following sections: INTRODUCTION, MATERIALS AND METHODS, RESULTS and DISCUSSION, and should include appropriate Figures and Tables. Data should be presented in the main text or in Figures and Tables, but not in both. The main text format of these sections, editorial, topic highlight, case report, letters to the editors, can be found at: http://www.wjgnet.com/1949-8470/g_info_20100313183720.htm.

Illustrations

Figures should be numbered as 1, 2, 3, *etc*., and mentioned clearly in the main text. Provide a brief title for each figure on a separate page. Detailed legends should not be provided under the figures. This part should be added into the text where the figures are applicable. Figures should be either Photoshop or Illustrator files (in tiff, eps, jpeg formats) at high-resolution. Examples can be found at: http://www.wjgnet.com/1007-9327/13/4520.pdf; http://www.wjgnet.com/1007-9327/13/4554.pdf; http://www.wjgnet.com/1007-9327/13/4891.pdf; http://www.wjgnet.com/1007-9327/13/4986.pdf; http://www.wjgnet.com/1007-9327/13/4498.pdf. Keeping all elements compiled is necessary in line-art image. Scale bars should be used rather than magnification factors, with the length of the bar defined in the legend rather than on the bar itself. File names should identify the figure and panel. Avoid layering type directly over shaded or textured areas. Please use uniform legends for the same subjects. For example: Figure 1 Pathological changes in atrophic gastritis after treatment. A: ...; B: ...; C: ...; D: ...; E: ...; F: ...; G: …*etc*. It is our principle to publish high resolution-figures for the printed and E-versions.

Tables

Three-line tables should be numbered 1, 2, 3, *etc*., and mentioned clearly in the main text. Provide a brief title for each table. Detailed legends should not be included under tables, but rather added into the text where applicable. The information should complement, but not duplicate the text. Use one horizontal line under the title, a second under column heads, and a third below the Table, above any footnotes. Vertical and italic lines should be omitted.

Notes in tables and illustrations

Data that are not statistically significant should not be noted. $^{a}P < 0.05$, $^{b}P < 0.01$ should be noted ($P > 0.05$ should not be noted). If there are other series of *P* values, $^{c}P < 0.05$ and $^{d}P < 0.01$ are used. A third series of *P* values can be expressed as $^{e}P < 0.05$ and $^{f}P < 0.01$. Other notes in tables or under illustrations should be expressed as ^{1}F, ^{2}F, ^{3}F; or sometimes as other symbols with a superscript (Arabic numerals) in the upper left corner. In a multi-curve illustration, each curve should be labeled with ●, ○, ■, □, ▲, △, *etc*., in a certain sequence.

Acknowledgments

Brief acknowledgments of persons who have made genuine contributions to the manuscript and who endorse the data and conclusions should be included. Authors are responsible for obtaining written permission to use any copyrighted text and/or illustrations.

REFERENCES

Coding system

The author should number the references in Arabic numerals ac-

cording to the citation order in the text. Put reference numbers in square brackets in superscript at the end of citation content or after the cited author's name. For citation content which is part of the narration, the coding number and square brackets should be typeset normally. For example, "Crohn's disease (CD) is associated with increased intestinal permeability[1,2]". If references are cited directly in the text, they should be put together within the text, for example, "From references[19,22-24], we know that..."

When the authors write the references, please ensure that the order in text is the same as in the references section, and also ensure the spelling accuracy of the first author's name. Do not list the same citation twice.

PMID and DOI

Pleased provide PubMed citation numbers to the reference list, e.g. PMID and DOI, which can be found at http://www.ncbi.nlm.nih.gov/sites/entrez?db=pubmed and http://www.crossref.org/SimpleTextQuery/, respectively. The numbers will be used in E-version of this journal.

Style for journal references

Authors: the name of the first author should be typed in bold-faced letters. The family name of all authors should be typed with the initial letter capitalized, followed by their abbreviated first and middle initials. (For example, Lian-Sheng Ma is abbreviated as Ma LS, Bo-Rong Pan as Pan BR). The title of the cited article and italicized journal title (journal title should be in its abbreviated form as shown in PubMed), publication date, volume number (in black), start page, and end page [PMID: 11819634 DOI: 10.3748/wjg.13.5396].

Style for book references

Authors: the name of the first author should be typed in bold-faced letters. The surname of all authors should be typed with the initial letter capitalized, followed by their abbreviated middle and first initials. (For example, Lian-Sheng Ma is abbreviated as Ma LS, Bo-Rong Pan as Pan BR) Book title. Publication number. Publication place: Publication press, Year: start page and end page.

Format

Journals

English journal article (list all authors and include the PMID where applicable)

1 **Jung EM**, Clevert DA, Schreyer AG, Schmitt S, Rennert J, Kubale R, Feuerbach S, Jung F. Evaluation of quantitative contrast harmonic imaging to assess malignancy of liver tumors: A prospective controlled two-center study. *World J Gastroenterol* 2007; **13**: 6356-6364 [PMID: 18081224 DOI: 10.3748/wjg.13.6356]

Chinese journal article (list all authors and include the PMID where applicable)

2 **Lin GZ**, Wang XZ, Wang P, Lin J, Yang FD. Immunologic effect of Jianpi Yishen decoction in treatment of Pixu-diarrhoea. *Shijie Huaren Xiaohua Zazhi* 1999; **7**: 285-287

In press

3 **Tian D**, Araki H, Stahl E, Bergelson J, Kreitman M. Signature of balancing selection in Arabidopsis. *Proc Natl Acad Sci USA* 2006; In press

Organization as author

4 **Diabetes Prevention Program Research Group**. Hypertension, insulin, and proinsulin in participants with impaired glucose tolerance. *Hypertension* 2002; **40**: 679-686 [PMID: 12411462 PMCID:2516377 DOI:10.1161/01.HYP.0000035706.28494.09]

Both personal authors and an organization as author

5 **Vallancien G**, Emberton M, Harving N, van Moorselaar RJ; Alf-One Study Group. Sexual dysfunction in 1, 274 European men suffering from lower urinary tract symptoms. *J Urol* 2003; **169**: 2257-2261 [PMID: 12771764 DOI:10.1097/01.ju.0000067940.76090.73]

No author given

6 21st century heart solution may have a sting in the tail. *BMJ* 2002; **325**: 184 [PMID: 12142303 DOI:10.1136/bmj.325.7357.184]

Volume with supplement

7 **Geraud G**, Spierings EL, Keywood C. Tolerability and safety of frovatriptan with short- and long-term use for treatment of migraine and in comparison with sumatriptan. *Headache* 2002; **42** Suppl 2: S93-99 [PMID: 12028325 DOI:10.1046/j.1526-4610.42.s2.7.x]

Issue with no volume

8 **Banit DM**, Kaufer H, Hartford JM. Intraoperative frozen section analysis in revision total joint arthroplasty. *Clin Orthop Relat Res* 2002; (**401**): 230-238 [PMID: 12151900 DOI:10.1097/00003086-200208000-00026]

No volume or issue

9 Outreach: Bringing HIV-positive individuals into care. *HRSA Careaction* 2002; 1-6 [PMID: 12154804]

Books

Personal author(s)

10 **Sherlock S**, Dooley J. Diseases of the liver and billiary system. 9th ed. Oxford: Blackwell Sci Pub, 1993: 258-296

Chapter in a book (list all authors)

11 **Lam SK**. Academic investigator's perspectives of medical treatment for peptic ulcer. In: Swabb EA, Azabo S. Ulcer disease: investigation and basis for therapy. New York: Marcel Dekker, 1991: 431-450

Author(s) and editor(s)

12 **Breedlove GK**, Schorfheide AM. Adolescent pregnancy. 2nd ed. Wieczorek RR, editor. White Plains (NY): March of Dimes Education Services, 2001: 20-34

Conference proceedings

13 **Harnden P**, Joffe JK, Jones WG, editors. Germ cell tumours V. Proceedings of the 5th Germ cell tumours Conference; 2001 Sep 13-15; Leeds, UK. New York: Springer, 2002: 30-56

Conference paper

14 **Christensen S**, Oppacher F. An analysis of Koza's computational effort statistic for genetic programming. In: Foster JA, Lutton E, Miller J, Ryan C, Tettamanzi AG, editors. Genetic programming. EuroGP 2002: Proceedings of the 5th European Conference on Genetic Programming; 2002 Apr 3-5; Kinsdale, Ireland. Berlin: Springer, 2002: 182-191

Electronic journal (list all authors)

15 Morse SS. Factors in the emergence of infectious diseases. Emerg Infect Dis serial online, 1995-01-03, cited 1996-06-05; 1(1): 24 screens. Available from: URL: http://www.cdc.gov/ncidod/eid/index.htm

Patent (list all authors)

16 **Pagedas AC**, inventor; Ancel Surgical R&D Inc., assignee. Flexible endoscopic grasping and cutting device and positioning tool assembly. United States patent US 20020103498. 2002 Aug 1

Statistical data

Write as mean ± SD or mean ± SE.

Statistical expression

Express *t* test as *t* (in italics), *F* test as *F* (in italics), chi square test as χ^2 (in Greek), related coefficient as *r* (in italics), degree of freedom as υ (in Greek), sample number as *n* (in italics), and probability as *P* (in italics).

Units

Use SI units. For example: body mass, m (B) = 78 kg; blood pressure, p (B) = 16.2/12.3 kPa; incubation time, t (incubation) = 96 h, blood glucose concentration, c (glucose) 6.4 ± 2.1 mmol/L; blood CEA mass concentration, p (CEA) = 8.6 24.5 μg/L; CO_2 volume fraction, 50 mL/L CO_2, not 5% CO_2; likewise for 40 g/L formaldehyde, not 10% formalin; and mass fraction, 8 ng/g, *etc.* Arabic numerals such as 23, 243, 641 should be read 23 243 641.

The format for how to accurately write common units and quantums can be found at: http://www.wjgnet.com/1949-8470/g_info_20100313185816.htm.

Abbreviations

Standard abbreviations should be defined in the abstract and on first mention in the text. In general, terms should not be abbreviated unless they are used repeatedly and the abbreviation is helpful to the reader. Permissible abbreviations are listed in Units, Symbols and Abbreviations: A Guide for Biological and Medical Editors and Authors (Ed. Baron DN, 1988) published by The Royal Society of Medicine, London. Certain commonly used abbreviations, such as DNA, RNA, HIV, LD50, PCR, HBV, ECG, WBC, RBC, CT, ESR, CSF, IgG, ELISA, PBS, ATP, EDTA, mAb, can be used directly without further explanation.

Italics

Quantities: *t* time or temperature, *c* concentration, *A* area, *l* length, *m* mass, *V* volume.
Genotypes: *gyrA*, *arg* 1, *c myc*, *c fos*, *etc.*
Restriction enzymes: *Eco*RI, *Hin*dI, *Bam*HI, *Kbo* I, *Kpn* I, *etc.*
Biology: *H. pylori*, *E coli*, *etc.*

Examples for paper writing

Editorial: http://www.wjgnet.com/1949-8470/g_info_20100313182341.htm

Frontier: http://www.wjgnet.com/1949-8470/g_info_20100313182448.htm

Topic highlight: http://www.wjgnet.com/1949-8470/g_info_20100313182639.htm

Observation: http://www.wjgnet.com/1949-8470/g_info_20100313182834.htm

Guidelines for basic research: http://www.wjgnet.com/1949-8470/g_info_20100313183057.htm

Guidelines for clinical practice: http://www.wjgnet.com/1949-8470/g_info_20100313183238.htm

Review: http://www.wjgnet.com/1949-8470/g_info_20100313183433.htm

Original articles: http://www.wjgnet.com/1949-8470/g_info_20100313183720.htm

Brief articles: http://www.wjgnet.com/1949-8470/g_info_20100313184005.htm

Case report: http://www.wjgnet.com/1949-8470/g_info_20100313184149.htm

Letters to the editor: http://www.wjgnet.com/1949-8470/g_info_20100313184410.htm

Book reviews: http://www.wjgnet.com/1949-8470/g_info_20100313184803.htm

Guidelines: http://www.wjgnet.com/1949-8470/g_info_20100313185047.htm

SUBMISSION OF THE REVISED MANUSCRIPTS AFTER ACCEPTED

Please revise your article according to the revision policies of *WJR*. The revised version including manuscript and high-resolution image figures (if any) should be re-submited online (http://www.wjgnet.com/1949-8470office/). The author should send the copyright transfer letter, responses to the reviewers, English language Grade B certificate (for non-native speakers of English) and final manuscript checklist to wjr@wjgnet.com.

Language evaluation

The language of a manuscript will be graded before it is sent for revision. (1) Grade A: priority publishing; (2) Grade B: minor language polishing; (3) Grade C: a great deal of language polishing needed; and (4) Grade D: rejected. Revised articles should reach Grade A or B.

Copyright assignment form

Please download a Copyright assignment form from http://www.wjgnet.com/1949-8470/g_info_20100313185522.htm.

Responses to reviewers

Please revise your article according to the comments/suggestions provided by the reviewers. The format for responses to the reviewers' comments can be found at: http://www.wjgnet.com/1949-8470/g_info_20100313185358.htm.

Proof of financial support

For paper supported by a foundation, authors should provide a copy of the document and serial number of the foundation.

Links to documents related to the manuscript

WJR will be initiating a platform to promote dynamic interactions between the editors, peer reviewers, readers and authors. After a manuscript is published online, links to the PDF version of the submitted manuscript, the peer-reviewers' report and the revised manuscript will be put on-line. Readers can make comments on the peer reviewer's report, authors' responses to peer reviewers, and the revised manuscript. We hope that authors will benefit from this feedback and be able to revise the manuscript accordingly in a timely manner.

Science news releases

Authors of accepted manuscripts are suggested to write a science news item to promote their articles. The news will be released rapidly at EurekAlert/AAAS (http://www.eurekalert.org). The title for news items should be less than 90 characters; the summary should be less than 75 words; and main body less than 500 words. Science news items should be lawful, ethical, and strictly based on your original content with an attractive title and interesting pictures.

Publication fee

WJR is an international, peer-reviewed, Open-Access, online journal. Articles published by this journal are distributed under the terms of the Creative Commons Attribution Non-commercial License, which permits use, distribution, and reproduction in any medium, provided the original work is properly cited, the use is non commercial and is otherwise in compliance with the license. Authors of accepted articles must pay a publication fee. The related standards are as follows. Publication fee: 1300 USD per article; Reprints fee: 350 USD per 100 reprints, including postage cost. Editorial, topic highlights, book reviews and letters to the editor are published free of charge.